THE UNIVERSITY OF MICHIGAN

COLLEGE OF ENGINEERING
Department of Nuclear Engineering

Technical Report

AN ELECTRON SPIN RESONANCE STUDY OF VANADIUM IN CALCIUM TUNGSTATE CRYSTAL

Nasser Mahootian
Chihiro Kikuchi

ORA Project 06029

under contract with:

HARRY DIAMOND LABORATORY
CONTRACT NO. DA-49-186-AMC-80(X)
WASHINGTON, D.C.

administered through:

OFFICE OF RESEARCH ADMINISTRATION ANN ARBOR

August 1966

ERRATA

Page	Line	Correction
2	4	spectra of
4		Add the following footnote: *K is a function of the spin-orbit coupling constant A, usually referred to as the A-value.
4	20	valence states
6	4	crystal were
7	16	This result is
7	21	was made
12	2	ESR spectrum
14		Add the following footnote: *Dr. Dunn has suggested that $(VO_4)^{3-}$ may be in the form of $[(V = 0)O_3]^{3-}$ where the V = 0 bond is considerably shorter than the other three and the paramagnetic electron upon irradiation comes from oxygen in the V = 0 bond.
16	Table 2.1, last line	6.3 ± 2.2
21	2nd paragraph	The ESR spectrum
23	1	1.96 Å
28	15	spectra are
29	21	(17.9 ± 0.2)
39	Table 4.2	A_1, A_2, and $\langle A \rangle$ are expressed in gauss
42	4	possess axial symmetry
42	Eq. (4.6)	H_0 - $Am/g\beta$
46	15	sets in the ab-plane

ERRATA--(CONTINUED)

Page	Line	Correction
52	13,14	tensors
55	Tables 4.3 and 4.4	estimated error for g_x and g_y is ± 0.005 and for A_x and A_y is ± 1 gauss.
66	20	77°K spectrum
68	7	set of lines is expected
74	4	admixture
87	lines 4 and 5 of Eq. (B.13)	E_β and E_α respectively
91	10	$L_x = (1/2)(L_+ + L_-)$

This report was also a dissertation submitted by the first author in partial fulfillment of the requirement for the degree of Doctor of Philosophy in The University of Michigan, 1966.

TABLE OF CONTENTS

LIST OF TABLES

LIST OF FIGURES

Abstract

In this study, the electron spin resonance (ESR) spectrum of vanadium ($_{23}V^{51}$, nuclear spin I = 7/2) is investigated in single crystals of calcium tungstate at microwave frequencies of about 9.5 Gc/sec. To some samples, rare-earth (RE) ions Tb^{3+} or Nd^{3+} were added as charge compensators for vanadium.

To produce vanadium paramagnetic centers, the samples were irradiated with 50 kvp, 35 ma X-rays for about 15 minutes ($\approx 10^8$ rad). It is believed that vanadium enters the crystal in diamagnetic pentavalent (V^{5+}) oxidation state and the observed spectra are due to the irradiation-produced V^{4+} (S = 1/2). Three vanadium paramagnetic centers were detected, at 77°K and 4.2°K, with the corresponding spectra designated as Groups A, B, and C, and intensities in the ratio of 100:5:70 respectively. Each group consists of sets of eight (2 I + 1) hyperfine lines, arisen from unequivalent paramagnetic sites, which become one set when the applied static magnetic field $\underline{H}$ is parallel to the c-axis of the crystal.

In general, the Group A lines, seen in the spectra of all samples, consist of four sets at 4.2°K. The maximum components of the g- and A-tensors are in the direction of the W-O bond in $CaWO_4$. Their magnitudes are

$$g_{max} = 2.044 \pm 0.003 \qquad A_{max} = (19.9 \pm 0.2) \times 10^{-4} \text{ cm}^{-1}$$

At 77°K, one set of lines emerges at the average position of the four low-temperature sets with isotropic g- and nearly isotropic A-tensors:

$$\begin{aligned} g &= 2.0245 \pm 0.0005 \\ A_{\parallel} &= (17.9 \pm 0.2) \times 10^{-4} \text{ cm}^{-1} \\ A_{\perp} &= (19.0 \pm 0.2) \times 10^{-4} \text{ cm}^{-1} \end{aligned}$$

where $A_{\parallel}$ is measured with $\underline{H}$ parallel to the c-axis. This group is attributed to V^{4+} ions at W^{6+} sites, i.e., to VO_4^{4-} complexes; the para-paramagnetic electron in this complex is supplied by one of the four oxygen ligands. The temperature dependence of the spectrum is interpreted in terms of thermal reorientation of the unpaired electron among the four possible V-O directions.

The Group B lines, shown by the (V,RE)-doped samples only, arise from two unequivalent sites with the g- and A-tensors given below:

$$A_{\parallel} = A_{\perp} = (8.5 \pm 0.2) \times 10^{-4}\ cm^{-1}$$

$$g_{\parallel} = 2.068 \pm 0.001$$

$$g_{\perp} = 2.004 \pm 0.001$$

$$\theta_1 = 90^\circ \quad , \quad \phi_1 = -10^\circ$$

$$\theta_2 = 90^\circ \quad , \quad \phi_2 = 80^\circ$$

where θ_i and ϕ_i are the polar and azimuthal angles of the g-ellipsoids symmetry axes. This group is also assigned to V^{4+} at a W^{6+} site. The anisotropy of the spectrum is attributed to a reduction of the local symmetry due, perhaps, to crystal imperfections.

The Group C lines are seen in the spectra of the samples in which vanadium is the only dopant or there is an excess of this element over the RE ions. This group arises from four nonequivalent sites: In general, four sets of eight lines are observed which become two in the ab-plane and unite to one when H $\parallel$ c-axis. Both the g- and A-tensors are anisotropic with only one common axis, taken as the z-axis, which is very close to the direction of the line joining two nearest Ca atoms of two adjacent planes in $CaWO_4$ lattice. The x- and y-axes of the g-tensor are rotated by about 30° in c.c.w. direction with respect to the corresponding A-tensor axes. The principal values and directions for these tensors for one site are shown below. The directions for the other three sites are obtained by adding $\pi/2$, π, and $3\pi/2$ to the azimuthal angle ϕ.

	x	y	z
g	1.990	1.965	1.901 ± 0.001
θ	69	51	46 ± 1
ϕ	112	220	0 ± 1
A	34	65	165.0 ± 0.3
θ	90	44	46 ± 1
ϕ	90	180	0 ± 1

A-values are given in $10^{-4}\ cm^{-1}$. The x and y components are approximate values calculated from measurements in the ab- and ac-planes.

From the ESR data the following models are proposed for site occupancies and charge compensation in $CaWO_4$: In the presence of charge compensator $(RE)^{3+}$tions, V^{5+} ions occupy W^{6+} sites and $(RE)^{3+}$ ions enter Ca^{2+} sites. In the absence of the rare-earth additives, V^{5+} ions substitute both W^{6+} and Ca^{2+} sites and charge compensation is accomplished according to the following scheme: 4 V^{5+} replace 4 W^{6+} while 2 V^{5+} substitute 2 Ca^{2+} and one Ca^{2+} vacancy is also formed in the nearest site.

CHAPTER I

INTRODUCTION

1. Present Investigation and Motivation

In recent years, calcium tungstate crystal has received great attention as an excellent host for laser-active rare-earth (RE) ions. Optical* and paramagnetic[1-9] properties of a number of these ions have been studied in this crystal lattice. Since RE ions, except Eu^{2+}, enter the crystal in their trivalent oxidation states[7-10] some charge compensation mechanism must exist in order to conserve the required electrical neutrality of the sample. Commonly, diamagnetic sodium (Na^{1+}) and niobium (Nb^{5+}) ions are used for these purposes. Effects of the charge compensation on laser activity of the crystal have been investigated by researchers at the Bell Telephone Laboratory.[12-14] There are, however, certain ambiguities concerning the lattice sites of the impurity ions. An example is the neodymium-doped crystal, $CaWO_4:Nd^{3+}$, which is a good laser material. In general, electron spin resonance (ESR) spectroscopy (described briefly in Section 2 of this chapter) provides us with an excellent tool for determining the site of paramagnetic ions

---

*A number of articles on the optical properties of the RE-doped calcium tungstate has been recently reviewed and discussed in a three-part paper by Görlich et al.[11]

in a crystal. But in this example, the ESR spectra, which vary with concentrations of Nd and the charge compensator ions, are too complex to reveal decisively the site or sites occupied by the RE ions.[3,4,5]

In the present investigation, ESR spectra or vanadium in calcium tungstate single crystals are studied. Some of the samples were also doped with Nd or Tb in addition to the vanadium. This research was undertaken as part of a general program for studying paramagnetic properties of vanadium ions in crystalline solids.* It is also an attempt to shed some light on the above-mentioned ambiguities and to obtain information on the RE laser centers in this crystal by using vanadium as an ESR probe. Vanadium is particularly well suited for this purpose because it lies immediately above niobium in the periodic table. Furthermore, as an ESR probe, it has several merits such as: (1) With an abundance of 99.76%, it is practically isotopically pure and hence its ESR spectrum does not present the complications usually encountered in the case of elements which have many isotopes; (2) due to the nuclear spin of I = 7/2, its spectrum is characterized by a hyperfine structure of 8 lines which is easily identified; (3) it shows spectrum at 77°K in contrast with accompanying Tb or Nd impurities; (4) its valence state can be changed easily by a few minutes X- or gamma-irradiation; (5) different valence states of this ion have been studied in a variety of crystalline field symmetries (see Table 1).

---

*In this program, vanadium has been studied experimentally in α-Al_2O_3, CaO, MgO powder and crystal, zinc-ammonium Tutton Salt, and SnO_2 (Ref. 15-19) and, theoretically, in rutile-type crystals SnO_2, TiO_2, and GeO_2 (Ref. 21-23).

2. A Brief Description of ESR Spectroscopy

This technique, which is also called electron paramagnetic resonance (EPR) spectroscopy, was introduced in physics about twenty years ago for studying systems that possess unpaired electrons and hence net angular momentum and magnetic moment. Accordingly, these systems are referred to as paramagnetic or spin systems. Unpaired electrons are found in ions of transition metals. These are five groups of elements which have one or more unfilled shells underneath their valence shell. Vanadium ($_{23}V^{51}$), for instance, with its electronic structure $1s^2\ 2s^2\ 2p^6\ 3s^2\ 3p^6\ 3d^3\ 4s^2$ belongs to the iron-group elements ($_{22}Ti$-$_{29}Cu$) where the 3d shell is only partially filled. On the other hand, $_{60}Nd$ and $_{65}Tb$ belong to the rare-earth group ($_{58}Ce$-$_{70}Yb$) where the 4f shell is unfilled. The other transition groups are palladium, platinum, and actinide groups. Unpaired electrons are also found in organic free radicals, odd-electron molecules, irradiated crystals, just to mention a few examples.

Usually, the paramagnetic system is composed of paramagnetic centers (e.g., transition metal ions) distributed uniformly, with a concentration of 1-0.001%, in a diamagnetic substance. All or most of the orbital degeneracies of the ion is lifted by its interaction with the electrostatic field of the surrounding ligands and by the spin-orbit coupling within the ion itself. For instance, in the case of V^{4+} ($S = 1/2$) in $CaWO_4$ crystal, the lowest energy level is an orbital singlet, but it is still two-fold degenerate in electronic spin. Now, when the sample is placed in a static magnetic field $\underline{H}$, this level splits into two (Zeeman splitting) corresponding to the spin quantum

numbers $M_s = \pm 1/2$. The energy separation between these levels, to first order, is $g\beta H$ where g and β are the spectroscopic g-factor and Bohr magneton. If the interaction between the electronic spin (S) and nuclear spin (I) is also taken into account, each of the spin levels splits further into (21 + 1) hyperfine components characterized by the nuclear spin quantum numbers M_I as depicted in Figure 1. With the hyperfine correction, splitting between the spin levels to first order is now $g\beta H + KM_I$ where K is a constant which gives the hyperfine separations. Transitions between levels of similar nuclear orientations ($\Delta M_I = 0$) can be induced by photons of energy $h\nu$. The resonance condition is thus,

$$h\nu = g\beta H + KM_I \qquad (1.1)$$

In practice, ν is commonly kept constant and (1.1) is satisfied by varying $\underline{H}$ slowly. Since, at thermal equilibrium, the lower energy levels are more populated, the resonant transitions are accompanied by a net absorption of energy from the radiation field.

From the values of the resonant magnetic field and the number of the absorption peaks and their separations we can obtain valuable information about the nuclear and electronic spins of the paramagnetic ions, their valence state, their lattice sites, and the crystal field symmetry and strength. By measuring the intensity of the absorption lines against that of a known standard, concentration of the paramagnetic ions in the sample can be found. These ESR quantitative measurements are easily extended to minute concentrations beyond detection of standard analytical techniques (chemical or optical).

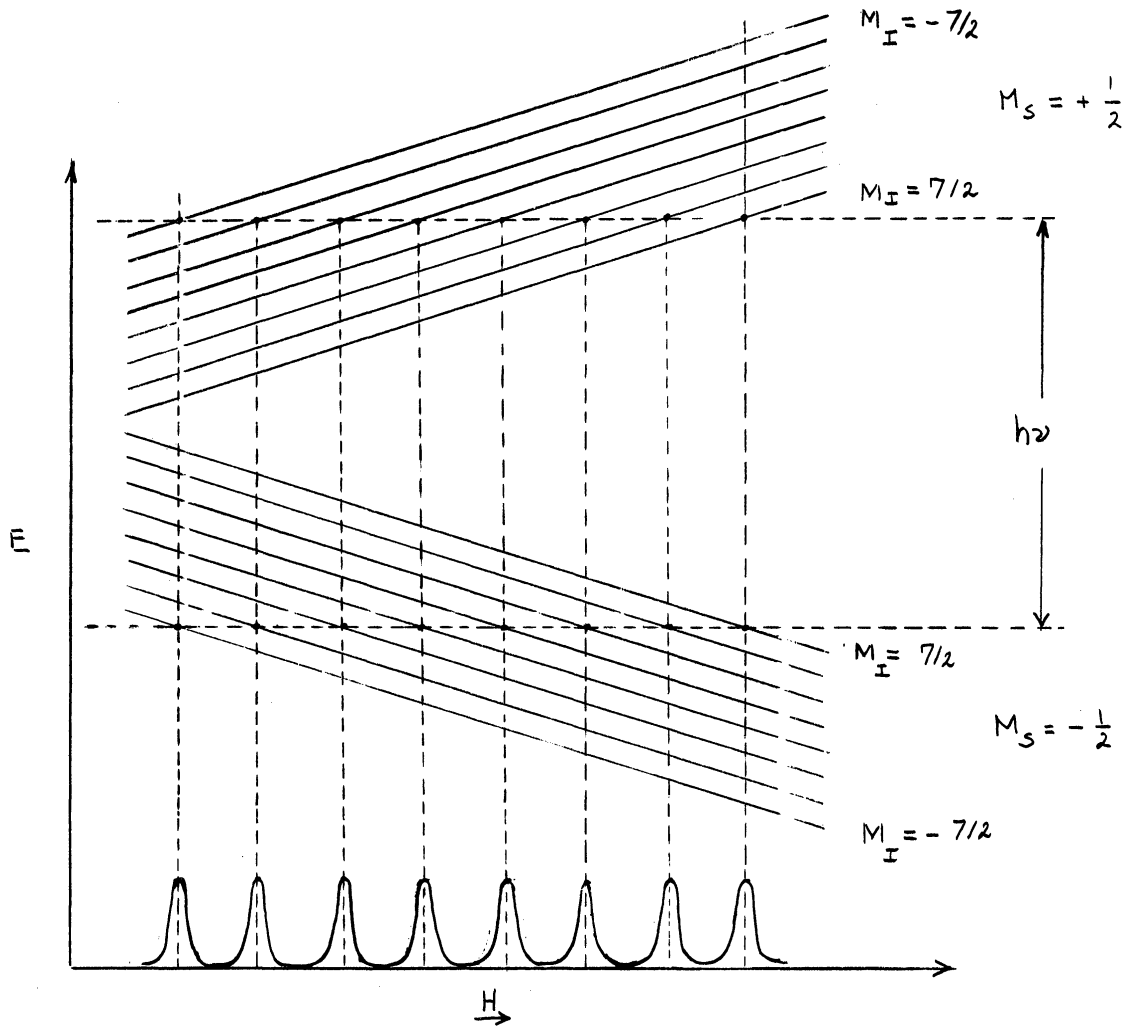

Fig. 1.1. Zeeman and nuclear splitting of the ground level of V^{4+}.

3. Literature Survey

This is a descriptive bibliography of ESR and some optical investigations on vanadium ions. The measured ESR parameters (g and hyperfine coupling constants) for different host crystals are shown in Table 1, to which we shall need to refer later.

Vanadium ions commonly met in ESR studies are V^{2+}, V^{3+}, and V^{4+} with $3d^3$, $3d^2$, and $3d^1$ configurations corresponding to the spectroscopic terms $^4F_{3/2}$, $^3F_2$, and $^2D_{3/2}$.

Divalent vanadium was first investigated in 1951 by Bleaney and coworkers[24] in the rhombic crystalline field of Tutton salt, $Zn(HN_4)_2(SO_4)_2.6H_2O$. Later, accurate measurements of the ESR parameters of V^{2+} in this crystal was carried out by Borcherts and Kikuchi.[19] In cubic site, V^{2+} was first investigated by Low[25] who used MgO as the host crystal. Later, it was investigated by Wertz and collaborators[26] who studied electron transfer processes among the iron group transition ions in MgO single crystals. Mahootian and Kikuchi[18] studied EPR spectrum of V^{2+} in MgO powder samples. They have also reported an anomalous angular dependence of the line width in MgO single crystals. Similar observation is reported by Van Wieringen and Rensen.[27] The observed anomaly is thought to be due to small tetragonal components, probably arising from internal strains.[28] In calcium oxide, V^{2+} was studied by Low and Rubins[29,30] and Azarbayejani and Kikuchi.[17] This ion was also studied in Si,[31] ZnO,[32] and the double fluoride $KMgF_3$.[33] Lambe and Kikuchi[15,16] were first to study V^{2+} in α-Al_2O_3. They produced this ion by X-irradiation of vanadium-doped corundum. As these authors have shown, before irradiation the paramagnetic vanadium ions in Al_2O_3 are V^{3+} and a small concentration of V^{4+}. The effect of irradiation is to convert V^{3+} to V^{2+}. Later, accurate measurements of the ESR parameters of V^{2+} in Al_2O_3 was made by Laurance and Lambe.[34] Sturge[35] studied energy levels of V^{2+} in MgO and Al_2O_3 by means of fluorescence and excitation optical spectra. Imbusch and collaborators[36] studied temperature dependence of the optical spectrum ($^2E \rightarrow {}^4A_2$ transitions) of V^{2+} in MgO.

Trivalent vanadium was first investigated in 1958 by Zverev and Prokhorov[37] in α-Al_2O_3. Lambe and Kikuchi,[16] in a systematic study of

various valence states (V^{2+}, V^{3+}, V^{4+}) of vanadium in sapphire, extended the measurements of the angular dependence of the V^{3+} spectrum to a wider range which was inaccessible to the former authors. Optical investigations of V^{3+} in sapphire was performed by Pryce and Runciman.[38] V^{3+} was also investigated in CdS by Woodbury and Ludwig[39] and in ZnS by Holton.[40] The latter observed both $\Delta M_s = 1$ and $\Delta M_s = 2$ transitions with isotropic g-, and A-values.

The ESR of V^{4+} has also been investigated in rutile-type crystals TiO_2, SnO_2, and GeO_2 (orthorhombic cation site symmetry). Gerritsen and Lewis[41] and Zverev and Prokhorov[42] studied V^{4+} in rutile, TiO_2. Later, this ion was studied in SnO_2,[43] and GeO_2.[44] In all these crystals, V^{4+} showed similar ESR spectra with an ambiguity in the sequence of the energy levels. In an attempt to remove this ambiguity, Karavelas and Kikuchi[21] have performed molecular orbital calculations for V^{4+} in TiO_2, GeO_2, and SnO_2. Their calculations indicated that the ground electron level was $3d(x^2-y^2)$. This result was further supported by the ESR investigations of Kikuchi, From and Dorain[20] who observed a large superhyperfine shift (SHFS) in $SnO_2:V^{4+}$. The mechanism of this SHFS was studied by Chen, Kikuchi, and Watanabe.[22] A systematic study of the theory of SHFS interaction of the iron group elements d electrons is made by Chen and Kikuchi.[23]

Tetravalent vanadium, in the form of unoriented vanadyl complex VO^{2+}, has been studied in various liquids, powders, and other amorphous media.[45,46,47,48,49,50,51,52] ESR spectrum of oriented VO^{2+} was studied by Borcherts and Kikuchi[19] in zinc-ammonium Tutton salt single crystals. They also showed that VO^{2+} could be reduced to V^{2+} by X-irradiation.

TABLE 1.1

g-VALUES AND HYPERFINE COUPLING CONSTANTS OF VANADIUM IONS IN VARIOUS HOST CRYSTALS

Ion	Host Crystal	Frequency Band	T(°K)	g	Hyperfine* Coupling Constants	Ref.
V^{2+}	MgO	X	290	1.9803(5)	74.24(2)	25
V^{2+}	MgO	X	300	1.980(.5)	74.19(5)	18
V^{2+}	MgO	X	290	1.9800(5)	74.1 (1)	27
V^{2+}	CaO	X	290	1.9683(5)	76.04(5)	29,30
V^{2+}	"	X	77	1.9683(5)	76.15(5)	"
V^{2+}	"	X	20	1.9683(5)	76.22(5)	"
V^{2+}	CaO	X	300	1.9687	76.30	17
V^{2+}	Si	X	1.3	1.9892	42.10	31
V^{2+}	ZnO	X	1.3	$g_{\parallel} = 1.977(1)$ $g_{\perp} \approx 2$	46.7 -	32
V^{2+}	$KMgF_3$	X	77	1.9720(2)	86.2(2)	33

TABLE 1.1--Continued

Ion	Host Crystal	Frequency Band	T(°K)	g	Hyperfine* Coupling Constants	Ref.
V^{2+}	Tutton salt	X,K	300	$g_z = 1.9717(5)$ $g_y = 1.9733(5)$	A = 86.63(5) B = 82.46(5)	19
V^{2+}	α-Al_2O_3	X	300	$g_{\parallel} = 1.991$ $g_{\perp} = 1.991$	A = 73.538(8) B = 74.267(30)	34
V^{3+}	α-Al_2O_3	X	4.2	1.98	102	15,16
V^{3+}	CdS		10	1.933	A = 63 A = 66	39
V^{3+}	ZnS	X	1.3	1.9433(5)	63.0(1)	40
V^{4+}	α-Al_2O_3	X	300	1.97	132	16
V^{4+}	TiO_2	X,K	4.2, 78	$g_{\tilde{1}10} = 1.956$ $g_{\bar{1}10} = 1.915$ $g_c = 1.913$	$A_{110} = 142$ $A_{\bar{1}10} = 31$ $A_c = 43$	41

TABLE 1.1--Continued

Ion	Host Crystal	Frequency Band	T(°K)	g	Hyperfine* Coupling Constants	Ref.
V^{4+}	TiO_2	X	77	$g_{110} = 1.955(1)$ $g_{\bar{1}10} = 1.913(1)$ $g_c = 1.912(1)$	$A_{110} = 141.5(7)$ $A_{\bar{1}10} = 30.9(3)$ $A_c = 44.1(3)$	42
V^{4+}	SnO_2	X	77	$g_{110} = 1.943$ $g_{\bar{1}10} = 1.939$ $g_c = 1.903$	$A_{110} = 144$ $A_{\bar{1}10} = 21$ $A_c = 44$	43
V^{4+}	GeO_2			$g_{110} = 1.963(.3)$ $g_{\bar{1}10} = 1.921(.6)$ $g_c = 1.921(.1)$	$A_{110} = 134.36(2)$ $A_{\bar{1}10} = 36.69(1)$ $A_c = 37.54(1)$	44
VO^{2+}	Tutton salt	X,K	300	$g_x = 1.9813(2)$ $g_y = 1.9801(2)$ $g_z = 1.9331(2)$	$A_x = 71.20(4)$ $A_y = 72.44(4)$ $A_z = 182.8\ (5)$	19

*Absolute values in units of 10^{-4} cm^{-1}.

CHAPTER II

SUMMARY OF RESULTS

In this study, electron spin resonance spectra of vanadium are investigated in calcium tungstate single crystals at microwave frequencies of about 9.5 Gc/sec. Some of the samples were also doped with the rare-earth elements Tb and Nd in addition to vanadium. Concentrations of the additives are shown in Table 3.1.

Prior to X-irradiation no vanadium ESR spectrum was observed. After the irradiation, spectra were seen only at 77°K and 4.2°K. It showed, in all samples, a hyperfine structure of 8 lines corresponding to a nuclear spin of $I = 7/2$, and effective electron spin of $S = 1/2$. The observed spectra are attributed to V^{4+} since a cobalt-doped $CaWO_4$ sample ($I_{Co} = 7/2$) failed to show any ESR signal. In general, three groups of lines were identified in the vanadium spectra and labeled as Groups A, B, and C. The intensities of these groups are in the ratio of about 100:5:70, respectively.

1. Group A Spectra

At 77°K, this group consists of a set of 8 lines, observed in the spectra of all samples, and characterized by an isotropic g- and nearly isotropic A-values.

$$g = 2.0245 \pm 0.0005$$

$$A_{\parallel} = 19.1 \pm 0.2 \quad \text{gauss}$$

$$A_{\perp} = 20.3 \pm 0.2 \quad \text{gauss}$$

At liquid helium temperature, the (V,Tb)-doped samples did not show any vanadium ESR spectra while the other samples did. This is discussed in detail in Chapter V where we have attempted to show that, due to cross-relaxation between V and Tb, such temperature dependence is expected.

At this temperature, the Group A lines were seen to split into four sets of 8 lines which coalesced to two in the ab-plane and to one when the applied static magnetic field was parallel to the c-axis. It was also observed that the average position of these sets coincided with the position of the Group A at 77°K, as shown in Table 4.2.

The maximum components of the g- and A-tensors at 4.2°K were found to be

$$g_{max} \equiv g_z = 2.044 \pm 0.003$$

$$A_{max} \equiv A_z = 21.3 \pm 0.2 \quad \text{gauss}$$

$$\theta = 60° \pm 3° , \quad \phi = 30° \pm 1$$

where θ and ϕ are the polar and azimuthal angles of the tensors z-axes which is very close to the W-O bond (see Figures 3.3 and 3.4). The values of g and A along the crystal axes were measured; the results are:

	a	b	c
g	2.033(1)	2.017(1)	2.024(1)
A(gauss)	21.2(1)	19.7(1)	19.1(1)

This group, with its positive Δ g (Δ g = g-g_e where g_e = g of free electron = 2.0023) and small hyperfine separation (HFS), is assigned to V^{4+} at the covalent tungsten site. A preliminary molecular-orbital calculation by Karavelas and Kikuchi[56] produced results in excellent agreement with the experimental g-value at 77°K.

For the low-temperature splitting of the Group A, we have tentatively adopted a model analogous to that proposed by Watkins and Corbett[70] for the interpretation of similar temperature dependences of the ESR spectra of the silicon E-center. Before X-irradiation, the vanadium at the W site is in the diamagnetic VO_4^{3-} form. Due to the irradiation, it acquires an electron from one of the oxygen ligands to become VO_4^{4-}, a paramagnetic complex ion with effective spin S = 1/2. The fact that g_z is in the direction of W-O bond lends some support to this model. Now, suppose the unpaired electron jumps randomly from one oxygen ligand to another in VO_4. Thus, there are four non-equivalent sites available to it. At 4.2°K, the jumping rate is slow, the life time of the spin at each of the four sites is long, and according to Gutowsky and Saika,[71] we expect to see distinct resonance spectra from each center. As the temperature is increased, the life time τ of the unpaired electron in each orientation becomes shorter and lines become broader until eventually the resonances from the four centers are not

distinguishable. At still higher temperatures (near 77°K), τ becomes so short that motional narrowing takes place with emergence of one set of lines at the average position of the four.[72]

2. Group B Spectra

This Group was seen only in the spectra of the samples which contained a rare-earth ion besides vanadium. It is composed of two sets of 8 lines which coalesce to one when the applied static magnetic field is parallel to the c-axis of the crystal. The ESR spectra arise from two non-equivalent sites with isotropic A- and axial g-tensors:

$$A_{\parallel} = A_{\perp} = 9.1 \pm 0.2 \quad \text{gauss}$$
$$g_{\parallel} = 2.068 \pm 0.001$$
$$g_{\perp} = 2.004 \pm 0.001$$

The symmetry axes of the two g-tensors are in the ab-plane and make angles $\phi_1 = -10$ and $\phi_2 = 80$ with the a-axis. This group, similar to the Group A, is also attributed to V^{4+} at W site, but with some reduction in the site symmetry to account for the observed anisotropic spectrum. The cause of this symmetry reduction is not quite understood. It may well be due to some local imperfections in the crystal. The fact that they did not appear in the spectrum of some newly prepared samples provides some support for this view. Due to its low intensity and power saturation effect, this group was not easily observable at 4.2°K.

3. Group C Spectra

This group was observed only in the ESR spectra of the samples which contained only vanadium or an excess of vanadium over the rare-earth dopants (e.g., $CaWO_4$:V, Nd, 1.0%, 0.1% concentrations in the melt). The spectrum at 4.2°K is similar to that at 77°K except for some line deformation and broadening due power saturation at the lower temperature.

The Group C is characterized by anisotropic spectra consisting, in general, of four sets of hyperfine lines which coalesce to two in the ab-plane and to one when $\underline{H}$ is parallel to the c-axis. This shows that the ESR spectra arise from four non-equivalent sites. The principal values and directions of the g- and A-tensors for these centers are shown in Table 4.3.

Because of its negative Δ g and large HFS, this group is assigned to V^{4+} in the ionic site in $CaWO_4$, i.e., the calcium site. In fact, as Table 1.1 shows, the g- and A-values of V^{4+} and other valence states of vanadium in ionic bonds are in the range of the values we have found for the Group C. Also, the assignment of V^{4+} to the Ca site is supported by the results of our crystal field calculations shown in Table 2.1.

4. Conclusions

Correlating the ESR results of the three groups, A, B, and C, we have concluded that:

1) As mentioned earlier, vanadium enters the calcium tungstate lattice in pentavalent oxidation state which is diamagnetic. As a

TABLE 2.1

EXPERIMENTAL VERSUS CALCULATED Δ g
FOR THE GROUP C LINES

g-shift	Experiment	Crystal Field Calc.
Δg_x	< 0	< 0
Δg_y	< 0	< 0
Δg_z	< 0	< 0
$\Delta g_z / \Delta g_x$	> 1	> 1
$\Delta g_z / \Delta g_y$	> 1	> 1
$\frac{1}{2}\left(\frac{\Delta g_z}{\Delta g_x} + \frac{\Delta g_z}{\Delta g_y}\right)$	4.4 ± 1.2	8

result of X-irradiation, it is converted to paramagnetic V^{4+} with one unpaired electron. Similar reducing effect of X-ray on vanadium ions has also been observed by others.[16,18,19,26]

2) In samples where the rare-earth ions Tb or Nd are present, V^{5+} ions occupy the W sites while the rare-earth ions, as trivalent ions, enter the Ca sites. This scheme also satisfies the required electrical neutrality of the crystal.

3) In samples where the vanadium ions are the only intended dopants, V^{5+} ions occupy both the Ca and W sites. We propose the following model for charge compensation: Four V^{5+} ions occupy four W^{6+} sites while two other V^{5+} ions substitute two Ca^{2+} ions and one calcium vacancy is also generated. According to this scheme, the intensities of

the Groups A and C must be in the ratio of 2:1. This is in agreement with results of our quantitative measurements (using $CuSO_4$ as an intensity standard) within $\pm$ 20% which is the usual error limit in the ESR quantitative measurements of this nature. Also, according to this scheme, every two vanadium ions at the Ca sites are coupled to a nearest calcium vacancy. The direction of this coupling makes an angle of 42°, 40' with the c-axis in the ac- or bc-plane (see Figure 3.2). This is also in good agreement with the direction of the common z-axis of the g- and A-tensors for the Group C.

A number of temperature annealing and growth rate* experiments were carried out in an attempt to see if there exist some electron transfer processes between the paramagnetic centers of the A and C spectra. From the results, it appears there is no simple charge-exchange correlation between the two centers.

---

*Rate of increase of the paramagnetic vanadium due to X-irradiation as a function of the irradiation time.

CHAPTER III

EXPERIMENTAL PROCEDURE AND CRYSTAL STRUCTURE

1. The ESR Spectrometer

The ESR spectroscopy of the $CaWO_4$ single crystals was achieved at 77°K and 4.2°K at X-band frequencies ($\nu \approx 9.5$ Gc/sec.) using a Varian 4012-35 12" rotating electromagnet, a V-153c Klystron, a cylindrical cavity operating in the TE_{011} mode, and a balanced bridge homodyne detection. Data at 4.2°K were obtained at 60-70 db below klystron power level (300 mw) using superheterodyne detection.

The microwave cavity was made of lavite, coated with the thermal silver paint Hanovia 32A on the inside and electroplated at 30 ma for about one hour.

The static magnetic field was measured by means of a proton probe connected to a Varian Fluxmeter Model F-85. A Beckman Transfer Oscillator 7580 and Beckman Universal EPUT and Timer 7380 were also connected to the fluxmeter for more accurate measurements. Magnetic field measurements were made at a point just underneath the cavity. The measurements were corrected for the distance between the sample and the magnetic probe, using the ESR signal of a small DPHH* standard glued to

---

* α , α -diphenyl β -picryl hydrazyl, $(C_6H_5)_2N\text{-}NC_6H_2(NO_2)_3$.

the sample.

The klystron frequency was measured using a Hewlett-Packard K-532A absorption type wavemeter. This device, with divisions to 0.010 Gc, allowed easily the frequency measurements to be extended to 1/4 of a division, i.e., to 0.0025 Gc/sec. For more accurate measurements the transfer oscillator was used.

2. Sample Preparation and Composition

Calcium tungstate crystals used in this study were grown at the Harry Diamond Laboratory, Washington, D. C., using the Czochralski technique as employed by Nassau and Broyer.[10] Vanadium and rare-earth dopants were added to the melt in the form of their most stable oxides, i.e., V_2O_5 and $(RE)_2O_3$.

To produce paramagnetic centers, the samples were X-irradiated for about fifteen minutes by a tungsten target Machlett AEG-50 S X-ray tube with beryllium window. The tube was operated at 50 Kvp x 35 ma. The dose rate at the location of the sample was about 6.0×10^6 rad/min.[19] The concentration of the paramagnetic vanadium was found to reach about 95% of its maximum value after fifteen minutes of irradiation. The maximum paramagnetic conversion ratio was about 6% of the vanadium present in the sample. This was measured by comparing the vanadium ESR signal intensity to that of a standard $CuSO_4$ single crystal. Figure 3.1 shows variation of the concentration with the irradiation time.

The vanadium concentrations in the samples were determined for us, using arc discharge spectroscopy, by the Physics Instrumentation

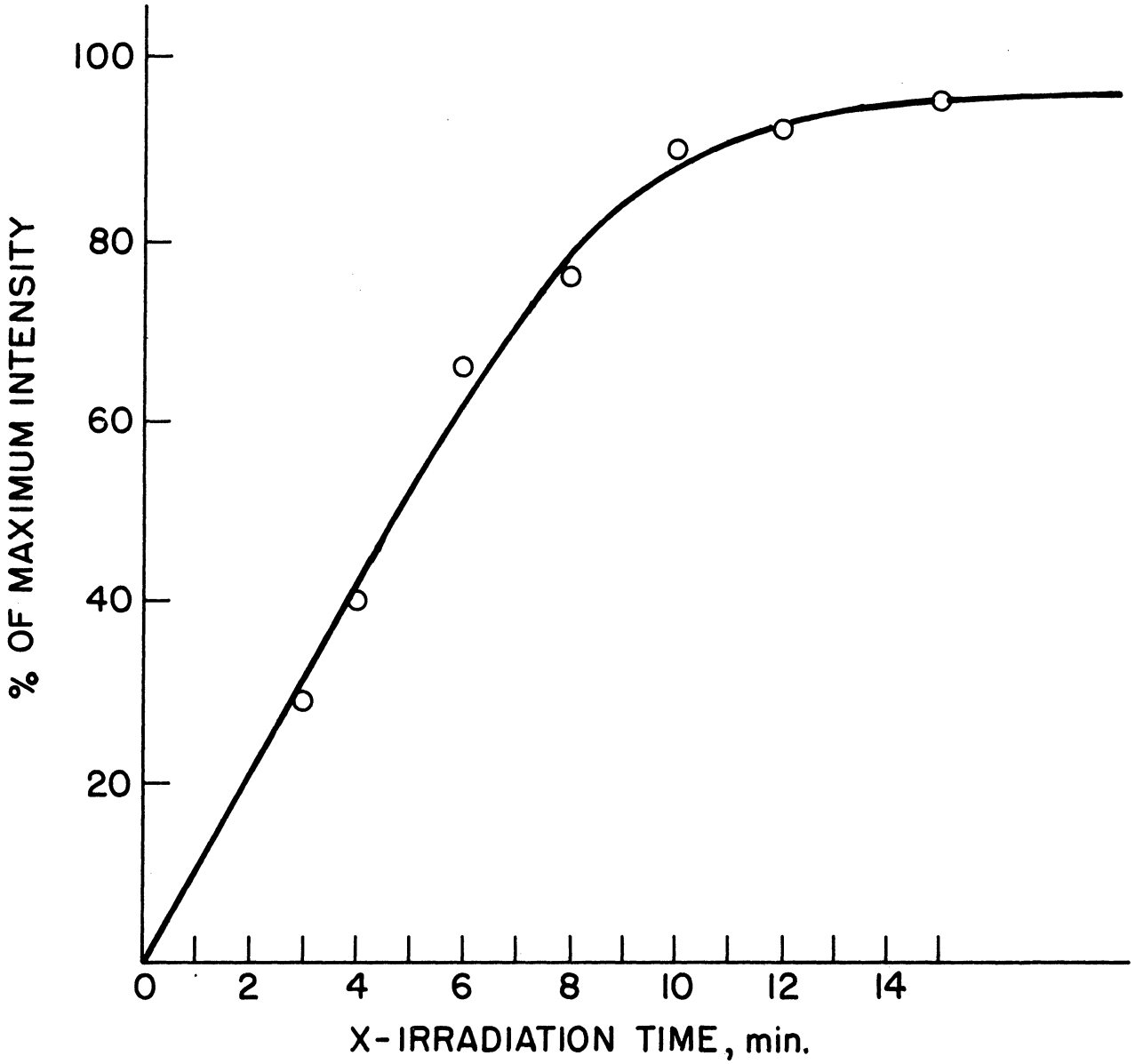

Fig. 3.1. Conversion of V^{5+} to V^{4+} by X-irradiation.

Laboratory, Department of Industrial Health, of the University of Michigan. The results are shown in Table 3.1.

TABLE 3.1

ATOMIC CONCENTRATIONS OF VANADIUM AND RARE-EARTH (RE) IONS IN $CaWO_4$ SAMPLES

Sample	In Melt		In Crystal	
	V/Ca (%)	RE/Ca (%)	V/Ca (%)	RE/Ca (%)
$CaWO_4$: V	0.5	0	0.05	0
$CaWO_4$: V,Tb	1	1	0.13	0.3
$CaWO_4$: V,Nd	1	1	0.13	0.2

The concentrations in melt were given to us by the Harry Diamond Laboratory. The last column in the table shows the rare-earth concentrations estimated from their distribution coefficients[10] $K = C_c/C_m$ where C_c and C_m denote concentrations in the crystal and in the melt, respectively.

ESR spectrum of Mn^{2+} was also detected in all $CaWO_4$ samples. In some cases, the intensity of the Mn^{2+} signal was comparable to that of the vanadium.

3. Crystal Structure and Orientation

The structure of calcium tungstate (Scheelite) is characterized by the space group C_{4h}^6 or the tetragonal $I4_1/a$ with four molecules in the unit cell.[53] Recently, the dimensions of the tetragonal body

centered unit cell of this crystal were determined thoroughly by neutron[54] and X-ray[55] diffraction techniques. The results obtained by the two methods are in excellent concordance within experimental error. In our calculations of angles and distances, we have used the X-ray diffraction data given below.

Unit cell dimensions:

$$a = b = 5.243 \pm 0.002\text{Å}$$

$$c = 11.376 \pm 0.003\text{Å}$$

Oxygen coordinates, using a W atom as the origin:

$$x = (0.2415 \pm 0.0014)a$$

$$y = (0.1504 \pm 0.0013)a$$

$$z = (0.0861 \pm 0.0006)c$$

The site symmetry of both Ca and W is S_4. The structure of $CaWO_4$ may be viewed as composed of WO_4^{2-} anions ionically bonded to Ca^{2+} cations. The metallic sites are found on planes separated by a distance of c/4 from each other and perpendicular to the c-axis, as shown in Figure 3.2. The symmetry configuration of metal ion sites on planes at c/4 and 3c/4 are mirror images of those on the ab- or c/2 planes with respect to a (001) plane. The lines joining each metal ion with the nearest metal ions in the adjacent planes make an angle 42°, 40' with the c-axis.

Each tungsten ion in $CaWO_4$ crystal is bonded to four oxygens to form a slightly squashed tetrahedron with dimensions 2.11Å x 2.11Å x

1.90Å and W-O distance of 1.78Å. The diagonal plane of the tetrahedron makes an angle of 31°54' with the a-axis. The WO_4 tetrahedron and its projection on the ab-plane are shown in Figures 3.3 and 3.4.

The calcium atoms, on the other hand, are surrounded each by eight oxygens which form two distorted tetrahedra with Ca-O distances of 2.44Å and 2.48Å. These tetrahedra and their projections on the ab-plane are shown in Figures 3.5, 3.6, and 3.7.

Crystal orientation and alignment were made by X-rays. To place the samples in the resonator cavity, they were glued to the end of thin wall quartz tubings.

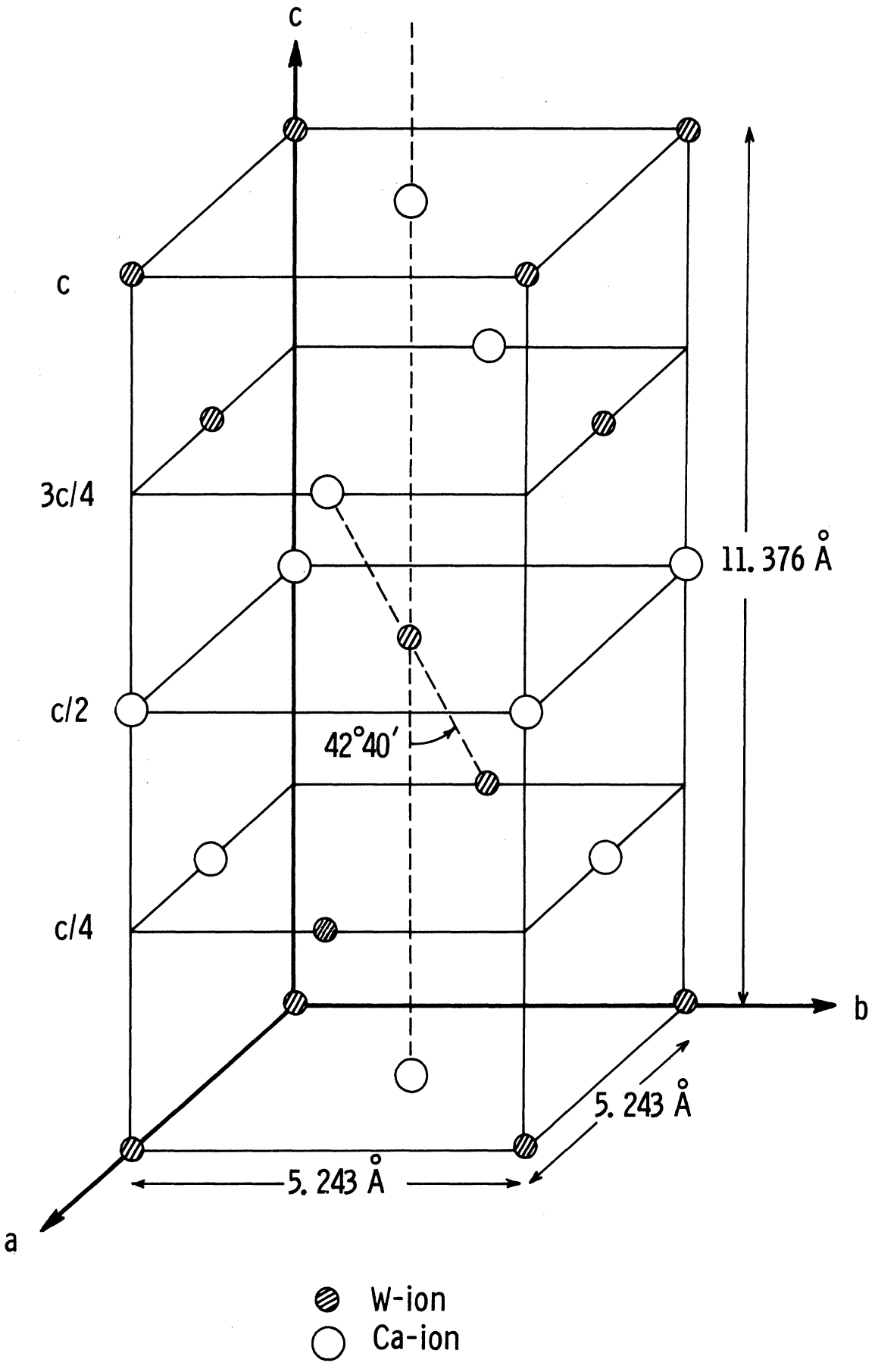

Fig. 3.2. Metal ions in $CaWO_4$ unit cell.

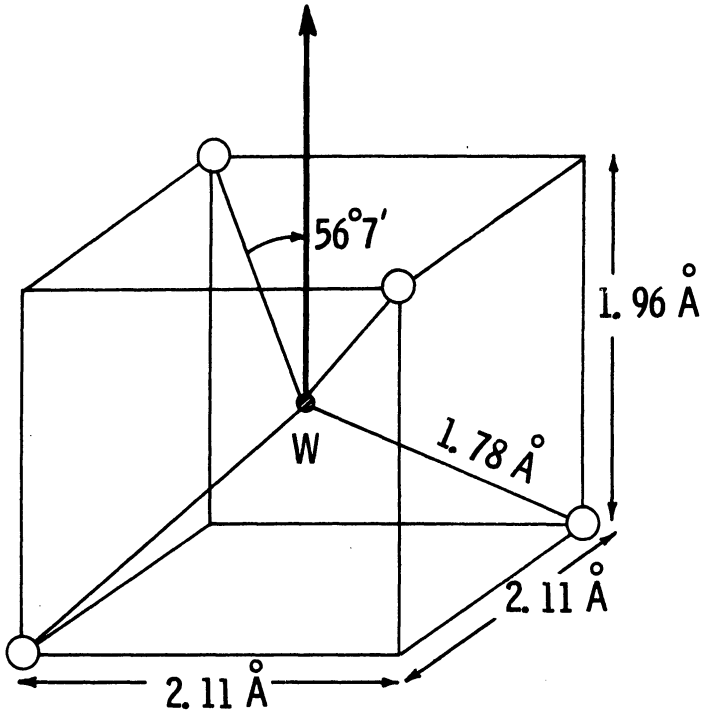

Fig. 3.3. $(WO_4)^{2-}$ tetrahedron.

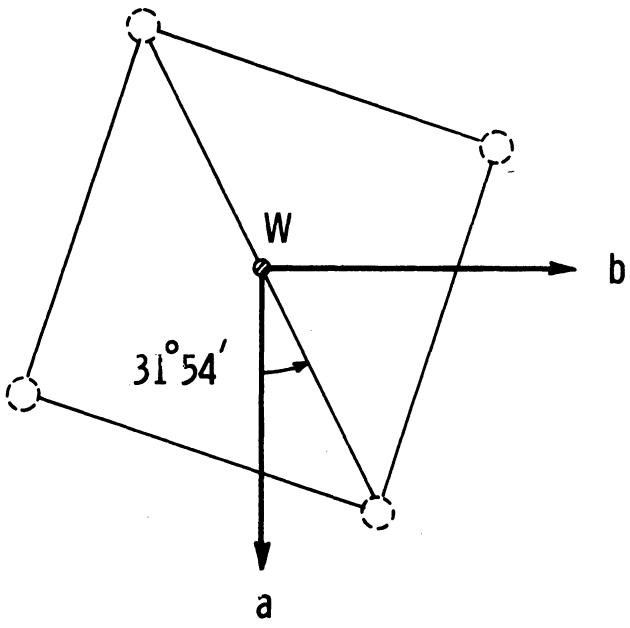

Fig. 3.4. Projection of $(WO_4)^{2-}$ tetrahedron on the ab-plane.

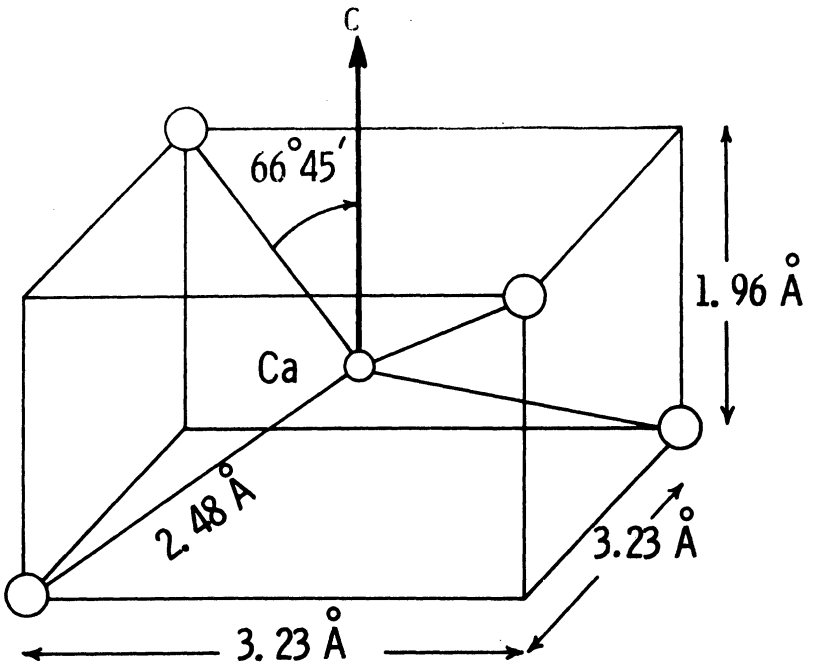

Fig. 3.5. (Ca, O) "long bond" tetrahedron.

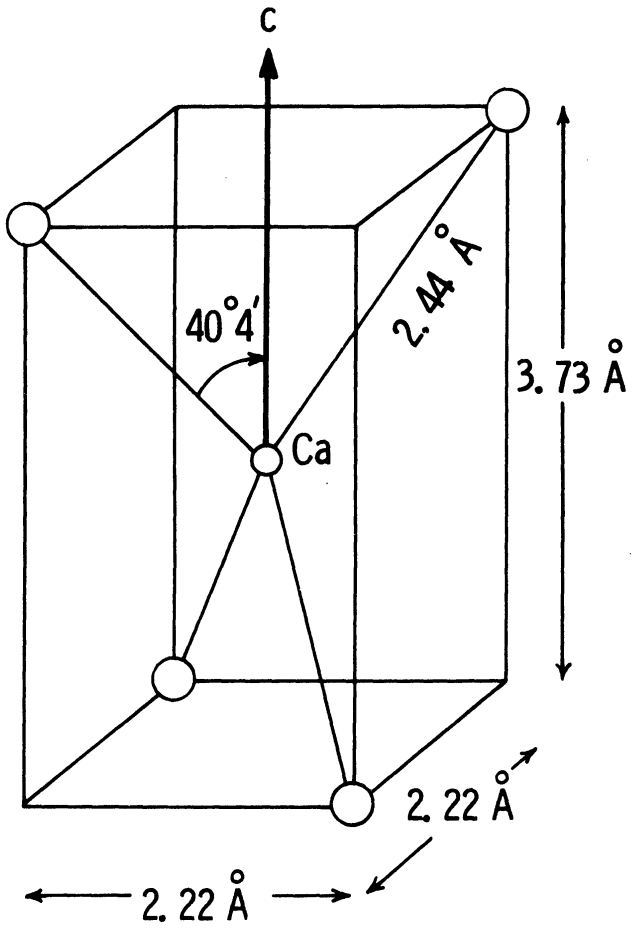

Fig. 3.6. (Ca, O) "short bond" tetrahedron.

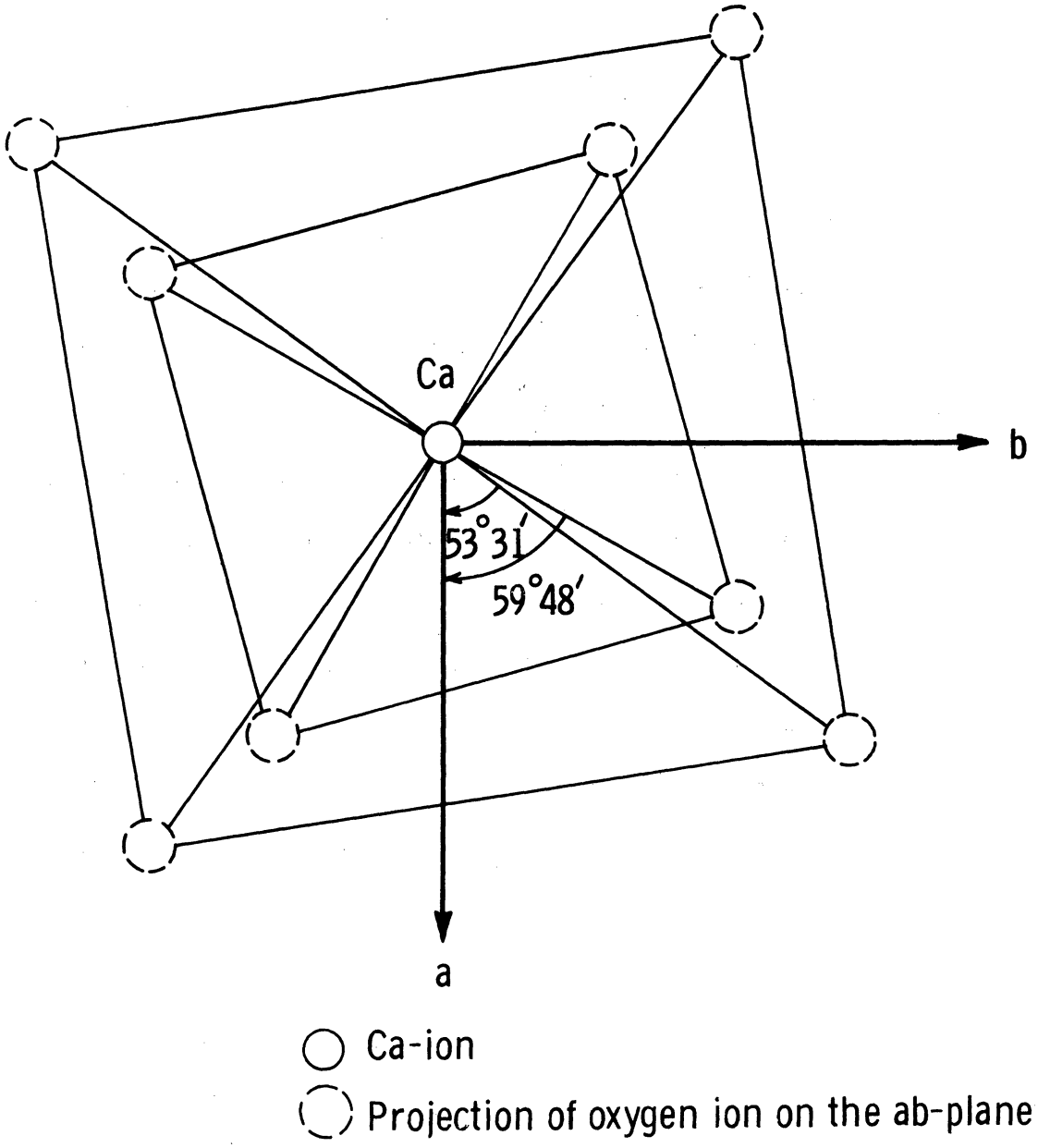

Fig. 3.7. Projection of the (Ca, O) double-tetrahedron on the ab-plane.

CHAPTER IV

EXPERIMENTAL RESULTS

Electron spin resonance absorption spectra of vanadium-doped $CaWO_4$ single crystals, with or without the rare-earth dopant Tb or Nd, were studied at microwave frequencies of about 9.5 Gc/sec ($\lambda \cong 3$cm). Concentrations of the additives are shown in Table 3.1.

The only spectra observed, before X-irradiation, were those of Tb^{3+} or Nd^{3+} (seen only at 4.2°K) and the unintended Mn^{2+} impurity. After the irradiation, new groups of lines were detected at liquid air (77°K) and liquid helium (4.2°K) temperatures. The resonant magnetic fields were in the range of about 3-4 kilogauss corresponding to a spectroscopic g-factor in the vicinity of 2. The additional absorption spectrum consisted, essentially, of sets of 8 lines, of almost equal separations and intensities, thus suggesting a hyperfine structure of $(2I + 1)$ with $I \cong 7/2$. Since, besides vanadium, cobalt has also a nuclear spin of 7/2, a sample doped with this element was examined but the additional lines failed to show. Hence, the new spectra were attributed to vanadium.

In general, the position of the spectral lines showed a dependence upon the direction of the applied static magnetic field with respect to the crystal axes. From the angular dependence, we have

classified the vanadium spectra in three groups which will be referred to as the Groups A, B, and C. The intensities of the three groups are in the ratio of 100 : 5 : 70, respectively.

The Group A, sharper than the other two, was seen in the spectra of all samples. At 77°K, it consists of 8 isotropic lines, separated by about 20 gauss with a positive Δ g (Figures 4.1, 4.2). At 4.2°K, and for a general direction of the magnetic field, each line of the Group A splits into 4 lines as we shall see later. The Group B lines were observed only in the spectra of the samples which contained, in addition to vanadium, either Tb or Nd as shown in Figure 4.1. They are characterized by an isotropic hyperfine separation (HFS) of about 10 gauss and an axial g-tensor with positive Δ g. The Group C was seen in the spectra of $CaWO_4$ crystals which contained only vanadium or an excess of vanadium over neodymium. This group has a large HFS varying from about 36 to 176 gauss and an anisotropic g with negative Δ g (Figures 4.2 and 4.3).

1. Group A Spectra

At liquid air temperature, this group consists of 8 lines with an isotropic g = 2.0245 + 0.0005. The hyperfine coupling constant A, however, was found to be slightly anisotropic:

$$A_{\parallel} = A = 19.1 \pm 0.2 \text{ gauss} = (18.2 \pm 0.2) \times 10^{-4} \text{ cm}^{-1}$$

$$A_{\perp} = B = 20.3 \pm 0.2 \text{ gauss} = (19.0 \pm 0.2) \times 10^{-4} \text{ cm}^{-1}$$

where $A_{\parallel}$ was measured along the c-axis. The experimental data at 77°K can be described by the spin Hamiltonian (see Appendix A),

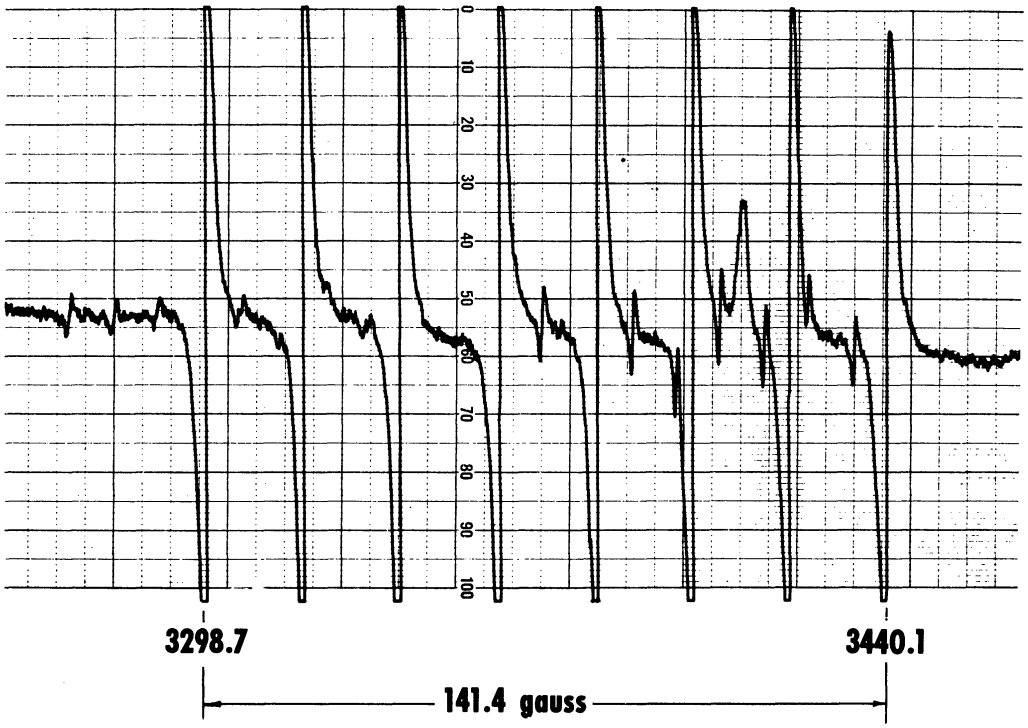

A. H IN THE ab-PLANE

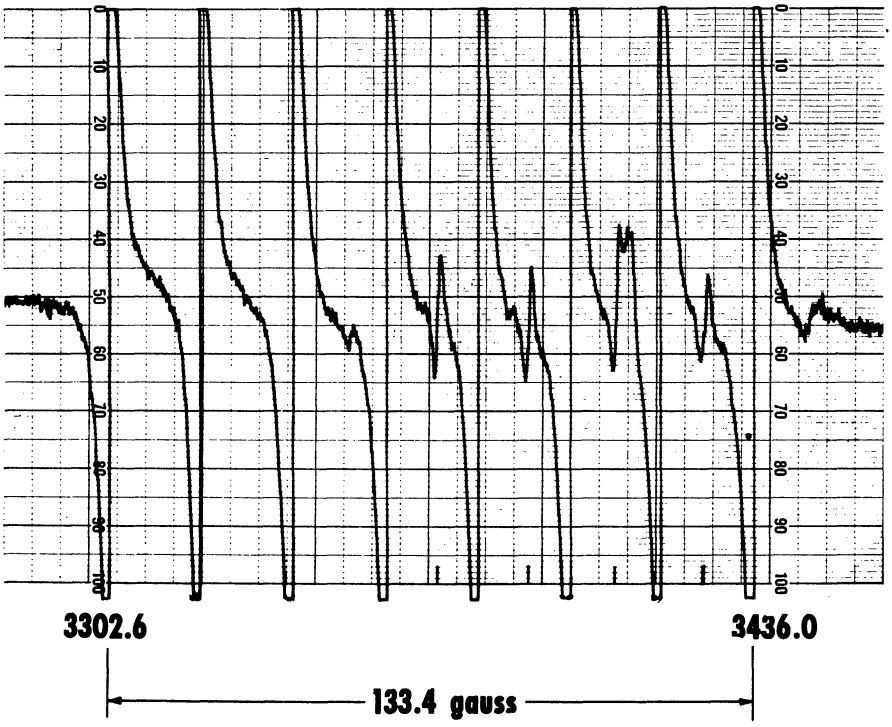

B. H PARALLEL TO c-AXIS

Fig. 4.1. ESR spectra of X-irradiated $CaWO_4$:V, Tb (0.13%, 0.3%) at 77°K.

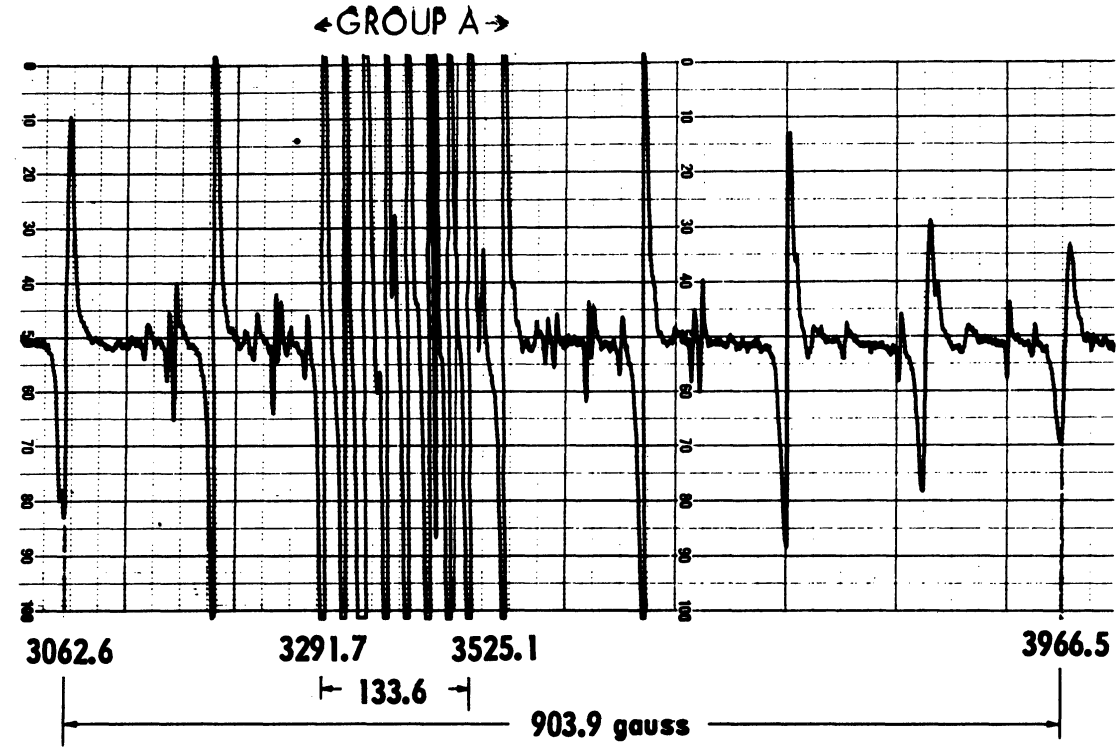

A. H PARALLEL TO c-AXIS

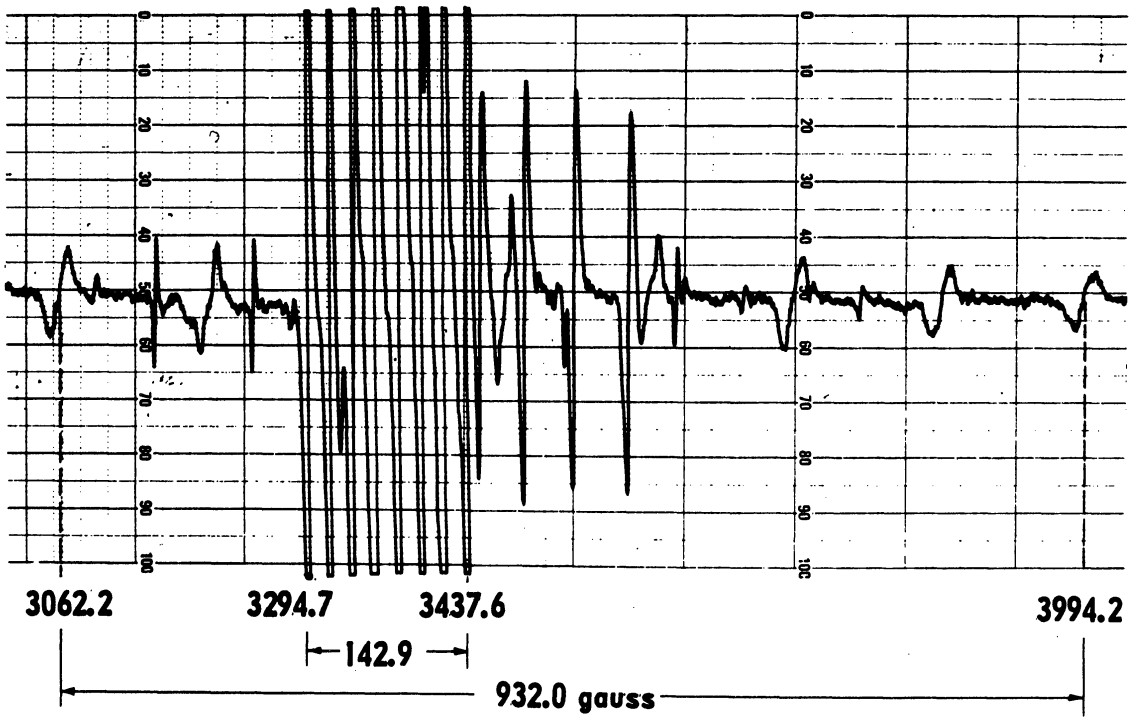

B. H PARALLEL TO a-AXIS

Fig. 4.2. ESR spectra of X-irradiated $CaWO_4$:V (0.05%) at 77°K. H ∥ a-axis and H ∥ c-axis.

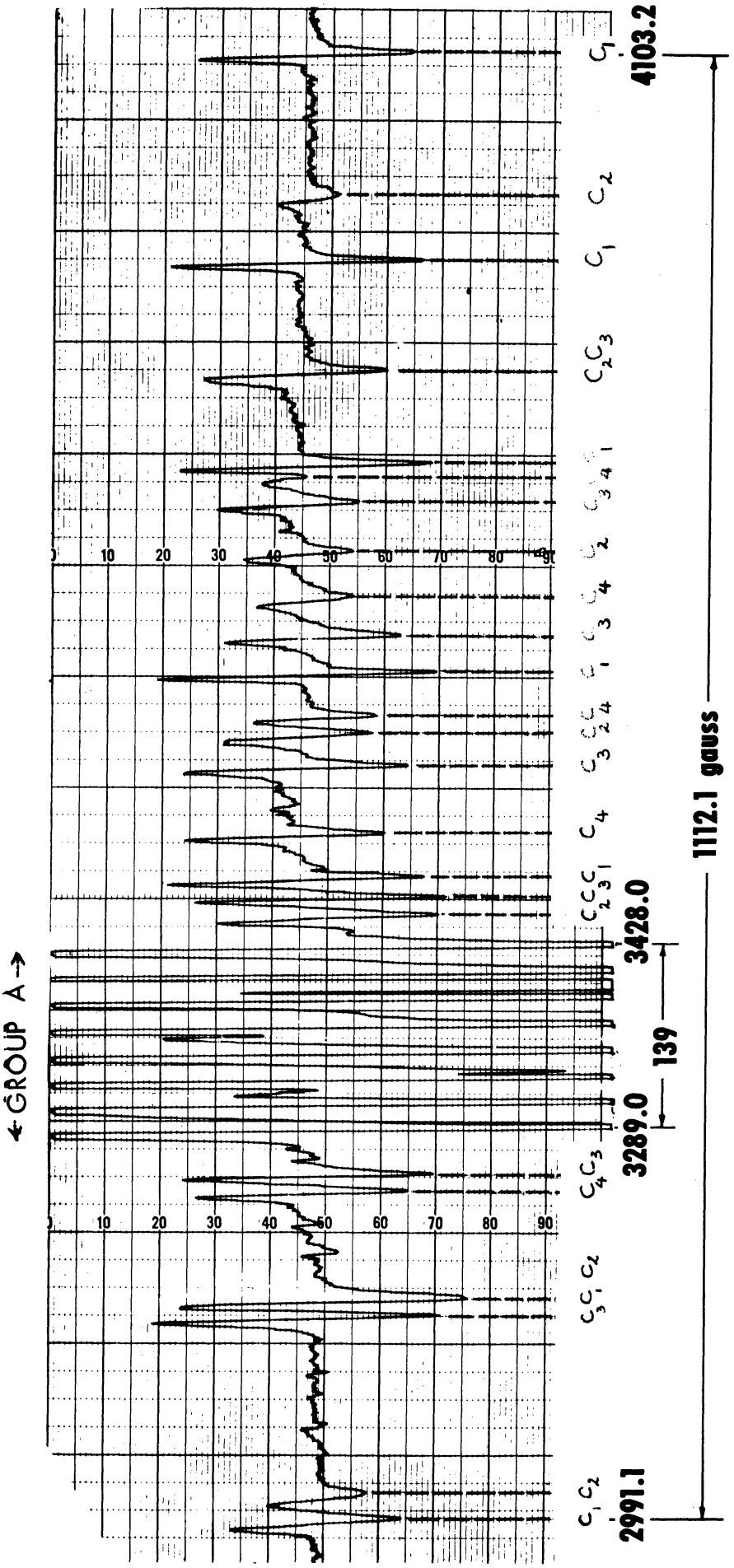

Fig. 4.3. ESR spectrum of X-irradiated $CaWO_4$:V (0.05%) at 77 °K. H is an arbitrary direction.

$$\mathcal{H}_s = g\beta\, \underline{H}\cdot\underline{S} + A S_z I_z + B(S_x I_x + S_y I_y) \tag{4.1}$$

with S = 1/2 and I = 7/2. The position of the resonant magnetic field for transitions ($M \rightarrow M-1$, Δ m = 0), obtained from (4.1), is

$$H(\theta,m) = H_0 - \frac{K}{g\beta} m - \left(\frac{B}{g\beta}\right)^2 \frac{1}{4H_0}\left[\frac{A^2+K^2}{K^2}\right]\left(\frac{63}{4} - m^2\right)$$
$$- \frac{m^2}{2(g\beta)^2 H_0}\left(\frac{A^2-B^2}{K}\right)\sin^2\theta\cos^2\theta \tag{4.2}$$

where,

β = Bohr magneton

m = nuclear magnetic quantum number

M = electron spin quantum number

$H_0 = h\nu/g\beta$, $h\nu$ = microwave photon energy

$K^2 = A^2\cos^2\theta + B^2\sin^2\theta$

and θ is the angle of the applied magnetic field with the symmetry axis, in our case the c-axis. For H $\|$ c-axis, θ = 0 and we have,

$$H(0,m) = H_0 - \frac{A}{g\beta} m - \frac{B^2}{2(g\beta)^2 H_0}\left[\frac{63}{4} - m^2\right] \tag{4.3}$$

and in the ab-plane,

$$H(\pi/2,m) = H_0 - \frac{B}{g\beta} m - \frac{A^2+B^2}{4(g\beta)^2 H_0}\left[\frac{63}{4} - m^2\right] \tag{4.4}$$

TABLE 4.1

CALCULATED AND MEASURED VALUES OF THE RESONANT MAGNETIC FIELD FOR THE GROUP A. T = 77 °K, H PARALLEL TO THE c-AXIS

m	Resonant Magnetic Field (Gauss)	
	Measured	Calculated
- 7/2	3430.3 ± 0.5	3430.2
- 5/2	3410.8	3410.8
- 3/2	3391.6	3391.4
- 1/2	3372.5	3372.2
+ 1/2	3353.5	3353.1
+ 3/2	3334.0	3334.1
+ 5/2	3315.7	3315.3
+ 7/2	3296.8	3296.5

Table 4.1 shows a comparison between the measured and calculated values of the resonant magnetic field when $\underline{H}$ is parallel to the c-axis.

The line width was found to depend on the direction of $\underline{H}$. This angular dependence was more pronounced for the RE-compensated samples as shown in Figure 4.4.

At liquid helium temperature, the Group A splits, in general, into four sets each of which consists of 8 lines with positive $\triangle$ g and hyperfine separations of about 20 gauss. They coalesce into two sets in the ab-plane and into one when $\underline{H}$ is parallel to the c-axis. Figure 4.5 shows the low-temperature splitting of this group. These sets largely superpose each other for all orientations of $\underline{H}$: the maximum separation between the centers of the lowest and the highest lying sets in the ab-plane spectrum is only about 40 gauss, whereas the total separation between the first and the last lines of each set is about 140 gauss. The measurements of g and A in different planes indicated that the maximum values of these tensors occurred when $\underline{H}$ was in the direction given by the polar coordinates

$$\theta = 60° \pm 3 \quad , \qquad \varphi = 30° \pm 2$$

$$g_{max} = 2.044 \pm 0.005$$

$$A_{max} = 21.3 \pm 0.5 \text{ gauss}$$

This is, within the experimental error, the same as the direction of the W-O bond in calcium tungstate (see Figures 3.3 and 3.4). The g- and A-values along the three crystal axes are

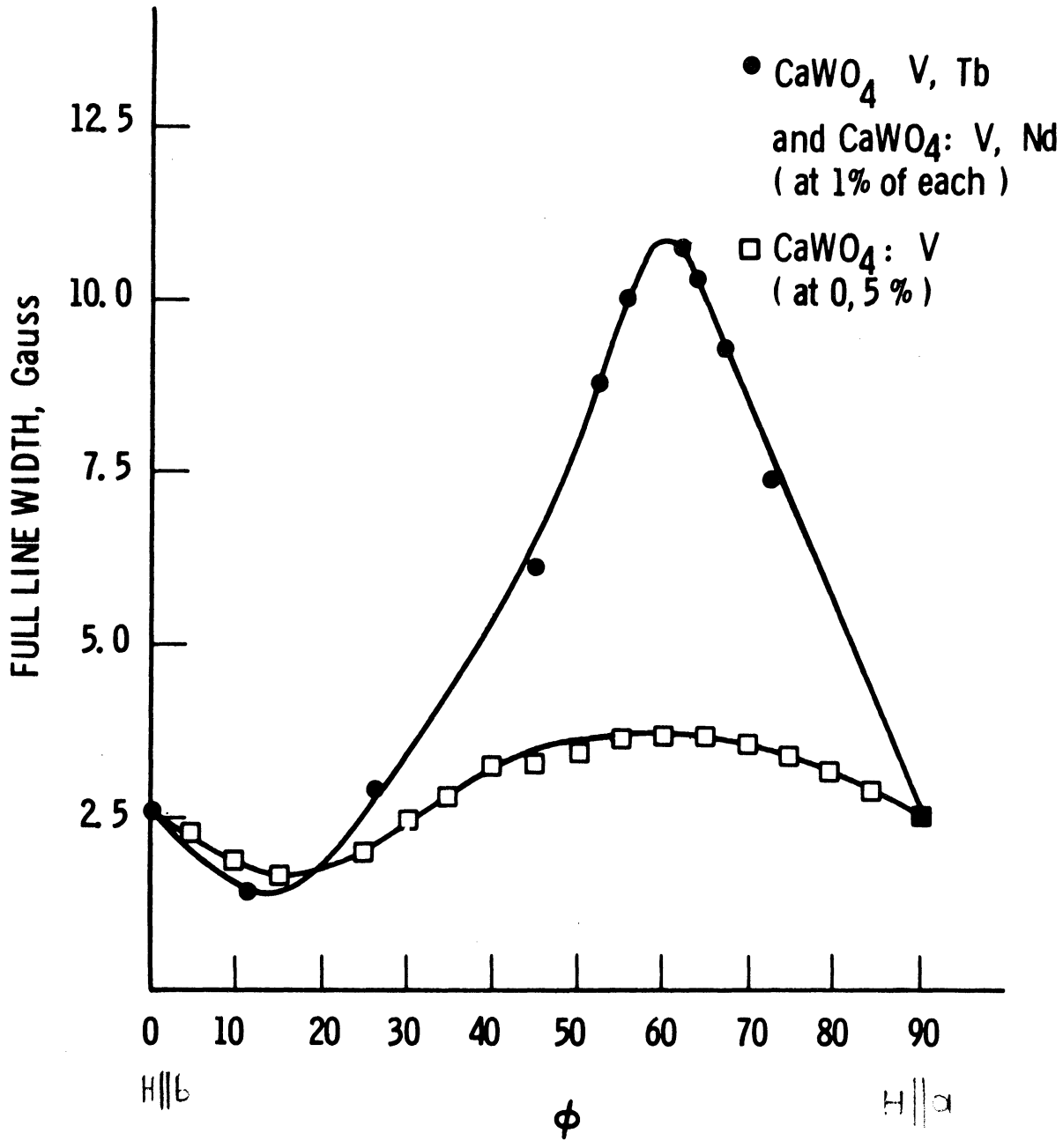

Fig. 4.4. Angular variation of the line width of the Group A spectra in the ab-plane at 77°K.

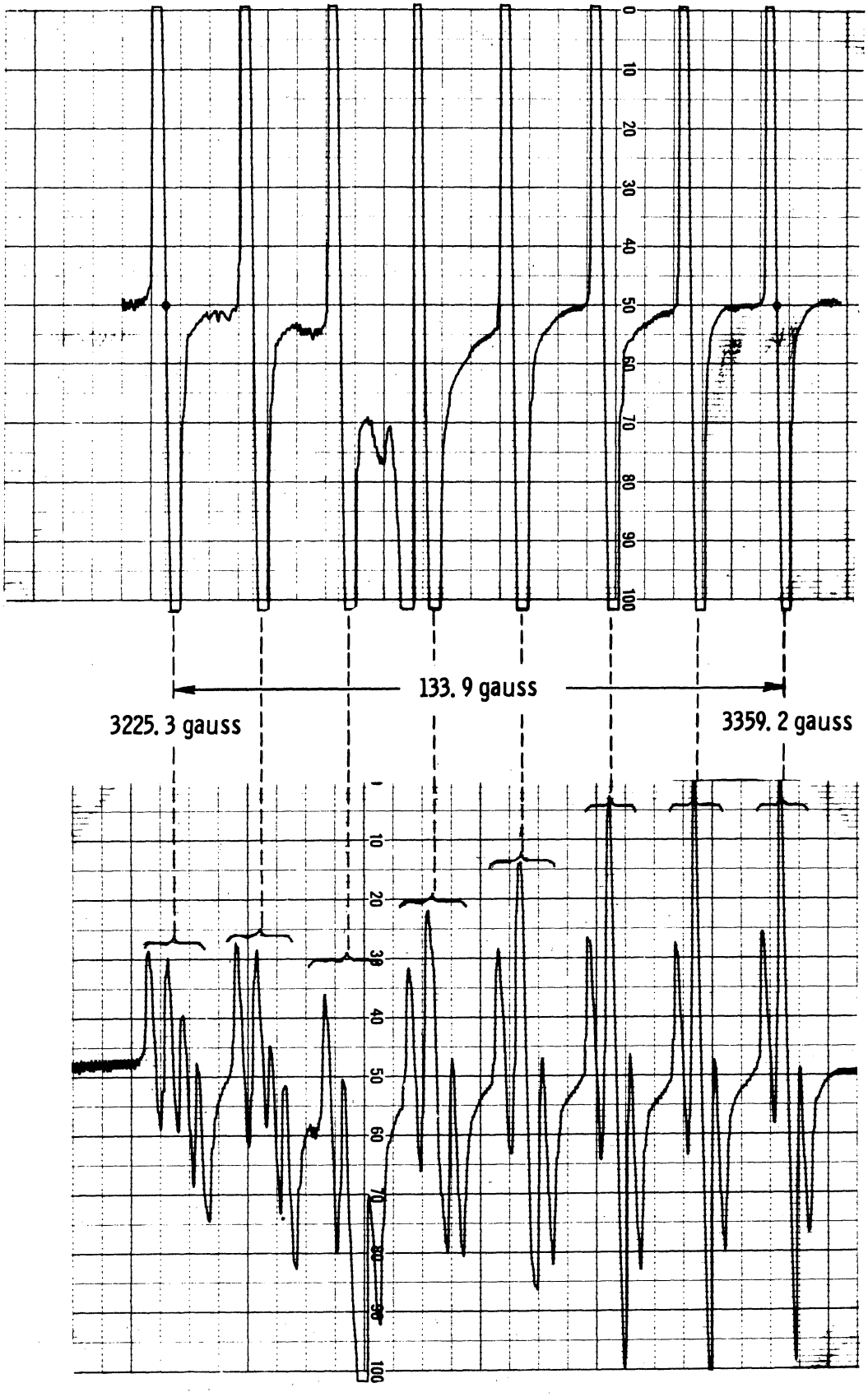

Fig. 4.5. Group A lines at 77°K (top) and at 4.2°K (bottom).

	a	b	c
g	2.033	2.017	2.024
A(gauss)	21.2	19.7	19.1

The angular dependence of the g-factor in the ab-plane and in the plane defined by the c-axis and the azimuthal angle $\phi = 30°$ is shown in Figures 4.6 and 4.7, respectively.

It was found that the average position (defined by <g> and <A>) of the four sets, which emerge from the Group A at 4.2°K, was the same as the position of this group at 77°K. This is shown in Table 4.2 for H in the ab-plane. In this plane, as we have seen, the four low-temperature sets reduce to two. Subscripts 1 and 2 are used to designate g- and A-values of these sets. We notice, in this table, that

$$\langle g \rangle_{4.2°K} = 2.025 \pm 0.001$$

$$\langle A \rangle_{4.2°K} = 20.3 \pm 0.1 \quad \text{gauss}$$

which agree well with the values found at 77°K.

2. Group B Spectra

At 77°K, this group is composed, in general, of two sets of 8 lines which collapse to one when H is parallel to the c-axis. The relative positions of the Groups A, B, and the DPPH absorption line are shown in Figure 4.8.

The angle dependence of the g-factor for the two sets in the ab-plane were the same except for a 90° phase difference as shown in

TABLE 4.2

AVERAGE VALUES OF g AND A OF THE TWO SETS EMERGING FROM THE GROUP A AT 4.2°K IN THE ab-PLANE
Φ IS MEASURED FROM THE a-AXIS

Φ	g_1	g_2	$\langle g \rangle \equiv (g_1+g_2)/2$	A_1	A_2	$\langle A \rangle \equiv (A_1+A_2)/2$
0	2.007	2.033	2.025	19.7	21	20.3
10	2.04	-	-	19.9	-	-
20	2.012	2.039	2.025	20.0	20.7	20.4
25	2.011	2.039	2.025	20.0	20.7	20.4
30	2.011	2.039	2.025	20.1	20.6	20.4
40	2.012	2.038	2.025	20.3	20.5	20.4
50	2.012	2.036	2.024	20.2	20.2	20.2
60	2.018	2.030	2.024	20.4	20.0	20.2
70	2.024	2.026	2.025	20.9	19.8	20.3
80	2.029	2.022	2.025	21.0	19.8	20.4
90	2.033	2.017	2.025	21.2	19.7	20.5

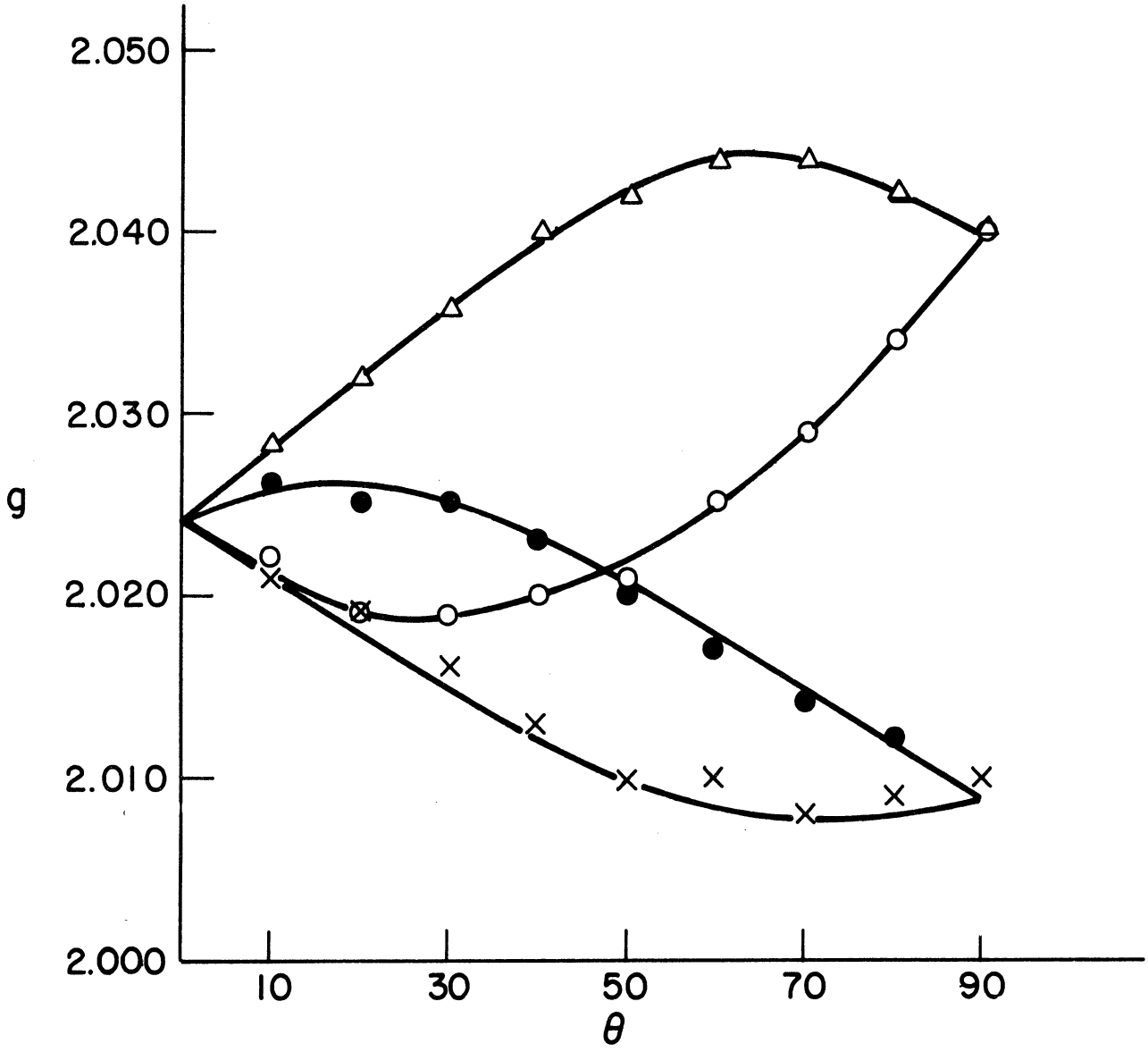

Fig. 4.6. Angular variation of the Group A g-value at 4.2°K. $\underline{H}$ varies in a plane containing the c-axis and making $\theta = 30°$ with the ac-plane.

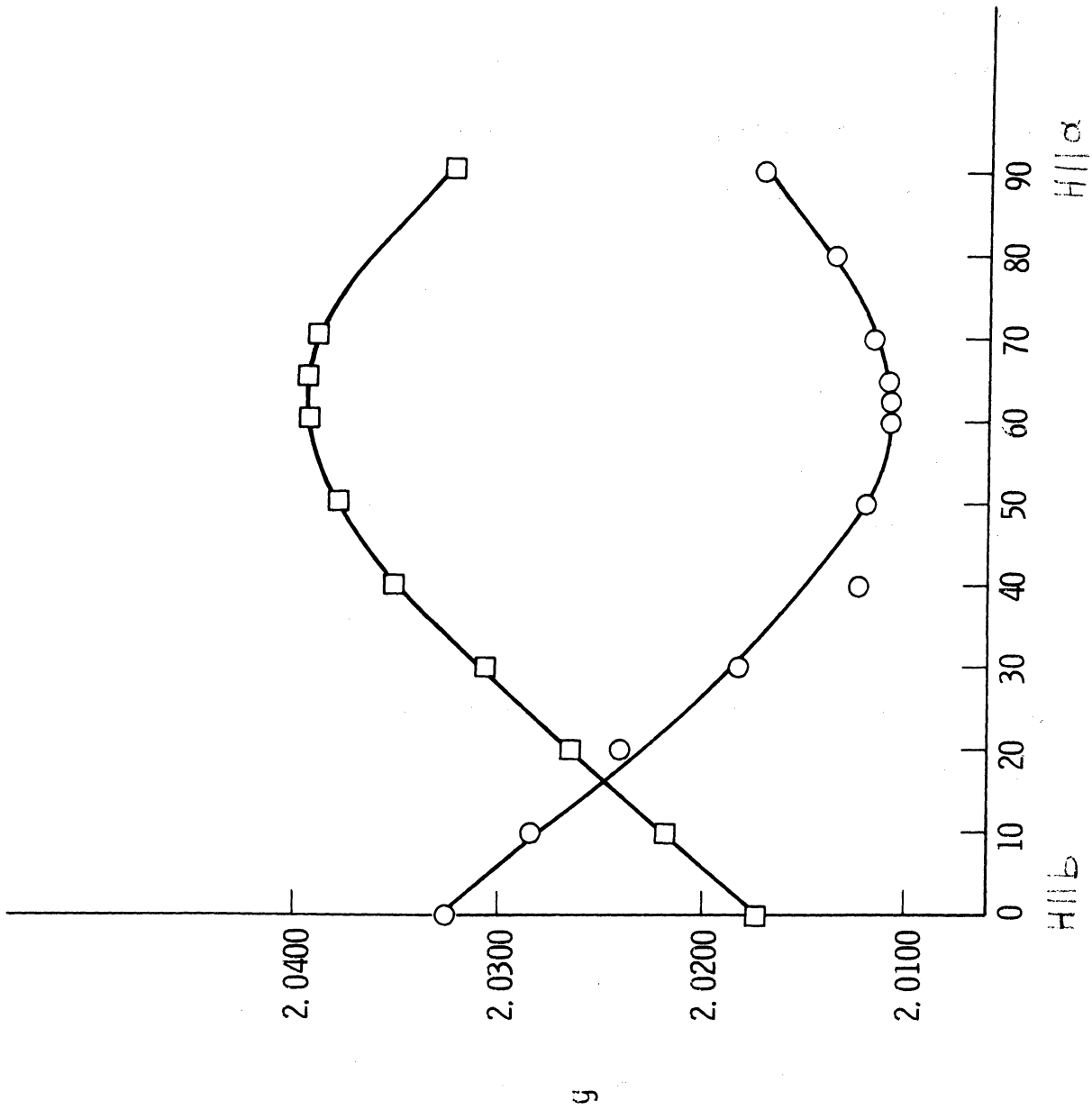

Fig. 4.7. Angular variation of the Group A g-value at 4.2°K. H varies in the ab-plane.

Figure 4.9. The g-value remained unchanged in the planes which contain the c-axis and make an angle $\phi_1 = -10°$ or $\phi_2 = 80°$ with the a-axis (Figure 4.10). This suggested that the g-tensors for the two sites possessed axial symmetry. The symmetry axes are given by the polar coordinates ($\theta_1 = 90°$, $\phi_1 = -10°$) and ($\theta_2 = 90°$, $\phi_2 = 80°$). The principal values for the g-tensors are,

$$g_{\parallel} = 2.068 \pm 0.001$$

$$g_{\perp} = 2.004 \pm 0.001$$

The hyperfine separation was found to be isotropic within experimental error. Its value is

$$A_{\parallel} = A_{\perp} = 9.1 \pm 0.2 \text{ gauss}$$

Hence, the experimental data can be described by an axial spin Hamiltonian with,

$$A_x = A_y = A_z = A$$

Thus,

$$\mathcal{H}_s = \beta\left[g_{\parallel} H_z S_z + g_{\perp}(H_x S_x + H_y S_y)\right] + A\,\underline{I}\cdot\underline{S} \qquad (4.5)$$

with an effective spin S = 1/2 and nuclear spin I = 7/2. The position of the resonance absorption lines, obtained from (4.5), is given by

$$H = H_0 - Am - \frac{A^2}{2H_0(g\beta)^2}\left(\frac{63}{4} - m^2\right) \qquad (4.6)$$

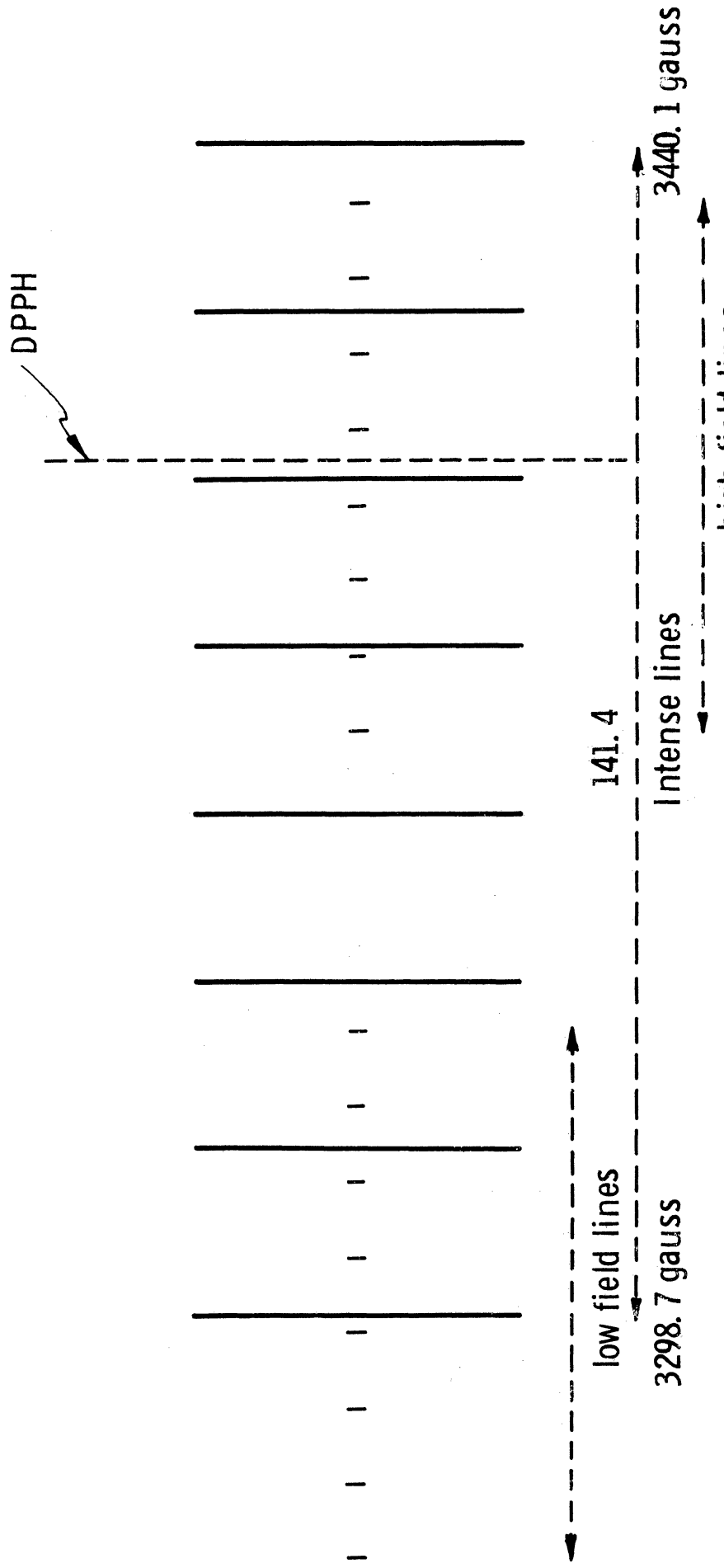

Fig. 4.8. Relative position of the Group A, B, and the DPPH line at 77°K.

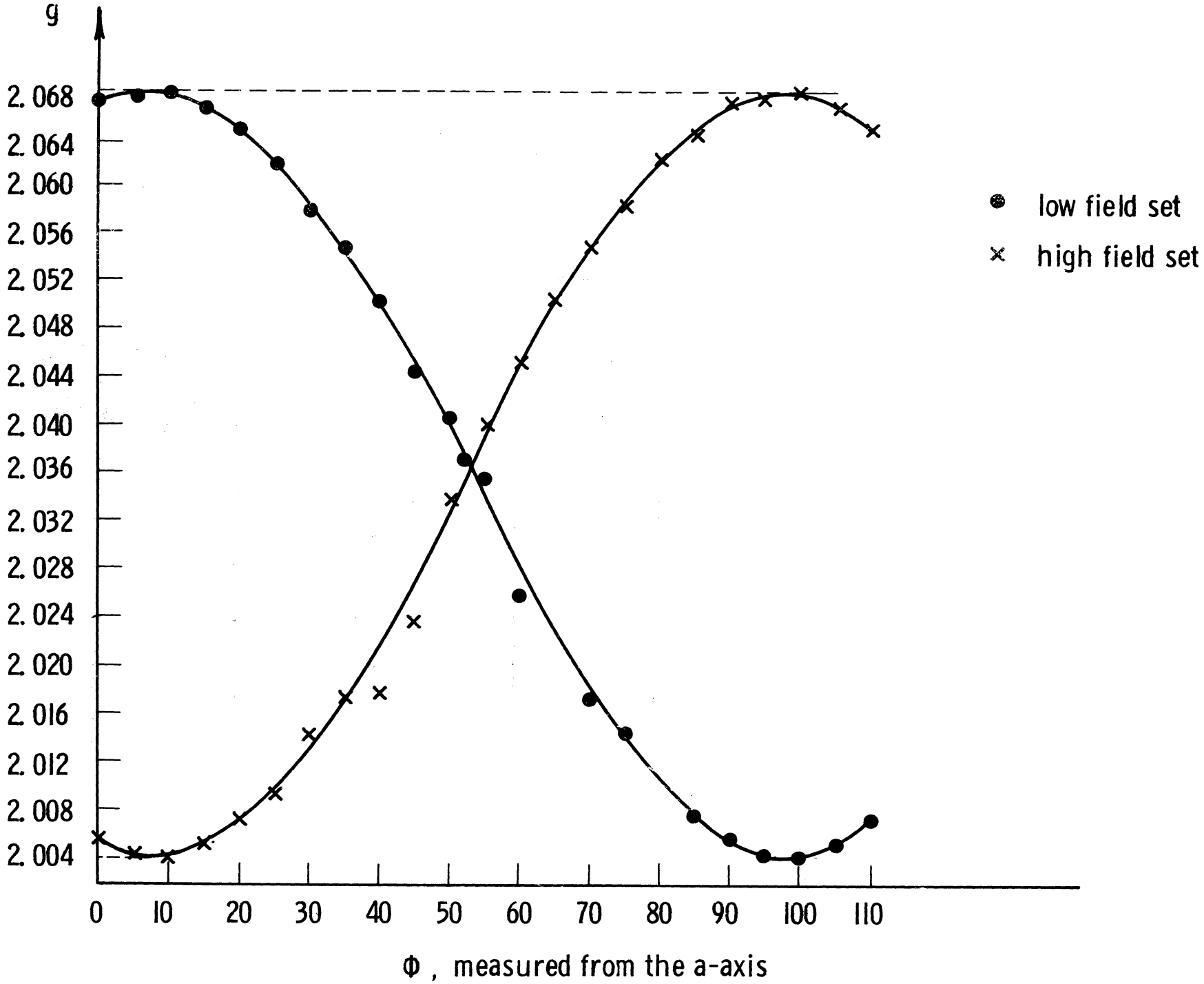

Fig. 4.9. Angular variation of the g-value for the Group B lines of CaWO$_4$:V^{4+},Tb in the ab-plane at 77°K

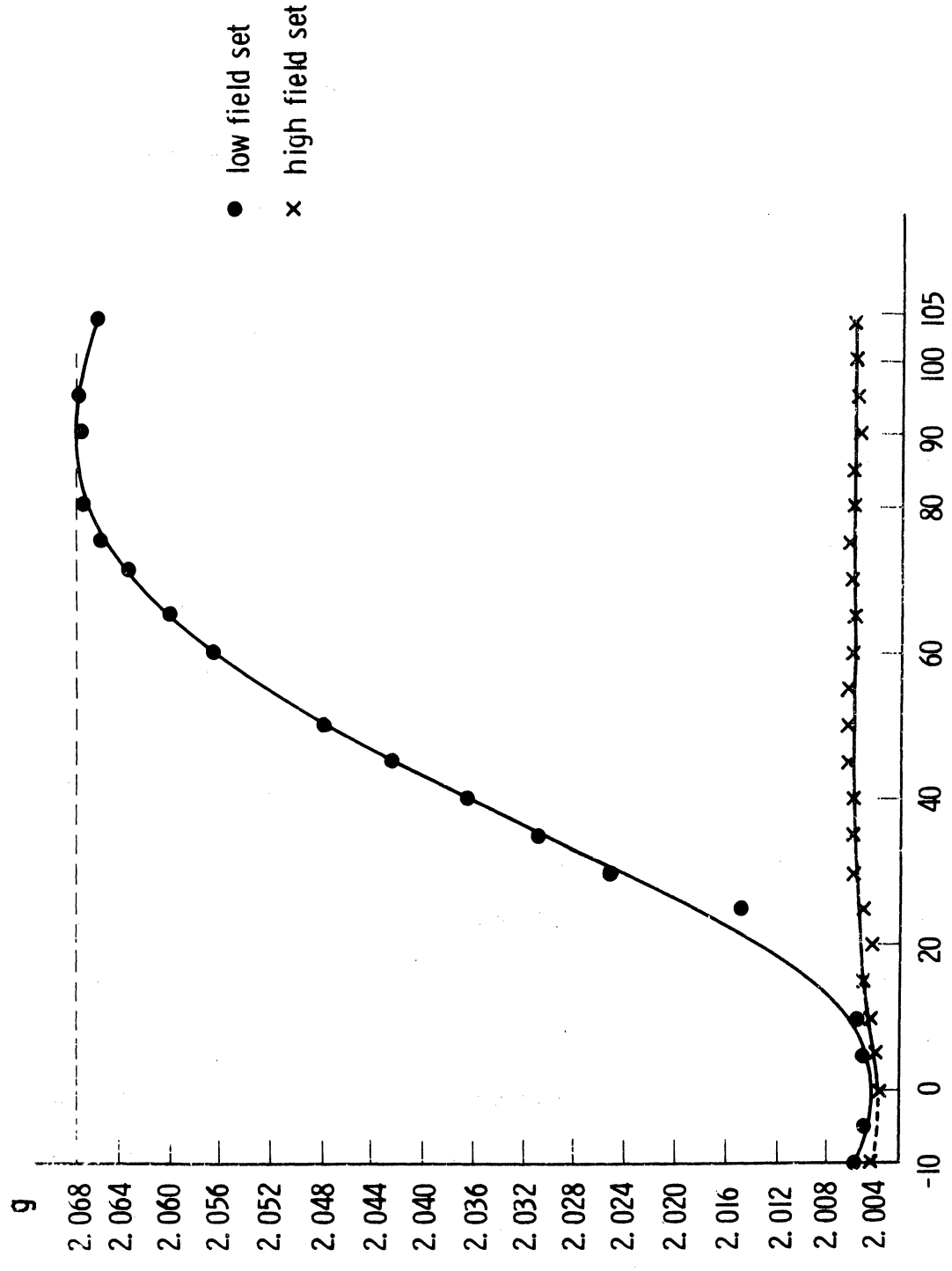

Fig. 4.10. Angular variation of the g-value for the Group B lines of $CaWO_4$:V, Tb at 77°K. $\underline{H}$ varies in a plane containing the c-axis and one of the g-tensor's principal axes.

where, $H_0 \equiv h\nu / g\beta$, and

$$g^2 = g_{\parallel}^2 \cos^2\theta + g_{\perp}^2 \sin^2\theta \qquad (4.7)$$

where θ is the angle of the static magnetic field with the symmetry axis. Figure 4.11 shows that the angular variation of the g-value measured in the ab-plane are in good agreement, within the experimental error, with the values calculated from (4.7).

At 4.2°, the spectra of the B and C groups showed some line broadening and deformation due to power saturation. This made the identification of the low-intensity Group B very difficult.

3. Group C Spectra

The spectrum at 4.2° was similar to that at 77° except for the above-mentioned saturation effect at the lower temperature. All the measurements were made at 77°K.

The Group C, in general, consists of four sets of 8 lines which unite to two sets of the ab-plane and to one when H is parallel to the c-axis as shown in Figures 4.2 and 4.3. The spectrum, arising from four non-equivalent sites, is characterized by anisotropic g- and A-values, with a negative Δ g and a relatively large HFS varying from about 36 to 176 gauss. Figures 4.12 through 4.15 show the angular variation of g- and A-values in the ab- and ac-planes. The two tensors have rhombic symmetry with only one coinciding principal axes chosen as the z-axis; x- and y-axes of the g-tensor seem to be rotated by about 30° in the counter clockwise direction with respect to the corresponding axes of

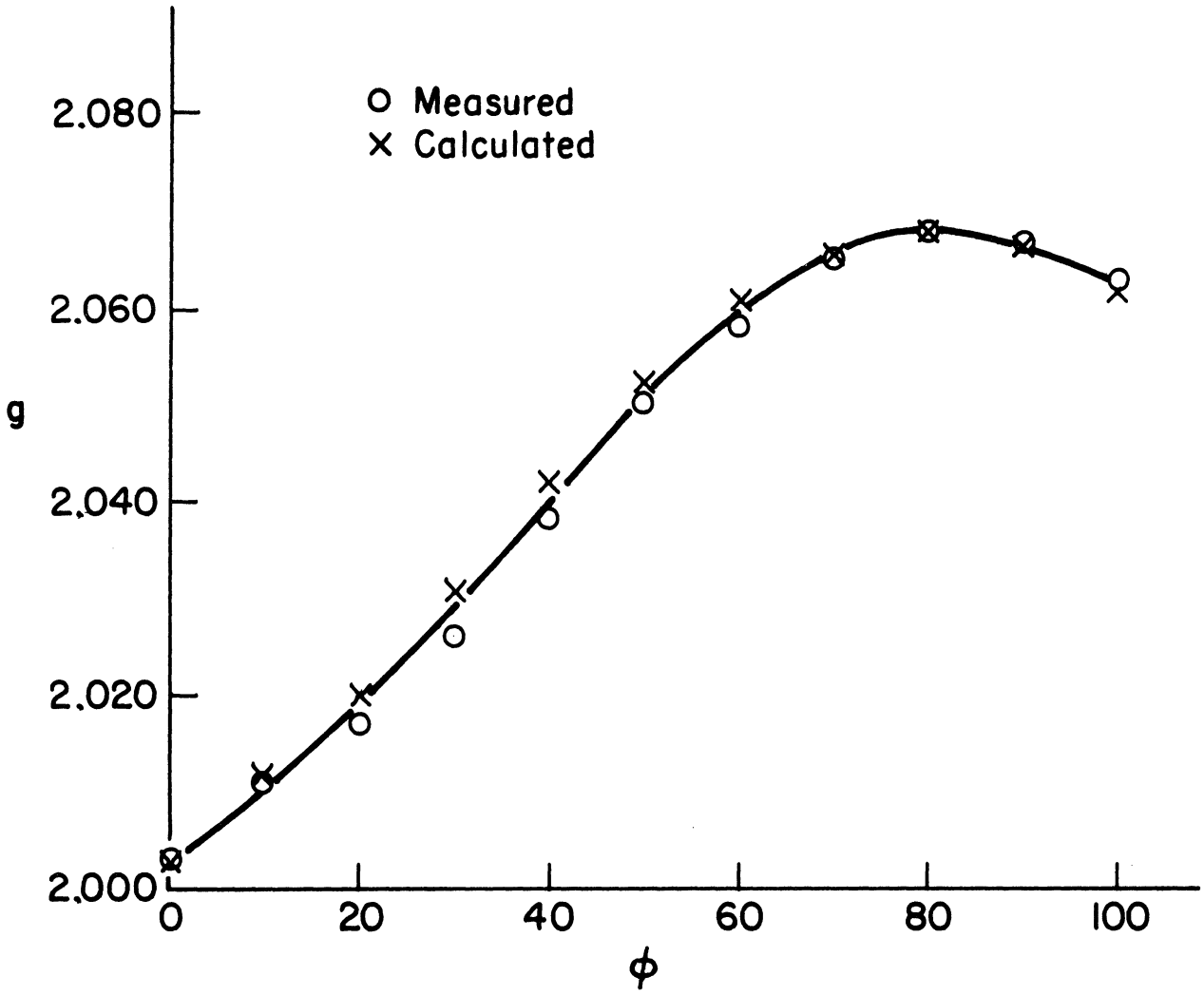

Fig. 4.11. Calculated versus measured g-values of the Group B in the ab-plane at 77°K.

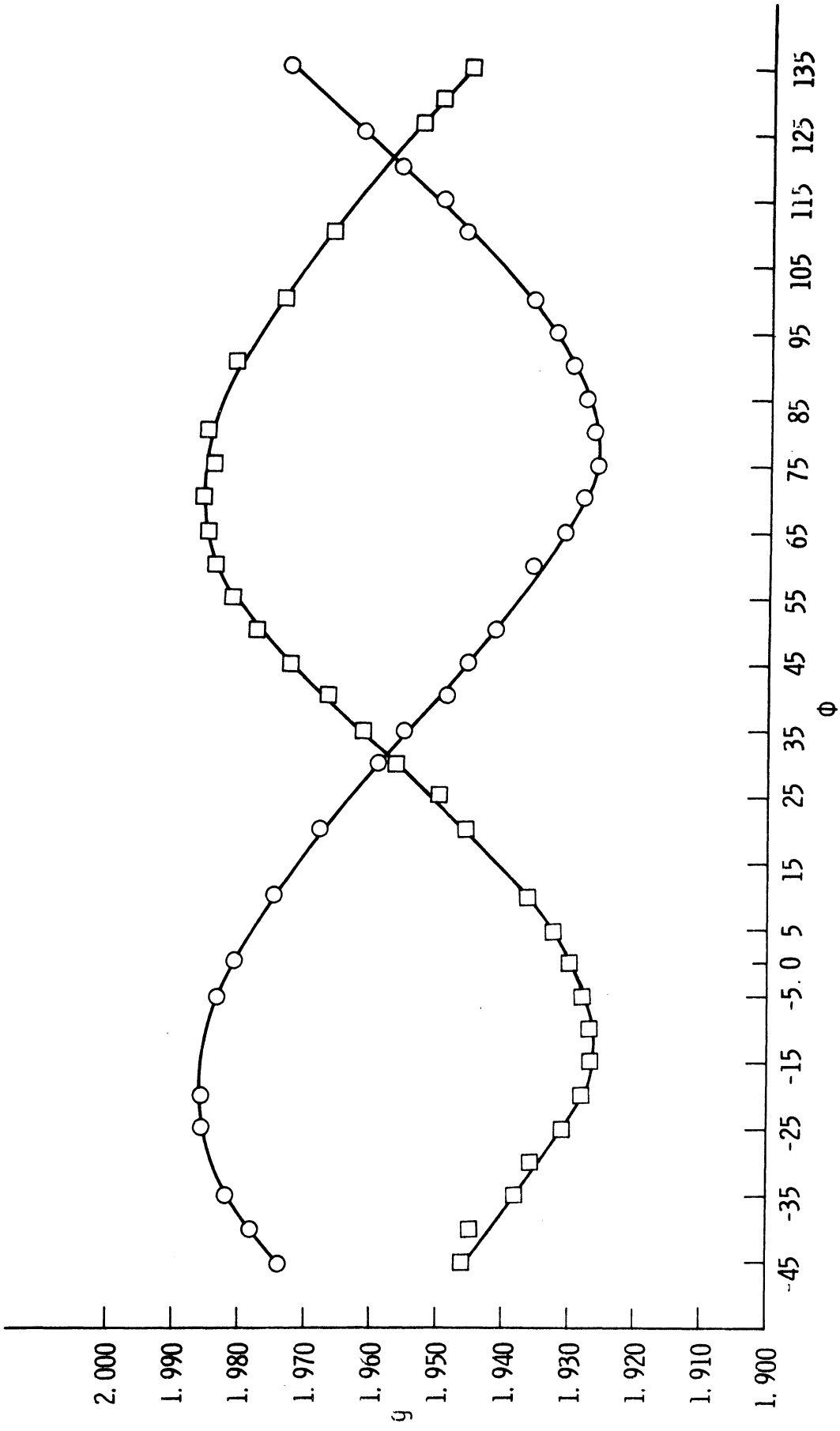

Fig. 4.12. Angular variation of the g-value for the Group C in the ab-plane at 77°K.

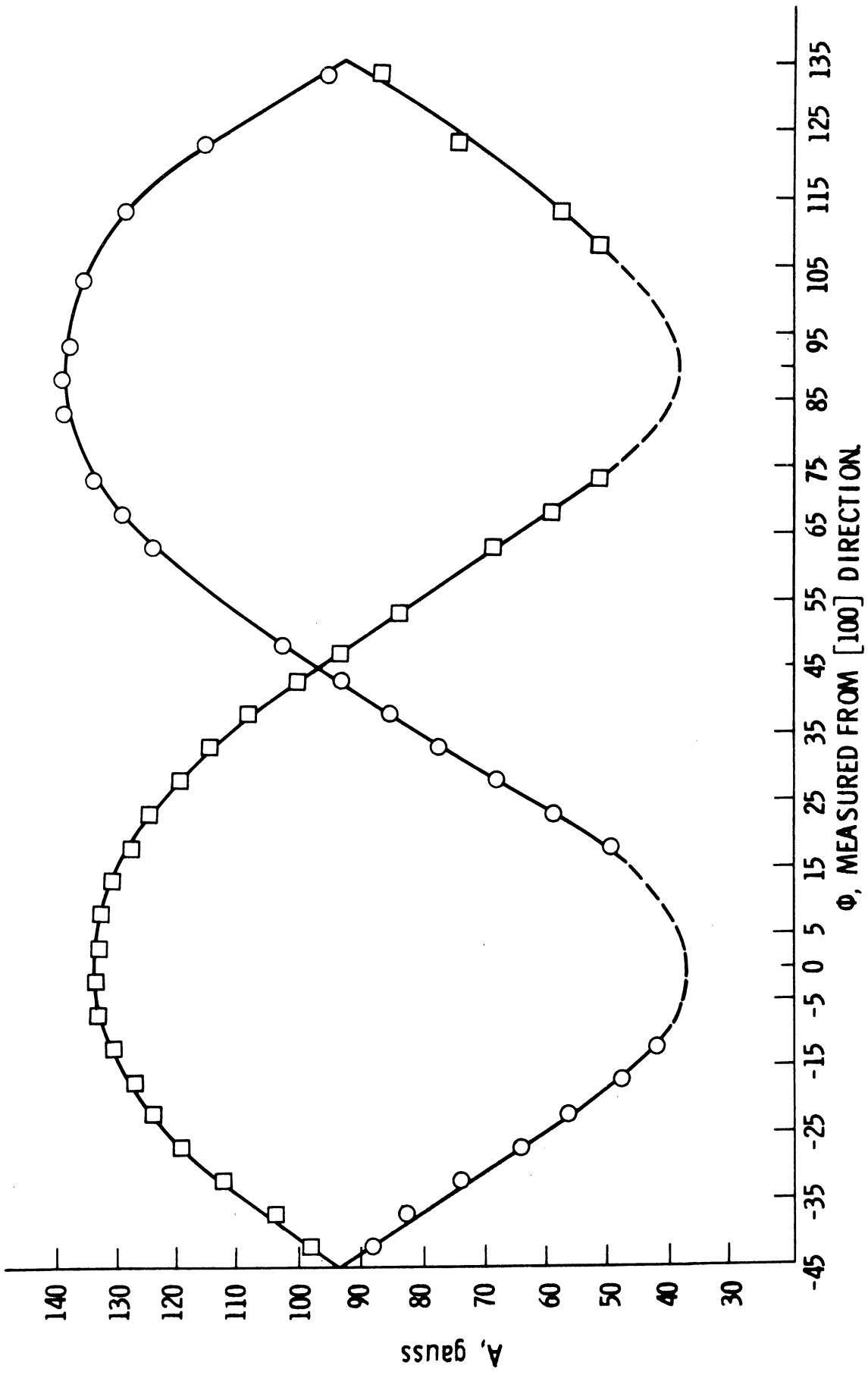

Fig. 4.13. Angular variation of the HFS for the Group C in the ab-plane at 77°K.

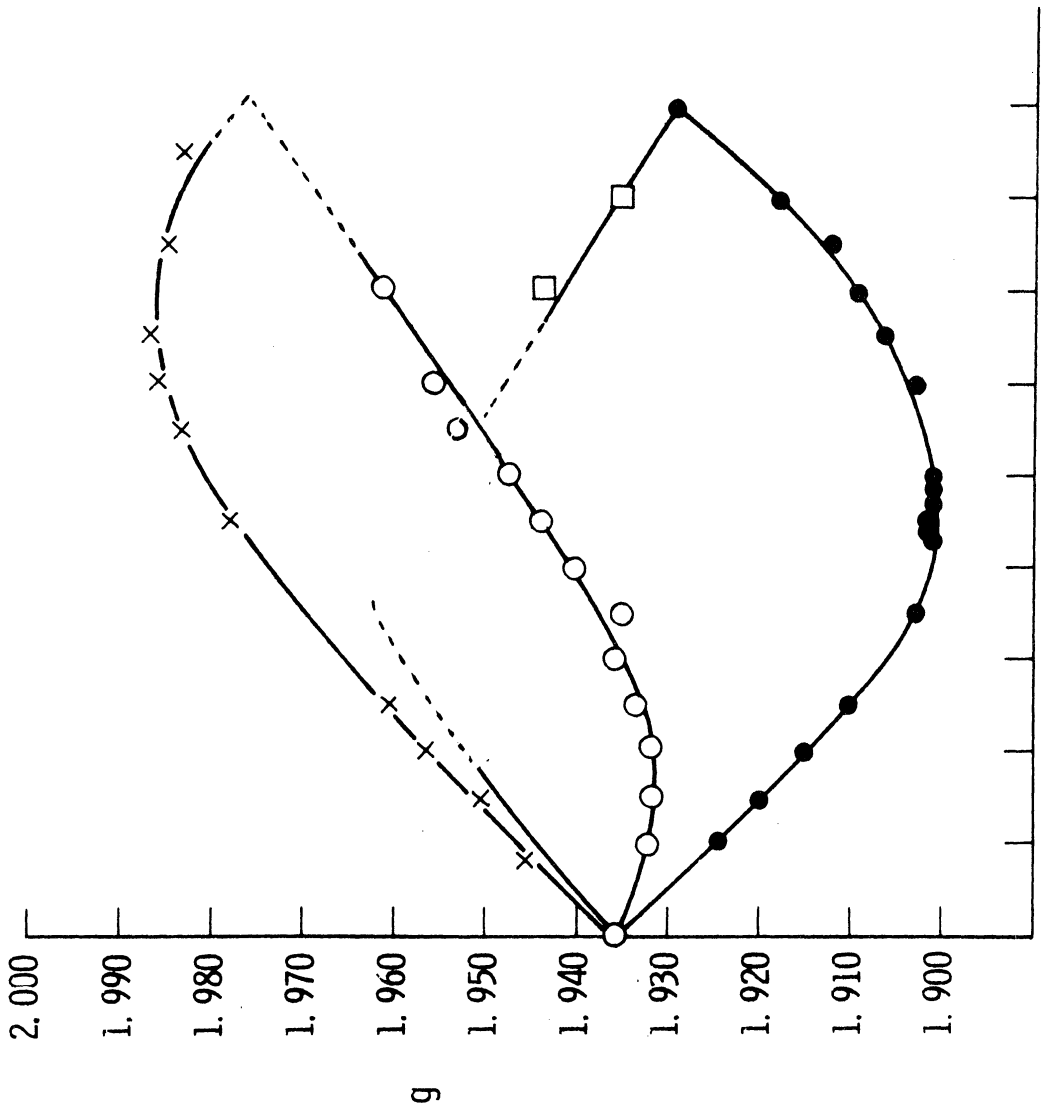

Fig. 4.14. Angular variation of the g-value for the Group C in the ac-plane at 77°K.

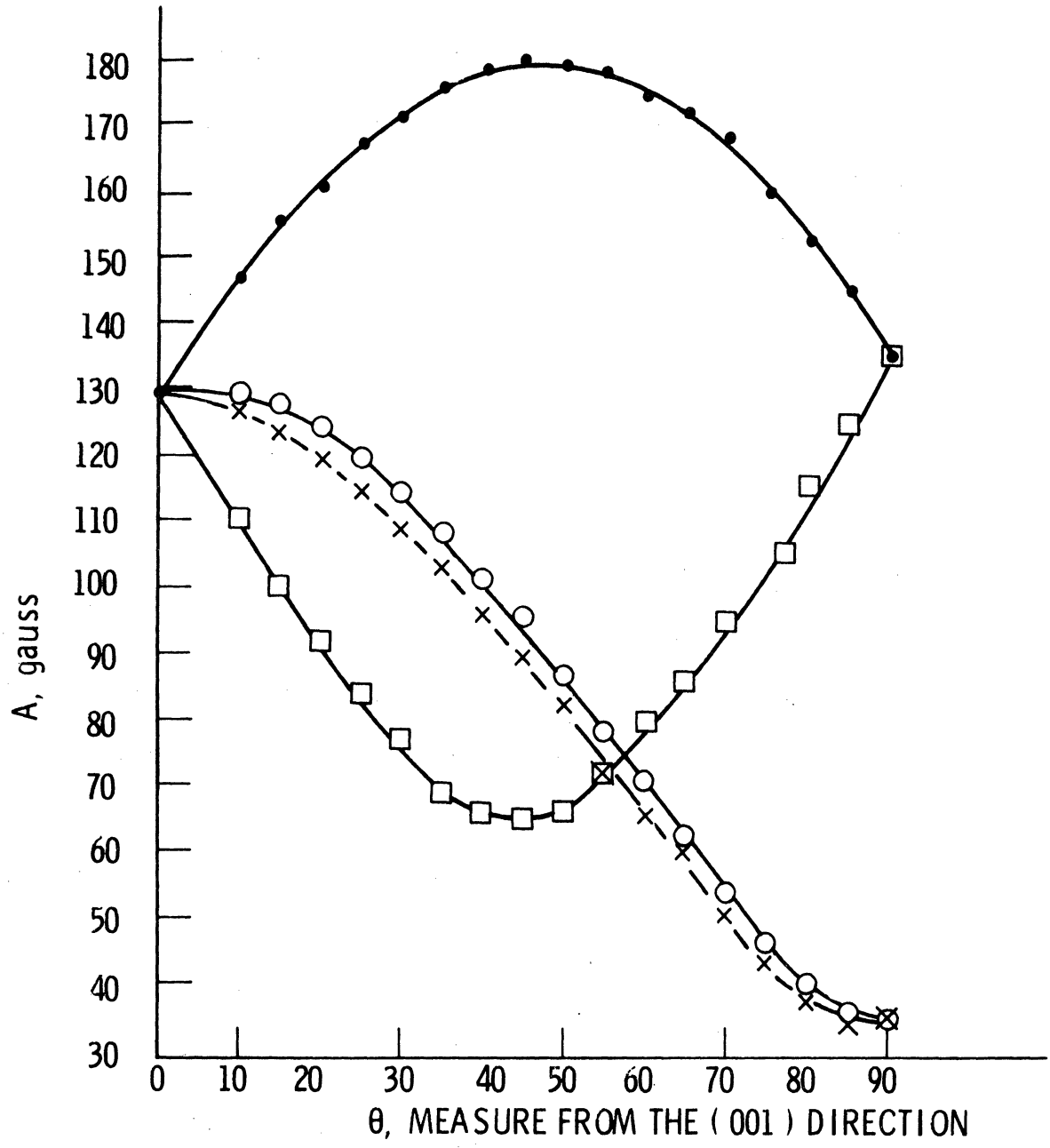

Fig. 4.15. Angular variation of the HFS for the Group C in the ac-plane at 77°K.

the A-tensor, as shown in Figure 4.16. g_z and A_z are the minimum and maximum values of these tensors. The large difference between the magnitude of these and the x, y components made the accurate measurements of the former possible. In contrast, the x and y components were difficult to determine experimentally due to the admixture of the four sets of lines and strong second order effect in the xy-plane. Approximate values and directions of these components were calculated (by computer) from the measurements in the ab- and ac-planes, using relationships

$$g^2 = g_x^2 n_1^2 + g_y^2 n_2^2 + g_z^2 n_3^2$$
$$A^2 = A_x^2 m_1^2 + A_y^2 m_2^2 + A_z^2 n_3^2$$

where n_i and m_i are direction cosines of g and A with respect to the tensor's axes. The results are shown in Tables 4.3 and 4.4. In the tables, θ and ϕ are polar and azimuthal angles of the tensor's axes. Indices 1 to 4 are used to designate the ϕ coordinates of the tensors for the four unequivalent sites.

The Group C lines can be described by a modified rhombic spin Hamiltonian of the form,

$$\mathcal{H}_s = \beta [g_z H_z S_z + g_x H_x S_x + g_y H_y S_y] + A_z I_z S_z + B_x I_x S_x + B_y I_y S_y + \sum_{i,j}{}' F_{ij} [S_i I_j + I_i S_j] \qquad (4.8)$$

where the last term is added to the usual rhombic spin Hamiltonian to account for the non-coinciding x and y axes of the g- and A-tensors. The constants B_x and B_y and F_{ij} are given by[19]

$$B_x = A_x \cos^2 \delta + A_y \sin^2 \delta$$

$$B_y = A_x \sin^2 \delta + A_y \cos^2 \delta$$

$$F_{xy} = F_{yx} = 1/2(A_x - A_y) \sin \delta \cos \delta \qquad (4.9)$$

where $\delta = 30°$ is the angle between x- or y-axes of the g- and A-tensors and A_x, A_y, and A_z are the principal values of the hyperfine coupling constants. Putting experimental data into (4.9), we obtain for the constants of the spin Hamiltonian (4.8)

$$B_x = 42 \times 10^{-4} \text{ cm}^{-1}$$

$$B_y = 57 \times 10^{-4} \text{ cm}^{-1}$$

$$F_{ij} = F_{ji} = 0.217(A_i - A_j), \; i,j = x,y,z$$

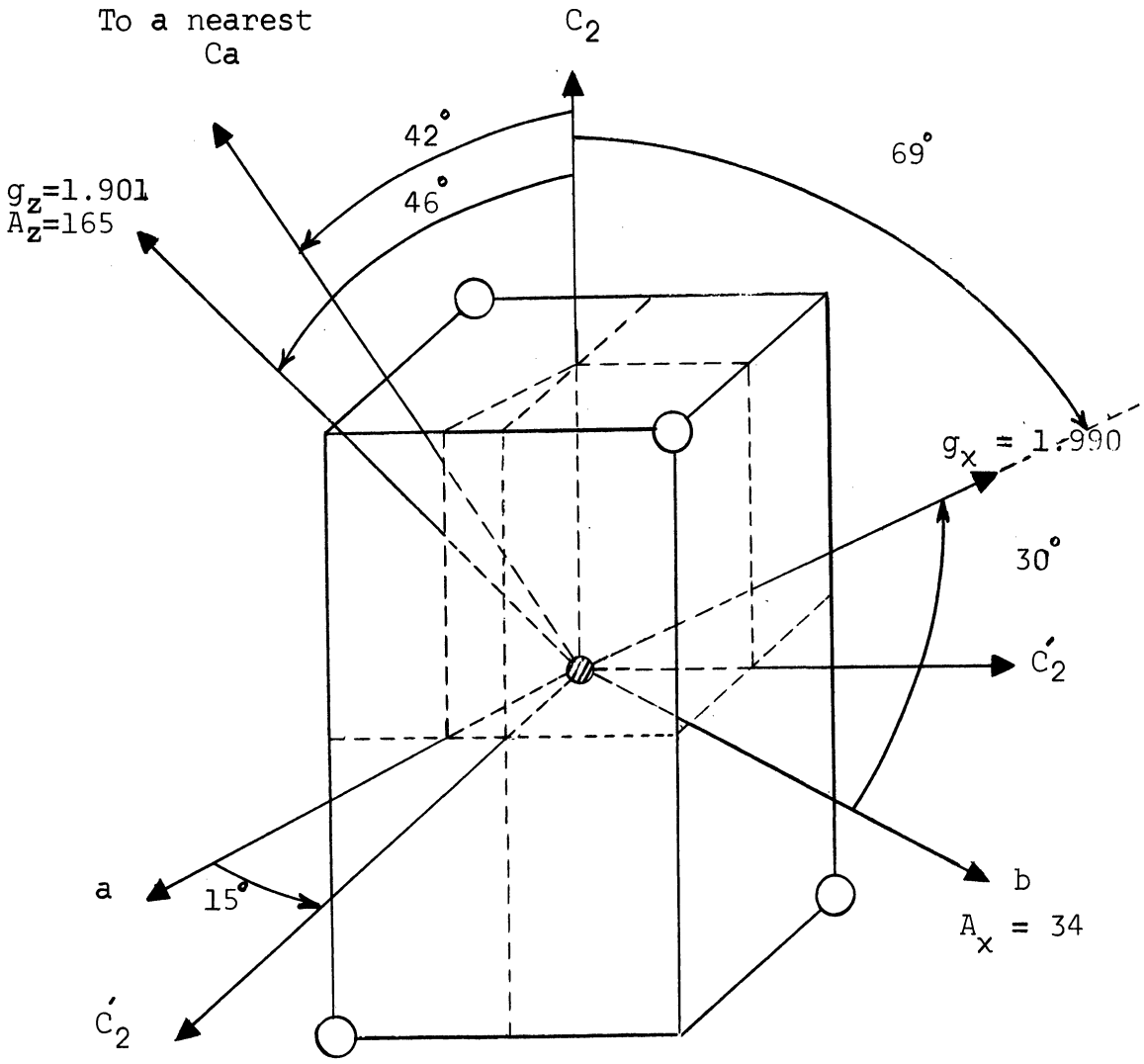

$g_y = 1.965$ $\quad A_y = 65 \times 10^{-4} cm^{-1}$

$\theta = 51°$ $\quad \theta = 44°$

$\phi = 220°$ $\quad \phi = 180°$

Fig.4.16. Group C, g- and A-tensors.

TABLE 4.3

PRINCIPAL VALUES AND DIRECTIONS OF THE
g-TENSOR FOR THE GROUP C LINES
T=77°K

	g_x 1.990	g_y 1.965	g_z 1.901 ± 0.001
θ	69°	51°	46° ± 1
ϕ_1	112°	220°	0° ± 1
ϕ_2	203°	310°	90° ± 1
ϕ_3	293°	40°	180° ± 1
ϕ_4	23°	130°	270° ± 1

TABLE 4.4

PRINCIPAL VALUES* AND DIRECTIONS OF THE
A-TENSOR FOR THE GROUP C LINES
T = 77°K

	A_x 34	A_y 65	A_z 165 ± 0.3
θ	90°	44°	46° ± 1
ϕ_1	90°	180°	0° ± 1
ϕ_2	180°	270°	90° ± 1
ϕ_3	270°	0°	180° ± 1
ϕ_4	0°	90°	270° ± 1

*In units of 10^{-4} cm^{-1}.

CHAPTER V

DISCUSSION AND CONCLUSIONS

1. Site Occupancies of V and Re Ions in $CaWO_4$

In the previous chapter we found the following correspondance between the doped calcium tungstate samples and the observed ESR spectra:

Sample	Spectra
$CaWO_4$: V	Group A (60%) + Group C (40%)
$CaWO_4$: V, RE	Group A (95%) + Group B (5%)

where RE represents Tb or Nd ions and the % shows the percentage of the total spectral intensity. From the ESR results, presented in Chapter IV, we draw the following conclusions concerning the paramagnetic centers of these groups.

a) It was seen that before X-irradiation the samples did not show any vanadium ESR spectrum. On the other hand, after the irradiation spectra arising from V^{4+} ions were detected in all samples. Hence, it is reasonable to assume that before the irradiation the vanadium in $CaWO_4$ is in the diamagnetic pentavalent oxidation state V^{5+}. Then, as a

result of the irradiation, it is reduced to paramagnetic V^{4+} ion with S = 1/2. In fact, the reducing effect of X- or γ-rays on vanadium ions has been observed in vanadium-doped magnesium oxide,[18,26] aluminum oxide,[16] and Tutton salt.[19] Also, we could not detect V^{3+} ions in the samples before the irradiation.

b) The Group C lines, in the spectrum of the uncompensated $CaWO_4$:V samples, arise from the V^{4+} ions at ionic Ca sites. One evidence for this assignment is the negative Δ g of this group: This is generally observed for ions at ionic sites as shown in Table 1.1. Crystal field calculations for V^{4+} in a Ca site result in the following energy levels (see Appendix B).

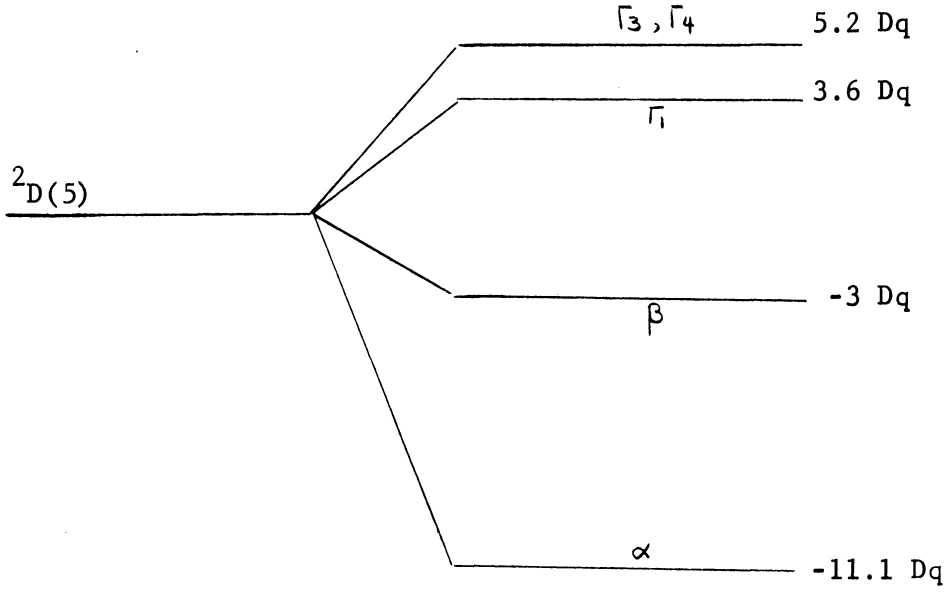

where,

$\Gamma_1 = \psi_{20}$ $\quad (\psi_\ell , m_\ell)$

$\Gamma_3 = \psi_{21}$

$\Gamma_4 = \psi_{2-1}$

$$\alpha = \frac{0.362}{\sqrt{2}} (\psi_{22} + \psi_{2-2}) + i \frac{0.932}{\sqrt{2}} (\psi_{22} - \psi_{2-2})$$

$$\beta = \frac{0.932}{\sqrt{2}} (\psi_{22} + \psi_{2-2}) + i \frac{0.362}{\sqrt{2}} (\psi_{22} - \psi_{2-2})$$

Using this energy scheme, we have calculated the shift of the g-factor. In the z-direction, we have

$$\Delta g_z = - \frac{8}{8.1 \text{ Dq}}$$

and for the x or y components,

$$\Delta g_\perp \equiv \Delta g_x = \Delta g_y = \frac{-2}{16.3 \text{ Dq}}$$

where the spin-orbit coupling coefficient λ is positive (less than half filled shell). The calculations not only predict $\Delta g < 0$ but also that

$$|\Delta g_z| > |\Delta g_\perp|$$

Or, in fact,

$$\Delta g_z / \Delta g_\perp \approx 8$$

Experimentally, we have found

$$\Delta g_z = - 0.1013 \pm 0.0005$$

$$\Delta g_x = -0.0123 \pm 0.005$$

$$\Delta g_y = - 0.0373 \pm 0.005$$

Thus,

$$\Delta g_z / \Delta g_x = 10 \pm 4$$

$$\Delta g_z / \Delta g_y = 2.7 \pm 0.4$$

The agreement between the calculated and experimental results is good when we consider the approximate nature of the former and the relatively high error in Δ g measurements for g-values close to g_e. The reason why the theoretical calculations make no distinction between g_x and g_y is that we have assumed perfect S_4 symmetry at the paramagnetic ion site in our crystal field calculations. In fact, one would expect the site symmetry to be disturbed by charge compensation mechanisms specially in the case in point (the Group C lines) where vacancy compensation is operative. Such a perturbation can cause splitting of the degenerate $\Gamma_{3,4}$ level. It is easy to show that if we assume new wave functions for these levels such as,

$$\Gamma_3' = a\,\Gamma_3 + b\,\Gamma_4$$
$$\Gamma_4' = c\,\Gamma_3 + d\,\Gamma_4$$

then in general $\Delta g_x \neq \Delta g_y$.

Another evidence for associating the Group C with V^{4+} in calcium site is the large HFS of this group. In Table 5.1 average values of the g- and A-tensors for V^{4+} ions in several host crystals are shown.

As we observe, $\langle A \rangle$ for the Group C lies between those of V^{4+} in the rutile structure crystals and in the zinc-ammonium Tutton salt which

TABLE 5.1

AVERAGE VALUES OF V^{4+} g- AND A-TENSORS IN SEVERAL CRYSTALS

Ion	Host Crystal	$< g >$	$< A >$*
V^{4+}	TiO_2	1.928	72
V^{4+}	SnO_2	1.928	69.7
V^{4+}	GeO_2	1.935	69.5
VO^{2+}	Tutton Salt	1.9648	108.8
V^{4+} (Group C)	$CaWO_4$	1:952	88

*In units of 10^{-4} cm^{-1}.

is a strongly ionic crystal. Hence, we conclude that the C spectrum originates from V^{4+} at ionic calcium sites.

c) Judging by the spectrum alone, the Group A may be associated with V^{4+} at either a W or a Ca site both of which possess a S_4 symmetry. But this group, in contrast with the Group C, has positive Δ g and small HFS, and thus it cannot be related to a Ca site. Also, Karavelas and Kikuchi[56] have made a preliminary molecular orbital calculation for vanadium orthovanadate VO_4^{3-} which is converted to VO_4^{4-} upon X-irradiation. Allowing for a charge compensation correction (for the extra electron at the orthovanadate complex), they anticipate $g_{\parallel} = 2.0268$ and $g_{\perp} = 2.0231$ which give $<g> = 2.024$ in excellent agreement with the experimental value g = 2.0245. Hence, the Group A is assigned to V^{4+} ions in W sites.

d) The Group B lines, with positive Δ g and small HFS, are also associated with a W site with some reduction of the local symmetry. Since the g-tensor principal axes do not bear any relationship with bonds directions in the crystal and also because of the low intensity of its spectrum, this group is believed to arise from local imperfections in the crystal. This view is further supported by the fact that crystals prepared at some later time did not show the Group B lines.

From the above conclusions we now propose a model for the charge compensation in the impurity-doped $CaWO_4$.

It was seen that in the RE-compensated samples, vanadium (as V^{5+}) occupies the W^{6+} site. Thus, a simple and reasonable scheme for the charge compensation is for the RE ions to enter Ca sites in trivalent oxidation state. This agrees well with the substitution model of Nassau and Loiacono[13] who used Nb^{5+}, instead of V^{5+}, for charge compensator in their Nd-doped calcium tungstate. Also, substitution of W^{6+} (in WO_4^{2-}) by V^{5+} is chemically possible for VO_4^{3-} is a complex vanadium ion, actually known to exist.[69] Finally, in occupation of lattice sites by impurity ions, the match between the sizes of the substituent and the substituted ions is an important factor.[13] Table 5.2 shows how well the ionic radii of V^{5+} and Nd^{3+} (or Tb^{3+}) compare with those of W^{6+} and Ca^{2+} which they replace.[57]

The case of $CaWO_4$:V samples, however, is different. Here, vanadium is the only impurity ion in the lattice, and thus contributions to the charge compensation must come from the vanadium ions itself; vacancies might also be generated. In fact, the anisotropic spectrum of

TABLE 5.2

IONIC RADII OF METAL IONS AND THEIR SUBSTITUTES IN $CaWO_4$

Ion	W^{6+}	Ca^{2+}	V^{5+}	Nd^{3+}	Tb^{3+}
Ionic radius (Å)	0.62	0.99	0.59	1.03	1.00

the Group C is a strong evidence for possible existence of vacancies in this crystal. Hence, we suggest the following model for the charge compensation in this sample. Four V^{5+} ions enter four W^{6+} sites while two other V^{5+} ions occupy two Ca^{2+} sites and one calcium vacancy is also formed. Then, upon X-irradiation, V^{5+} ions at W and Ca sites are converted to V^{4+} which give rise to the Groups A and C spectra, respectively. According to this model the intensities of the Groups A and C must be in the ratio of 2:1. This is in agreement with the experimental results within 20%, the error limit of ESR quantitative measurements. Also, the model suggests that each pair of vanadium ions at calcium sites are coupled to a nearest calcium vacancy. The direction of this coupling, as shown in Figure 3.2, makes an angle of 42° 40' with the c-axis in the ac- or bc-plane. This is in good agreement with the direction of the common z-axis of the g- and A-tensors of the Group C (see Figure 4.16).

A number of temperature annealing and growth rate* experiments

*Conversion rate of $V^{5+} \rightarrow V^{4+}$ as a function of X-irradiation dose.

were carried out in an attempt to see if an electron transfer process existed between the ESR centers of A and C. From the results, it appears that there is no simple correlation between the two centers.

The above observations lead us to the following conclusions on site occupancies of the vanadium and RE ions in $CaWO_4$.

i) In the charge-compensated $CaWO_4$:V, Tb and $CaWO_4$:V, Nd samples, vanadium ions, in V^{5+} oxidation state, occupy W^{6+} sites while the trivalent rare-earth ions enter Ca^{2+} sites.

ii) In the uncompensated $CaWO_4$:V sample, V^{5+} ions occupy both W^{6+} and Ca^{2+} sites. In this case, each pair of vanadium ions at calcium sites are coupled to a nearest calcium vacancy.

2. Line Width and Temperature Dependence of Vanadium Spectra

For many years, line shape and relaxation of paramagnetic signals have been the subjects of extensive experimental and theoretical studies. In spite of this, still in most cases only a qualitative analysis of experimental data is possible. In this section, we too will attempt to interpret qualitatively our observations of the line width and the temperature dependence of the Group A spectra on the basis of relaxation phenomena. A brief description of these processes and the related formulas, which are going to be used in our description, are presented in Appendix C. For convenience, the following notations will be used in reference to the samples under consideration:

S_1 for $CaWO_4$:V

S_2 for $CaWO_4$:V, Nd

S_3 for $CaWO_4$:V, Tb

We shall also express the full width (at half-maximum) of the absorption line in terms of $\Delta\omega$, i.e., the deviation from the resonance frequency ω_0 as shown in Figure C.1. To first order, $\Delta\omega$ is proportional to ΔH, the measured line width in gauss through

$$\hbar \Delta\omega \approx g\beta \Delta H$$

a) The observed angular variation of the line width of the Group A at 77°K suggests that a sizable contribution to the line broadening comes from the dipolar spin-spin coupling. Perhaps there are small contributions from other sources of line broadening such as mosaic spread of the crystal and inhomogeneity in the static magnetic field across the sample. Also, the electron-nucleus dipolar interactions may not be quite negligible in our case.

Experimentally, we have observed that the ESR absorption lines of S_2 and S_3 are much broader than that of S_1 (see Figure 4.4). This can be explained by spin-spin interactions (dipolar broadening) between vanadium ions as well as between vanadium and the RE ions. According to Equations (C.3) and (C.4) of Appendix C, the dipolar interactions tend to increase the line width as the concentrations of the impurity ions increase. The concentration of vanadium in S_1 is almost half as much as that in S_2 and S_3 (see Table 3.1). Furthermore, the last two samples

contain RE ions which make substantial contribution to $\Delta\omega$ through Equation (C,4).

b) As we recall, at liquid helium temperature samples S_1 and S_2 showed similar ESR spectra whereas S_3, which contains V and Tb, did not show any vanadium spectra even at 60-70 db below the 300 mw power level of the microwave source. The Tb^{3+} ESR lines, however, could be observed at very low magnetic field intensities.* Similar phenomena have been reported by others,[66,67] and it can be explained in terms of cross-relaxation mechanism: In S_1 samples, vanadium ions occupy both Ca and W sites with two different but close g-values. At liquid helium temperature, these two spin species couple magnetically and the cross-relaxation takes place with $T_2 < T_{12} \ll T_1$ where T_1, T_2, and T_{12} are the spin-lattice, the spin-spin, and the cross-relaxation times. Since the resonance frequencies of the two centers are not much different from each other, we expect[64] T_{12} to be closer to T_2. The fact that we see the ESR spectra of S_1 at 4.2°K implies that the non-saturation condition (C.6) is satisfied. That is,

$$\gamma^2 H_1^2 T_1 T_2 < 1$$

where γ is a constant and $(2H_1)$ is the amplitude of the magnetic component of the radiation field. Now, in the (V,Nd)-doped samples S_2, almost all vanadium ions go to W sites and Nd^{3+} occupy Ca sites. The g-values of Nd^{3+} ions in S_2 are close to that of vanadium; in fact, the

---

*For Tb^{3+} in $CaWO_4$, $g_{\parallel} = 17.777$ and $g_{\perp} < 0.15$ (Ref. 2).

two sets of spectra overlap in a wide region in the ab-plane. This is a favorable condition for establishment of the cross-relaxation. Again, since the g-values are similar to the preceding case S_1, we would expect to see the vanadium spectrum, in concordance with the experimental results.

The case of the S_3 samples, however, is different. Here, we have V^{4+} and Tb^{3+} in W and Ca sites, respectively. Due to the large difference between the resonance frequencies of these ions we expect T_{12} to be very large.[64] This makes

$$\gamma^2 H_1^2 T_1 T_{12} > 1$$

and hence the saturation condition prevails. The reason we are able to see the Tb spectrum is that the spin-lattice relaxation time T_1 for Tb^{3+} is smaller than that for V^{4+} (Tb^{3+} does not show spectrum at 77°K while V^{4+} does). Apparently the smallness of T_1 compensates for large T_{12} so that the saturation condition is removed.

3. Splitting of the Group A Lines at 4.2°K

As we have seen in Chapter IV, at liquid helium temperature, the Group A spectrum splits, in general, into four sets of lines. The maximum component of the g-tensor was found to be in the direction of the W-O bond in WO_4^{2-}. Also, the 77°K spectra was found to be at the average position of the four low-temperature sets (Table 4.2).

This behavior cannot be accounted for only by temperature dependence of the line width: the separation between the centers of the

lowest lying and the highest lying sets at 4.2° reaches a maximum of about 40 gauss while the maximum line width of the Group A at 77°K, for $CaWO_4$:V samples, is only about 4 gauss. Watkins and Corbett[70] have observed similar phenomena in the ESR of the silicon E-centers and attributed it to "thermal reorientation" of the centers. We shall tentatively apply their method to our case.

Before irradiation, vanadium in W^{6+} site forms the diamagnetic complex VO_4^{3+}. After the irradiation, it acquires one electron and becomes paramagnetic VO_4^{4-}. If we assume that the unpaired electron comes from one of the oxygen atoms, then there are four possible V-O orientations differing in the spin resonance frequencies by $\delta\nu = 2\pi\delta\omega$. This is in agreement with the ESR spectra observed at 4.2°K. Now, suppose the unpaired electron in VO_4^{4-} jumps randomly from one V-O direction to another with an average life time of τ in each direction. At low temperatures the jumping rate is slow and, as Gutowsky and Saika[71] have shown, if $\tau \gg 1/\delta\omega$ then we expect one distinct resonance absorption for each orientation with an intensity proportional to the probability of finding the electron in that orientation. We can identify this case with the Group A at 4.2°K assuming the electron executes random jumps among the four V-O orientations with the same probability. Thus, we expect to see four lines with equal intensities as it is actually observed in experiment.

As the temperature is increased, the jumping rate increases (τ decreases) and the resonance lines undergo life time broadening. Experimentally, we have observed this when the liquid helium in the system is

all evaporated and the temperature of the sample is rapidly approaching that of the liquid nitrogen coolant in the outer dewar. Analogous observations have been reported by others.[70,73]

As the temperature is further increased, τ becomes smaller until eventually $\tau \ll \frac{1}{\delta\omega}$ which is the condition for "fast exchange" and manifestation of motional narrowing.[72] In this case, one set of spectrum is expected to emerge at the average position of the four low-temperature lines with a line width proportional to τ. We have associated this case with the 77°K spectra of the Group A (see Table 4.2).

APPENDIX A

THE SPIN HAMILTONIAN AND POSITION OF THE SPECTRAL LINES

1. THE HAMILTONIAN

In EPR spectroscopy usually a phenomenological Hamiltonian, the "spin Hamiltonian," is employed to interpret experimental results. It is phenomenological in this sense that its form can be anticipated on the basis of physical considerations and the crystal field symmetry. It can also be derived from a general Hamiltonian for a paramagnetic ion in the electric field of the host material (a crystal, in our case) and the externally applied static magnetic field. We shall outline this derivation.

The Hamiltonian for the paramagnetic ion can be written as,

$$\mathcal{H} = \mathcal{H}_c + \mathcal{H}_{cf} + \mathcal{H}_{LS} + \mathcal{H}_{ss} + \mathcal{H}_{em} + \mathcal{H}_{Ne} + \mathcal{H}_{Nm} + \mathcal{H}_q \qquad (A.1)$$

where various interactions and their order of magnitude for the iron group elements are as follows.

$\mathcal{H}_c$, the coulomb interaction between the electrons and the nucleus ($\approx 10^5$ cm^{-1}) = $\sum_{i=1}^{n}\left(\frac{p_i^2}{2m} - \frac{Ze^2}{r_i}\right) + \sum_{i>k=1}^{n} e^2/r_{ik}$

$\mathcal{H}_{cf}$, the crystal field interaction. Its magnitude depends on the

ion. For most iron group elements, $\mathcal{H}_{LS} < \mathcal{H}_{cf} < \sum \frac{e^2}{r_i}$

The explicit form of $\mathcal{H}_{cf}$ depends, of course, on the crystal field symmetry. It will be treated in detail in Appendix B.

$\mathcal{H}_{LS}$, the spin orbit coupling interaction ($\approx 10^3$ cm^{-1}) =

$$\lambda \underline{L}.\underline{S} \quad , \qquad \text{assuming Russel-Saunders coupling.}$$

$\mathcal{H}_{ss}$, the spin-spin interaction (≈ 1 cm^{-1}) =

$$\sum_{j>k}^{n} 4\beta^2 \left[\frac{\underline{S}_j \cdot \underline{S}_k}{r_{jK}^3} - \frac{3(\underline{r}_{jk} \cdot \underline{S}_j)(\underline{r}_{jk} \cdot \underline{S}_k)}{r_{jk}^5} \right]$$

$\mathcal{H}_{em}$, interaction of the unpaired electrons with the applied static magnetic field (≈ 1 cm^{-1}) =

$$\beta \underline{H} \cdot (\underline{L} + 2\underline{S}) \qquad (\beta = \text{Bohr magneton})$$

It produces the splitting of the electronic levels between which the transitions are observed.

$\mathcal{H}_{ne}$, the effect of the nuclear magnetic moment on the magnetic field of electrons ($\approx 10^{-2}$ cm^{-1}) =

$$2 g_N \beta \beta_N \sum_{i=1}^{n} \left[\frac{\underline{l}_i \cdot \underline{S}_i}{r_i^3} + \frac{3(\underline{r}_i \cdot \underline{S}_i)(\underline{r}_i \cdot \underline{I})}{r_i^5} \right]$$

where g_N, β_N and I are nuclear g factor, nuclear magneton and nuclear spin, respectively.

$\mathcal{H}_{Nm}$, the interaction between the nuclear magnetic moment and the D.C. magnetic field ($\approx 10^{-3}$ cm^{-1}) = $-g_N \beta_N \underline{H} \cdot \underline{I}$

$\mathcal{H}_Q$, the interaction of the nuclear quadrupole moment with the electrons ($\approx 10^{-4}$ cm^{-1}) =

$$\frac{-e^2Q}{2I(2I-1)} \sum_i \left[I(I+1) r_i^{-3} - 3 \left(\underline{I} \cdot \underline{r}_i \right)^2 r_i^{-5} \right]$$

The effect of the crystalline field on the nuclear quadrupole moment is negligible.

Since in our case the crystal field energy $\mathcal{H}_{cf}$ is smaller than the coulomb interaction energy $\mathcal{H}_c$, but greater than all other energies in Eq. (A-1), the state of the free ion is usually described by $\mathcal{H}_c$. Then, the effects of the $\mathcal{H}_{cf}$ and the other interaction energies are taken into account by the application of two successive perturbations.

When the state of a free ion is described by the coulomb energy only, it is implied that the electrons move independently from each other while obeying the Pauli exclusion principle. The total orbital and spin angular momenta are then given by

$$\underline{L} = \sum_i \underline{l}_i$$

$$\underline{S} = \sum_i \underline{s}_i$$

and $\underline{J} = \underline{L} + \underline{S}$. Thus, in the absence of any external electric or magnetic field, each energy level is $(2J + 1)$ - fold degenerate. The

single electron orbitals are the usual $1s^2$ $2s^2$ $2p^6$ etc. V^{4+}, for instance, can be represented by $[A]3d^1$ where [A] stands for the closed argon shell. The ground state of the free ion depends on its unpaired electrons, i.e., those which are not comprised in the closed shell. For the V^{4+} ion, with just one unpaired 3d electron, the ground state can be readily written as $^2D_{3/2}$ (using the usual spectroscopic notation $^rL_{2J+1}$ where, r = 2 S+1 denotes the spin multiplicity of the state and J = L-S. The minus sign is used here because 3d shell of the V^{4+} ion is less than half-full).

The effect of the crystal field energy $\mathcal{H}_{cf}$ on splitting of the ground state of the free ion shall be discussed in Appendix B.

2. THE SPIN HAMILTONIAN

So far, we have considered only the first two terms of the Hamiltonian (A.1). The remaining perturbations will now be treated collectively to derive the spin Hamiltonian. Denoting these terms by $\mathcal{H}'$, we have

$$\mathcal{H}' = \mathcal{H}_{LS} + \mathcal{H}_{ss} + \mathcal{H}_{me} + \mathcal{H}_{N} + \mathcal{H}_{Nm} + \mathcal{H}_{Q} \tag{A.2}$$

Using the operator equivalent method on (A.2) and neglecting terms of second order in operators $\underline{L}$, $\underline{S}$, and $\underline{I}$, we obtain

$$\begin{aligned} \mathcal{H}' = {} & \lambda\, \underline{L}\cdot\underline{S} + \beta \underline{H}(\underline{L} + 2\underline{S}) + A\, \underline{I}\cdot\underline{S} + P\, \underline{L}\cdot\underline{I} \\ & - g_N \beta_N\, \underline{H}\cdot\underline{I} + Q'\left[I_z^2 - \tfrac{1}{3}(I+1) I \right] \end{aligned} \tag{A.3}$$

where Q' is related to the quadrupole moment Q by

$$Q' = \frac{3eQ}{4I(2I-1)} \left(\frac{\partial^2 V}{\partial z^2}\right)_0$$

In deriving (A.3), the spin-spin interaction term $\mathcal{H}_{ss}$ and the first term of $\mathcal{H}_Q$ which expresses the interaction between the nuclear quadrupole moment and the electric field of electrons, have been dropped because of their negligible contributions.

When, as in our case, the lowest energy level of the paramagnetic ion in the crystal field is an orbital singlet, the perturbation calculations with $\mathcal{H}'$ are carried out in two steps. First, operators $\underline{S}$ and $\underline{I}$ are regarded as non-commuting algebraic quantities and the ordinary perturbation calculations are done only with the orbital part of the wave functions. The result is an expression in $\underline{I}$ and $\underline{S}$ which is called the spin Hamiltonian. Next, this new Hamiltonian is used to find the actual energy levels. Thus, to second order, for instance

$$\mathcal{H}_s = \langle 0|\mathcal{H}'|0\rangle - \sum_{n\neq 0} \frac{|\langle 0|\mathcal{H}'|n\rangle|^2}{E_n - E_0}$$

where, $|0\rangle$ and $|n\rangle$ denote the ground state and the nth orbital excited state wave functions. The spin Hamiltonian obtained in this fashion has the general form

$$\begin{aligned}\mathcal{H}_s = {} & \beta \underline{H}\cdot\underline{\underline{g}}\cdot\underline{S} + \underline{S}\cdot\underline{\underline{D}}\cdot\underline{S} + \underline{I}\cdot\underline{\underline{A}}\cdot\underline{S} \\ & + \underline{I}\cdot\underline{\underline{Q}}\cdot\underline{I} + \beta_N \underline{H}\cdot\underline{\underline{g}}_N\cdot\underline{I} + \beta^2 \underline{H}\cdot\underline{\underline{\Lambda}}\cdot\underline{H}\end{aligned} \qquad \text{(A.4)}$$

where $\underline{\underline{g}}$, $\underline{\underline{D}}$, $\underline{\underline{A}}$, $\underline{\underline{Q}}$, $\underline{\underline{g}}_N$, and $\underline{\underline{\Lambda}}$ are tensors whose principal axes are assumed to coincide. The first term in (A.4) is the Zeeman splitting term. The spectroscopic factor, g, may be anisotropic and differ from 2.0023 due to the admixing of higher orbitals. The fine structure term, $\underline{S}.\underline{\underline{D}}.\underline{S}$, represents the splitting of the ground state in the absence of external magnetic field and the nuclear interaction. This term originates from the second order effects of the crystalline field and spin-orbit coupling. The hyperfine structure term, $\underline{I}.\underline{\underline{A}}.\underline{S}$, describes the interaction between the nuclear magnetic dipole and the magnetic field due to the electronic spin. The term $\underline{I}.\underline{\underline{Q}}.\underline{I}$, shows the contribution of the nuclear quadrupole moment due to its interaction with the crystalline electric field. The direct interaction between the externally applied magnetic field and the nuclear magnetic dipole moment is expressed by the term $\underline{H}.\underline{\underline{g}}_N.\underline{I}$. Finally, the last term, $\beta^2.\underline{H}.\underline{\underline{\Lambda}}.\underline{H}$, can be neglected because it is independent of nuclear and electronic variables and thus shifts all energy levels by an equal amount.

The eigenvalues of (A.4) cannot be obtained in a general manner: In each specific problem, the general spin Hamiltonian $\mathcal{H}_S$ must be modified to conform to the symmetry of the crystal field. For instance, for cubic symmetry the tensor quantities of (A.4) are all isotropic, i.e.,

$$g_x = g_y = g_z \equiv g$$

$$A_x = A_y = A_z \equiv A, \text{ etc.}$$

Hence, we have

$$(\mathcal{H}_S)_{cubic} = g\beta \underline{H}\cdot\underline{S} + D(S_x^2+S_y^2+S_z^2) + A\,\underline{I}\cdot\underline{S}$$
$$+ Q(I_x^2+I_y^2+I_z^2) - g_N\beta_N \underline{H}\cdot\underline{I}$$

Observe furthermore,

$$D(S_x^2+S_y^2+S_z^2) = D\,S(S+1) = \text{const.}$$

and can be neglected because it shifts all energy levels by the same amount. Thus, assuming the principal axes of the various tensors coincide, we find

$$(\mathcal{H}_S)_{cubic} = g\beta \underline{H}\cdot\underline{S} + A\,\underline{I}\cdot\underline{S} - g_N\beta_N \underline{H}\cdot\underline{I} \qquad \text{(A.5)}$$

Similarly, for the axial field,

$$\begin{aligned}(\mathcal{H}_{axial}) = {} & \beta\left[g_z H_z S_z + g_\perp (H_x S_x + H_y S_y)\right] \\ & + D\left[S_z^2 - \tfrac{1}{3}S(S+1)\right] + A\,I_z\cdot S_z \\ & + B(S_x I_x + S_y I_y) + Q'\left[I_z^2 - \tfrac{1}{3}I(I+1)\right] \\ & - \beta_N\left[g_{Nz} H_z I_z + g_{N\perp}(H_x I_x + H_y I_y)\right]\end{aligned} \qquad \text{(A.6)}$$

and for the more general case, the rhombic symmetry,

$$(\mathcal{H}_S)_{\text{rhombic}} = \beta(g_z H_z S_z + g_x H_x S_x + g_y H_y S_y) + D\left[S_z^2 - \tfrac{1}{3}S(S+1)\right]$$
$$+ E(S_x^2 - S_y^2) + A\, I_z \cdot S_z + B_x I_x S_x + B_y I_y S_y + Q'\left[I_z^2 - \tfrac{1}{3}I(I+1)\right]$$
$$+ Q''\left[I_x^2 - I_y^2\right] - \beta_N(g_{Nz} H_z I_z + g_{Nx} H_x I_x + g_{Ny} H_y I_y) \qquad \text{(A.7)}$$

When the principal axes of A- and g-tensors do not coincide, cross-terms of the form

$$\sum_{ij}{}' F_{ij}(S_i I_j + S_j I_i)$$

must be added to the rhombic spin Hamiltonian (A.7). Note further that for paramagnetic systems with S = 1/2, the effective axial or rhombic spin Hamiltonians do not contain terms in D or E.

3. ENERGY LEVELS AND LINE POSITIONS FOR S = 1/2 SYSTEMS

In general, the energy levels for the state $|M, m\rangle$ are eigenvalues of $\mathcal{H}_S$ and can be obtained by the usual degenerate perturbation calculations. The results for V^{4+} ions (S = 1/2), to second order and neglecting the nuclear and quadrupole interaction, are as follows.

$$E(M,m)_{\text{cubic}} = g\beta HM + AMm$$
$$+ \frac{A^2}{2g\beta H}\left[mI(I+1) + Mm(M-m) - \frac{3}{4}m\right] \qquad \text{(A.8)}$$

where M and m denote the electronic and nuclear spin quantum numbers, respectively. The energy for $\Delta M = \pm 1$, $\Delta m = 0$ resonance transitions is given by

$$E(M,m) - E(M-1,m) = h\nu$$

from which the resonant magnetic field H (i.e., the position of the resonance absorption lines in the magnetic field) is obtained as

$$H(m)_{\text{Cubic}} = H_0 - \frac{A}{g\beta} m - \left(\frac{A}{g\beta}\right)^2 \frac{1}{2H_0} \left[I(I+1) - m^2\right]$$

where, $H_0 = h\nu/g\beta$

Similarly, for the axial spin Hamiltonian we have,

$$E(M,m) - E(M-1,m) = h\nu$$

$$= g\beta H + Km + \frac{B^2}{4g\beta H_0}\left[\frac{A^2+K^2}{K^2}\right]\left[I(I+1) - m^2\right]$$

$$+ \frac{m^2}{2g\beta H_0}\left(\frac{A^2-B^2}{K}\right)^2\left(\frac{g_\parallel g_\perp}{g^2}\right)^2 \sin^2\theta\cos^2\theta$$

and the resonant field is,

$$H(m,\theta) = H_0 - \frac{K}{g\beta} m - \frac{B^2}{4(g\beta)^2 H_0}\left(\frac{A^2+K^2}{K^2}\right)\left[I(I+1) - m^2\right]$$

$$- \left(\frac{A^2-B^2}{K}\right)^2\left(\frac{g_\parallel g_\perp}{g^2}\right)^2 \frac{m^2}{2(g\beta)^2 H_0} \sin^2\theta\cos^2\theta$$

where,

$$K^2 g^2 = A^2 g_\parallel^2 \cos^2\theta + B^2 g_\perp^2 \sin^2\theta$$

$$g^2 = g_\parallel^2 \cos^2\theta + g_\perp^2 \sin^2\theta$$

$g_{\parallel}$ and $g_{\perp}$ are g-values measured parallel and perpendicular to the symmetry axis, respectively; θ is the angle between the magnetic field and the symmetry axis.

APPENDIX B

S_4 SYMMETRY AND SPLITTING OF THE ^2D GROUND STATE

In this appendix we shall apply crystal field calculations to $V^{4+}(3d^1$ ion, ^2D ground state) at the substitutional calcium site in $CaWO_4$ single crystal. The purpose of these calculations is to find the energies associated with splitting of the ion's ground state in the crystal field and, subsequently, to estimate $\triangle$ g.

1. THE CRYSTAL FIELD POTENTIAL

In these calculations we shall make the customary assumptions in the crystal field calculations, namely, (1) the impurity ion (the paramagnetic transition metal ion of interest) occupies a substitutional metallic site in the host crystal without distorting the field, (2) negative and positive charges in the lattice are non-overlapping point charges.

If we choose the paramagnetic ion as the origin of polar coordinates, Fig. B.1, then the electrostatic potential at a space point $\underline{r}$, due to negative charges Q_i located at $\underline{R}_i$, can be written as

$$V(\underline{r}) = e \sum_i \frac{Q_i}{|\underline{r} - \underline{R}_i|}$$

Or, using the law of cosines,

$$V(\underline{r}) = e \sum_i \frac{Q_i}{(r^2 + R_i^2 - 2\,\underline{r} \cdot \underline{R}_i)^{1/2}}$$

This, in turn, can be rewritten in terms of the Legendre polynomials as,

$$V(\underline{r}) = e \sum_i \frac{Q_i}{R_i} \sum_{l=0}^{\infty} \left(\frac{r}{R_i}\right)^l P_l(\cos \omega_i)$$

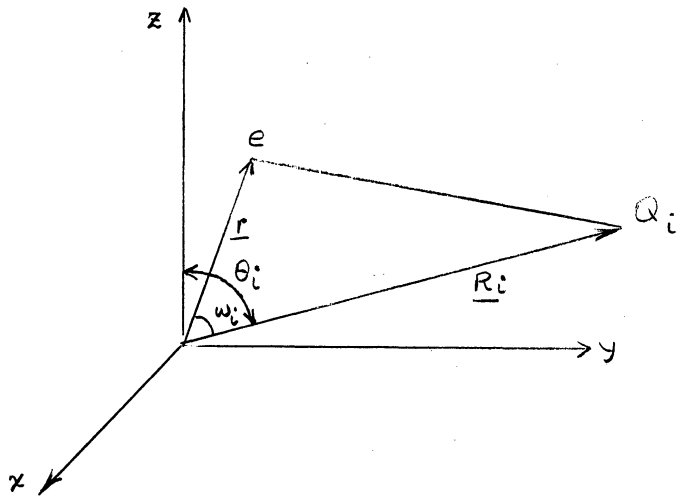

Fig. B.1. Point charge potential.

where ω_i denote angles between directions $\underline{r}$ and $\underline{R}_i$. Polynomials $P_l(\cos \omega_i)$ can be expressed in terms of (θ, ϕ) and (θ_i, ϕ_i), which define directions $\underline{r}$ and $\underline{R}_i$, by making use of the spherical harmonics addition theorem. Thus,

$$P_l(\cos \omega_i) = \frac{4\pi}{2l+1} \sum_{m=-l}^{l} (-1)^m Y_{l-m}(\theta_i, \phi_i) Y_{lm}(\theta, \phi) \qquad \text{(B.2)}$$

Using this in (B.1) we obtain

$$V(\underline{r}) = e \sum_i \sum_{m=-l}^{l} \sum_{l=0}^{\infty} (-1)^m \frac{4\pi}{2l+1} \frac{Q_i}{R_i} \left(\frac{r}{R_i}\right)^l Y_{l-m}(\theta_i, \phi_i) Y_{lm}(\theta, \phi) \qquad \text{(B.3)}$$

Eq. (B.3) can be rewritten as

$$V(\underline{r}) = \sum_{\ell=0}^{\infty} \sum_{m=-\ell}^{\ell} A_{\ell m} r^{\ell} Y_{\ell m}(\theta, \phi) \tag{B.4}$$

where $A_{\ell m}$ are given by

$$A_{\ell m} = e \frac{4\pi}{2\ell+1} (-1)^m \sum_i \frac{Q_i}{R_i^{\ell+1}} Y_{\ell -m}(\theta_i, \phi_i) \tag{B.5}$$

The number of terms in (B.4) which need to be considered is greatly reduced in each particular problem as follows. First of all, the final goal in these calculations is to find the energy levels of the paramagnetic ion in the crystal field. This is done, as we shall see later, by computing matrix elements of $V(\underline{r})$ with respect to the wave functions associated with these levels.

The paramagnetic ion in our case is V^{4+} with electronic configuration [A] $3d^1$ were [A] stands for the closed argon shell. Thus, the paramagnetic electron in this case is just one 3d electron. Accordingly, the wave functions do not contain terms with $\ell > 2$. Therefore, terms with $\ell > 4$ in $V(\underline{r})$ can be eliminated as they result in zero matrix elements. Similarly, the terms of odd ℓ (odd parity) are excluded from the crystal potential.

Further reduction in the number of terms in $V(\underline{r})$ can be obtained by symmetry considerations. The calcium site in $CaWO_4$ has S_4 symmetry with elements E, C_2, and S_4. The last element, for instance, requires that the crystal potential, anywhere in the lattice, remain invariant

under a rotation of 90° about the c-axis followed by a reflection in a plane perpendicular to this axis. Thus, applying S_4 to $\underline{r}$, we get

$$\phi \rightarrow \phi + \frac{\pi}{2}$$

$$\theta \rightarrow \pi - \theta$$

but,

$$V(\phi,\theta) = V\left(\phi + \frac{\pi}{2}\,,\ \pi - \theta\right)$$

which, by virtue of (B.4), requires

$$Y_{\ell m}(\theta,\phi) = Y_{\ell m}\left(\phi + \frac{\pi}{2}\,,\ \pi - \theta\right)$$

or,

$$P_{\ell m}(\cos\theta)\, e^{im\phi} = P_{\ell m}(-\cos\theta)\, e^{im(\phi + \pi/2)} \qquad \text{(B.6)}$$

Noting that $P_{\ell m}(\cos\theta)$ has the parity of $\ell - |m|$ with respect to the change in the sign of its argument, the only acceptable values of ℓ and m that can satisfy (B.6) are

ℓ	0	2	4
m	0	0	± 4

The term Y_{00} introduces just a constant shift in all energy levels and thus it can be neglected from the sum in (B.4). Hence, Y_{20}, Y_{40}, Y_{44}, and Y_{4-4} are the only terms to be considered in the calculation of $V(\underline{r})$, which now can be written as,

$$V(\underline{r}) = r^2 A_{20} Y_{20} + r^4 \left(A_{40} Y_{40} + A_{4-4} Y_{4-4} + A_{44} Y_{44}\right) \qquad \text{(B.7)}$$

The coefficients A_{lm} must be calculated from (B.5) by carrying out the indicated summation over the ligand charges. Taking Ca as the origin, the polar coordinates of the eight ligand oxygen ions, computed from the recent crystal structure data,[55] are shown in Table B.1.

TABLE B.1

POLAR COORDINATES OF THE EIGHT NEAREST OXYGEN NEIGHBORS OF Ca IN $CaWO_4$

Oxygen Number	R(in Å)	θ_i	ϕ_i
1	2.481	$66^\circ,45'$	53,31
2	2.481	$-66^\circ,45' + \pi$	53,31 + $\pi/2$
3	2.481	$66^\circ,45'$	53,31 + $2\pi/2$
4	2.481	$-66^\circ,45' + \pi$	53,31 + $3\pi/2$
5	2.436	$-40^\circ,4' + \pi$	59,48
6	2.436	$40^\circ,4'$	59,48 + $\pi/2$
7	2.436	$-40^\circ,4' + \pi$	59,48 + $2\pi/2$
8	2.436	$40^\circ,4'$	59,48 + $3\pi/2$

The angles θ_i and ϕ_i in the table are the polar and azimuthal angles of the ith oxygen, respectively.

From Eq. (B.5) the expression for A_{20} can be written as,

$$A_{20} = \frac{4\pi}{5} e \sum_{i=1}^{8} \frac{Q_i}{R_i^3} Y_{20}(\theta_i, \phi_i)$$

$$= \frac{4\pi}{5} Qe \left\langle \frac{1}{R^3} \right\rangle \sqrt{\frac{5}{16\pi}} \sum_{i=1}^{8} (3\cos^2\theta_i - 1) \qquad \text{(B.8)}$$

where Q is the effective charge of the oxygen ions and $\langle 1/R^3 \rangle$ is defined by

$$\left\langle \frac{1}{R^3} \right\rangle \equiv \frac{1}{2}\left(\frac{1}{R_1^3} + \frac{1}{R_2^3} \right)$$

with $R_1 = 2.481$ Å, and $R_2 = 2.486$ Å. From Table B.1, we obtain

$$\sum_{i=1}^{8} \left(3\cos^2\theta_i - 1 \right) = 0.898 \tag{B.9}$$

Thus, combining (B.8) and (B.9), we find

$$A_{20} = 0.898\sqrt{\frac{\pi}{5}} \left\langle \frac{1}{R^3} \right\rangle Qe \tag{B.10}$$

Similarly,

$$A_{40} = -1.130\sqrt{\pi} \left\langle \frac{1}{R^5} \right\rangle Qe$$

and,

$$A_{4-4} Y_{4-4} + A_{44} Y_{44} = -\sqrt{\frac{35\pi}{6}} \left\langle \frac{1}{R^5} \right\rangle Qe$$

$$(x)\left[1.198\left(Y_{44} + Y_{4-4} \right) - i\, 1.094\left(Y_{44} - Y_{4-4} \right) \right]$$

where,

$$\left\langle \frac{1}{R^5} \right\rangle \equiv \frac{1}{2}\left(\frac{1}{R_1^5} + \frac{1}{R_2^5} \right)$$

Hence, according to (B.7), we finally have

$$V(r) = 0.898\sqrt{\frac{\pi}{5}} \left\langle \frac{1}{R^3} \right\rangle eQ r^2 Y_{20}(\theta,\phi)$$

$$-1.130\sqrt{\pi} \left\langle \frac{1}{R^5} \right\rangle eQ r^4 Y_{40}(\theta,\phi)$$

$$-\sqrt{\frac{35\pi}{6_{72}}} \left\langle \frac{1}{R^5} \right\rangle eQ r^4 \left[1.198\,(Y_{44}+Y_{4-4}) - i\,1.094\,(Y_{44}-Y_{4-4})\right] \qquad \text{(B.11)}$$

For calculations of matrix elements of $V(\underline{r})$ it is more convenient to express V in the operator equivalent form as follows,

$$V(\underline{r}) = 0.2245\,\alpha\, eQ \left\langle \frac{r^2}{R^3} \right\rangle \left[3L_z^2 - \hat{L}^2\right]$$

$$-\beta eQ \left\langle \frac{r^4}{R^5} \right\rangle \left\{ \frac{1.695}{8}\left[35L_z^4 - 30\hat{L}^2 L_z^2 + 25L_z^2 - 6\hat{L}^2 \right. \right. \qquad \text{(B.12)}$$

$$\left. \left. + 3(\hat{L}^2)^2\right] - \frac{35}{64}\left[1.198\,(L_+^4 + L_-^4) - i\,1.094\,(L_+^4 - L_-^4)\right]\right\}$$

where,

$$\alpha = -\frac{2}{21} \quad , \qquad \beta = \frac{2}{63}$$

$$\hat{L}^2 \,|\psi(\ell,m)\rangle = \ell(\ell+1)\,|\psi(\ell,m)\rangle$$

$$\left\langle \frac{r^n}{R^{n+1}} \right\rangle \equiv \frac{\langle r^n \rangle}{\langle R^{n+1} \rangle}$$

$\langle r^n \rangle \equiv$ average of r^n over 3d radial wave function $=$

$$\int_0^\infty R_{n\ell}(r)\, r^n\, r^2\, dr$$

2. ENERGY LEVELS

The energy levels of the paramagnetic ion in the crystal field are the roots of the secular determinant

$$\| \langle \Gamma_i | V(\underline{r}) | \Gamma_j \rangle - E_i \, \delta_{ij} \| = 0$$

where Γ_i are appropriate basis functions for the S_4 symmetry. These functions are chosen, by considering the symmetry operations of the S_4 group, to diagonalize V or to reduce the number of the off-diagonal elements to a minimum. Thus we find,

$$\Gamma_1 = \psi_{20} \qquad (\psi_{\ell, m_\ell})$$

$$a\Gamma_2 = \frac{1}{\sqrt{2}} (\psi_{22} + \psi_{2-2})$$

$$b\Gamma_2 = \frac{1}{\sqrt{2}} (\psi_{22} - \psi_{2-2})$$

$$\Gamma_3 = \psi_{21}$$

$$\Gamma_4 = \psi_{2-1}$$

The non-zero matrix elements of V(r) are:

$$\langle \Gamma_1 | V | \Gamma_1 \rangle = 0.128 \, A - 0.483 \, B \equiv W_1$$

$$\langle a\Gamma_2 | V | a\Gamma_2 \rangle = -0.128 \, A - 0.580 \, B \equiv W_2$$

$$\langle b\Gamma_2 | V | b\Gamma_2 \rangle = -0.128 \, A + 0.418 \, B \equiv W_3$$

$$\langle a\Gamma_2 | V | b\Gamma_2 \rangle = -0.456 \, i \, B \equiv W_4$$

$$\langle {}_b\Gamma_2 | V | {}_a\Gamma_2 \rangle = 0.456\ i\ B \equiv W_4^*$$

$$\langle \Gamma_3 | V | \Gamma_3 \rangle = 0.064\ A + 0.322\ B \equiv W_5$$

$$\langle \Gamma_4 | V | \Gamma_4 \rangle = 0.064\ A + 0.322\ B \equiv W_5$$

where,

$$A = eQ\langle r^2 / R^3 \rangle \quad \text{and} \quad B = eQ\langle r^4 / R^5 \rangle$$

The secular determinant is set up as follows:

	$\lvert\Gamma_1\rangle$	$\lvert\Gamma_3\rangle$	$\lvert\Gamma_4\rangle$	$\lvert{}_a\Gamma_2\rangle$	$\lvert{}_b\Gamma_2\rangle$
$\langle\Gamma_1\rvert$	W_1-E	0	0	0	0
$\langle\Gamma_3\rvert$	0	W_5-E	0	0	0
$\langle\Gamma_4\rvert$	0	0	W_5-E	0	0
$\langle{}_a\Gamma_2\rvert$	0	0	0	W_2-E	W_4
$\langle{}_b\Gamma_2\rvert$	0	0	0	W_4^*	W_3-E

From this determinant, the energy levels are found to be:

$$\begin{aligned} E_1 &= 0.128\ A - 0.483\ B \\ E_3 &= 0.064\ A + 0.322\ B \\ E_4 &= 0.064\ A + 0.322\ B \\ E &= -0.128\ A + 0.595\ B \\ E &= -0.128\ A - 0.757\ B \end{aligned} \qquad \text{(B.13)}$$

In order to determine the sequence of energy levels we need to know, at least approximately, the ratio A/B. Accurate determination of

this ratio which involves integrals of the radial wave function is not possible. Pappalardo and Wood,[68] using the results of Hartree-Fock calculations by Watson,* have estimated**

$$< r^4 / R^4 > / < r^2 / R^2 > \quad = \quad 0.118$$

for Cu^{2+} (d^9) which is conjugate of V^{4+} (d^1). We shall use this value in our approximate calculations. Hence, employing the conventional Dq notation where,

$$Dq = eQ < r^4 / R^5 > \quad / \quad 6$$

we have $B \approx 6Dq$ and $A \approx 51Dq$. Using these parameters in B.13, we find the energy levels as shown in Figure B.2.

The corresponding eigenfunctions, which now diagonalize the perturbation Hamiltonian $V(\underline{r})$, are found to be

$$\Gamma_1 = \psi_{20}$$

$$\Gamma_3 = \psi_{21}$$

$$\Gamma_4 = \psi_{2-1}$$

$$\alpha = \frac{0.362}{\sqrt{2}}(\psi_{22} + \psi_{2-2}) + \frac{0.932\,i}{\sqrt{2}}(\psi_{22} - \psi_{2-2})$$

$$\beta = \frac{0.932\,i}{\sqrt{2}}(\psi_{22} + \psi_{2-2}) + \frac{0.362}{\sqrt{2}}(\psi_{22} - \psi_{2-2})$$

---

*Private communication with the former authors.

**The final result of Pappalardo and Wood on energy levels of Cu^{2+} in $CaWO_4$ is not correct due to some calculation errors.

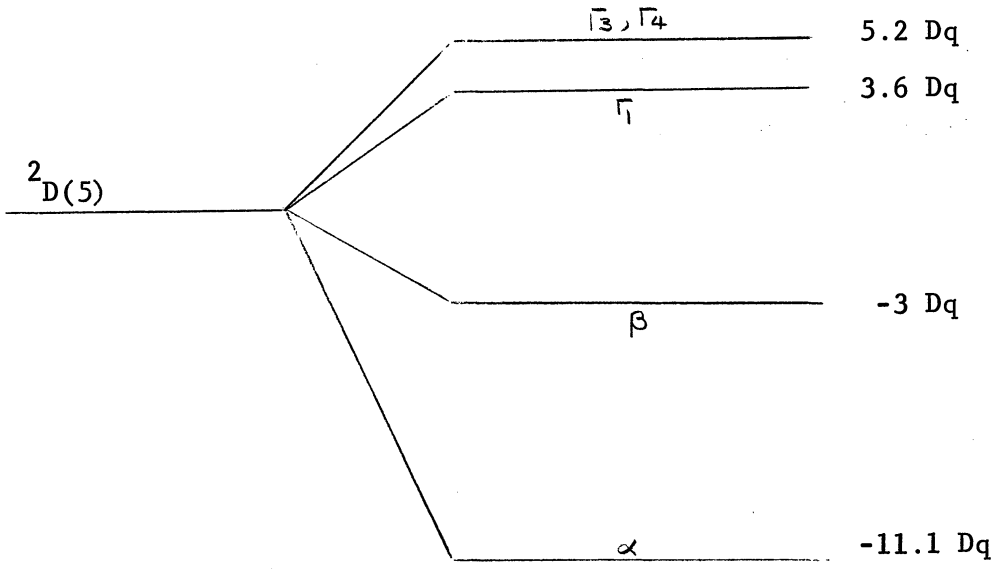

Fig. B.2. Energy levels of V^{4+} in a Ca site of $CaWO_4$.

3. SHIFT OF THE g-FACTOR

The g-factor for a free electron is $g_e = 2.0023$. However, the paramagnetic electron is not free and consequently its g-value differ from g_e by an amount $\Delta g = g - g_e$. Contributions to Δg come from coupling of the orbital angular momentum of the electron with its spin angular momentum and with the externally applied magnetic field. Denoting these perturbations by $\mathcal{H}_{pert}$, we have

$$\mathcal{H}_{pert} = \lambda \underline{L} \cdot \underline{S} + \beta \underline{L} \cdot \underline{H}$$

Δg is proportional to matrix elements of $\mathcal{H}_{pert}$ in the crystal field. For orbitally non-degenerate ground state (our case),

$$\langle 0 | \mathcal{H}_{pert} | 0 \rangle = 0$$

where $|0\rangle$ denotes the orbital part of the ground state wave function. Hence, to second order,

$$\Delta g \propto W = - \sum_f \frac{|\langle f | \mathcal{H}_{pert} | 0 \rangle|^2}{E_f - E_0}$$

where f denotes "final states." Let us choose $\underline{H}$ in the direction of the z-axis taken as the quantization axis. Thus, carrying out the perturbation calculations and collecting terms of first order in $S_z H_z$, we find

$$W = - \sum_f \frac{2 S_z H_z \beta \lambda}{E_f - E_0} |\langle f | L_z | 0 \rangle|^2$$

comparing this with the corresponding term in the spin Hamiltonian

$$\mathcal{H}_s = \beta g_z H_z S_z + \cdots$$

we find

$$\Delta g_z = - \sum_f \frac{2\lambda}{E_f - E_0} |\langle f | L_z | 0 \rangle|^2$$

Similar relationships can be obtained for x and y directions too. Hence, in general

$$\Delta g_i = - \sum_f \frac{2\lambda}{E_f - E_0} |\langle f | L_i | 0 \rangle|^2 \qquad \text{(B.14)}$$

$$i = x, y, z$$

Applying (B.14) to the energy levels of V^{4+} we find,

$$\Delta g_z = -2\lambda \left[\frac{|\langle \beta | L_z | \alpha \rangle|^2}{E_\beta - E_\alpha} + \frac{|\langle \Gamma_1 | L_z | \alpha \rangle|^2}{E_{\Gamma_1} - E_\alpha} + \frac{|\langle \Gamma_{3,4} | L_z | \alpha \rangle|^2}{E_{\Gamma_{3,4}} - E_\alpha} \right.$$

where,

$$\langle \beta | L_z | \alpha \rangle = 2i$$

$$\langle \Gamma_1 | L_z | \alpha \rangle = 0$$

$$\langle \Gamma_{3,4} | L_z | \alpha \rangle = 0$$

Thus

$$\Delta g = -\frac{8\lambda}{E_\beta - E_\alpha} = -\frac{8\lambda}{8.1\,Dq}$$

Similarly, for $\triangle\ g_x$, using the relationship

$$L_x = (1/2)(L_+ + L_-)$$

we have,

$$\Delta g_x = -\frac{1}{2}\lambda \left[\frac{|\langle \beta | L_+ + L_- | \alpha \rangle|^2}{E_\beta - E_\alpha} + \frac{|\langle \Gamma_1 | L_+ + L_- | \alpha \rangle|^2}{E_{\Gamma_1} - E_\alpha} + \frac{|\langle \Gamma_{3,4} | L_+ + L_- | \alpha \rangle|^2}{E_{\Gamma_{3,4}} - E_\alpha} \right.$$

where,

$$|\langle \beta | L_+ + L_- | \alpha \rangle|^2 = 0$$

$$|\langle \Gamma_1 | L_+ + L_- | \alpha \rangle|^2 = 0$$

$$|\langle \Gamma_3 | L_+ + L_- | \alpha \rangle|^2 = 2$$

$$|\langle \Gamma_4 | L_+ + L_- | \alpha \rangle|^2 = 2$$

Thus,

$$\Delta g_x = -2 \frac{\lambda}{E_{3,4} - E_\alpha} = \frac{-2\lambda}{16.3\,Dq}$$

For Δg_y, using the relationship $L_y = (L_+ + \underline{L}) / 2i$ in (B.14), we obtain

$$\Delta g_y = \frac{-2\lambda}{16.3\,Dq}$$

or

$$\Delta g_x = \Delta g_y$$

APPENDIX C

RELAXATION AND SATURATION PHENOMENA

In this appendix we shall describe briefly these processes and introduce the formulas which were used in our discussion, in Section 2 of Chapter V, on the line width and temperature dependence of the spectra. No effort, however, will be made here to present lengthy proofs or derivations since the subject is fully treated in a number of papers and books.

1. Relaxation Processes

Consider a system of two spin states ($M_s = \pm 1/2$) in a crystal lattice in a static magnetic field. Let us suppose that the spins are in thermal equilibrium with each other and with the lattice. That is, there are no interactions to change the total population of each level. The steady state condition is, then, characterized by

$$N_1^\circ W_{12} = N_2^\circ W_{21}$$

where N_i° are the equilibrium populations and W_{ij} are transition probabilities per unit time via spin-spin and spin-lattice interactions. On the other hand, assuming Boltzman distribution, the static equilibrium is governed by

$$N_2^\circ / N_1^\circ = e^{-\Delta E / kT}$$

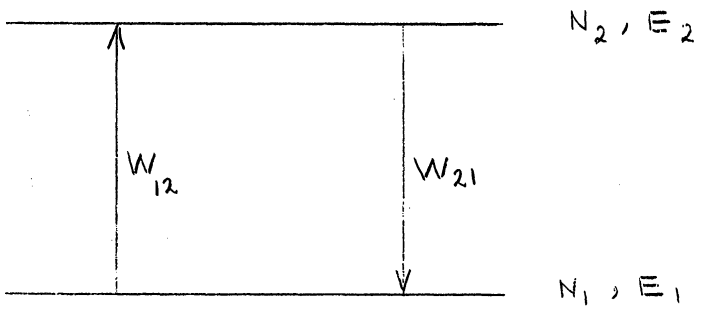

where $\Delta E = E_2 - E_1 > 0$. Hence, we have

$$W_{12} / W_{21} = e^{- \Delta E / kT}$$

Now we turn the microwave field on and disturb the equilibrium by inducing transitions between the spin levels. In this case the spins, by interacting with each other and with the lattice, try to re-establish the thermal equilibrium. The transient condition of the system can be expressed by

$$d / dt \ (N_1 - N_2) = 2 \ (N_2 W_{21} - N_1 W_{12})$$

or (C.1)

$$dn/dt = N \ (W_{21} - W_{12}) - n \ (W_{21} + W_{12})$$

where $N \equiv N_1 + N_2$, and $n \equiv N_1 - N_2$. Solution of Equation (C.1) is

$$n = n_o + Ae^{-t/\tau}$$

where,

$$n_o \equiv N \quad \frac{W_{21} - W_{12}}{W_{21} + W_{12}} \quad ,$$

$$\frac{1}{\tau} \equiv W_{21} + W_{12} \quad ,$$

and A is a constant of integration.

The approach of the spin system toward a thermal equilibrium is called "relaxation" and the associated characteristic time τ is defined as the "relaxation time." There are three major relaxation processes, namely, spin-lattice, general spin-spin interactions, and cross-relaxation.

i) Spin-Lattice Relaxation

This is the mechanism by which the spin system exchanges energy with the lattice and "cools-off." Here, the relaxation time (T_1), in general, is a function of temperature (T); the applied magnetic field H; and parameters Δ and λ, the crystal field strength and the spin-orbit coupling constant, respectively.[58] The explicit form of T_1 is one of the most disputed problems in relaxation, especially at low temperatures. Since the classic work of Casimir and du Pré,[59] many investigators have studied this problem both theoretically and experimentally.* The agreement among their results in most cases is only qualitative. However, they all agree that T_1 has $(1/T)^n$ - dependence.

---

*For recent literature on this subject see references 60 and 61.

For the purpose of our discussion we will use the recent formula of Van Vleck[60] for the low temperature region,

$$T_1 = \frac{b + cH^2}{a_0 + a_2 H^2 + a_4 H^4} \cdot \frac{1}{T} \qquad (C.2)$$

where a, a_0, a_2, a_4, b, and c are constants and H is the magnetic field strength.

ii) Spin-Spin Interactions

These are interactions which tend to establish a thermal equilibrium in the spin system via coupling of the spins with each other and with the nuclei of the host medium. These are: (1) magnetic dipole-dipole coupling; (2) electrostatic interactions between electrons which is usually called exchange effects; and (3) hyperfine coupling between the spin of the paramagnetic ion and the nuclear spin of the host material. Of these, the second one is important only in systems with high spin densities, e.g., undiluted paramagnetic salts, and the third one is usually negligible.

The theory of the magnetic dipole-dipole interaction was first developed by Van Vleck[62] who used moments method to calculate dipolar broadening of ESR lines. The spin-spin interaction was also recently studied by statistical approach[63] which extended Van Vleck's results to very dilute spin systems. The contribution of the magnetic dipole coupling to the line width stems from the fact that if two paramagnetic ions i and j are located at a distance r_{ij} from each other, then the classical magnetostatic energy between the two is given by

$$E_{ij} = \frac{g^2\beta^2}{r_{ij}^3}\left[\underline{S}_i \cdot \underline{S}_j - \frac{3(\underline{r}_{ij}\cdot\underline{S}_i)(\underline{r}_{ij}\cdot\underline{S}_j)}{r_{ij}^2}\right]$$

where $\underline{S}_i$ and $\underline{S}_j$ are the two spin angular momenta and $\underline{r}_{ij}$ is the radius vector from i to j. The energy for a system of N spin is then,

$$\mathcal{H} = \frac{1}{2}\sum_{i=1}^{N}\sum_{j=1}^{N} E_{ij}$$

Using this perturbation Hamiltonian, Van Vleck calculated the mean square derivation $\langle(\Delta\omega)^2\rangle$, of the resonance frequency, defined by

$$\langle(\Delta\omega)^2\rangle = \frac{\int_0^\infty (\omega - \langle\omega\rangle)^2 f(\omega)\,d\omega}{\int_0^\infty f(\omega)\,d\omega}$$

where f (ω) is a line-shape factor and

$$\langle\omega\rangle = \frac{\int_0^\infty \omega f(\omega)\,d\omega}{\int_0^\infty f(\omega)\,d\omega} \equiv \omega_0$$

In most spin resonance experiments, the frequency ω is held constant and the magnetic field $\underline{H}$ is varied. To first order, $\hbar\Delta\omega = g\beta\Delta H$ where Δ H is the line width measured in gauss.

Taking the static magnetic field in the z direction, chosen as the quantization axis, Van Vleck has obtained

$$\langle(\Delta\omega_1)^2\rangle_1 = \frac{3}{4\hbar^2} S_1(S_1+1) g_1^4\beta^4 \sum_j r_{0j}^{-6}(1-3\cos^2\theta_{0j}) \qquad \text{(C.3)}$$

where $\underline{r}_{oj}$ and θ_{oj} are the radius vector and polar angle of the jth ion with respect to one of the ions taken as the origin of coordinates. Now suppose the system contains a second kind of paramagnetic ions whose resonance frequency is different from the first one, e.g., $CaWO_4$:V, Nd system. In this case, if the resonance condition is set for the first ions, the contribution of the second ions to the spread of the resonance frequency, in the same coordinate system, is given by

$$\langle (\Delta\omega)_1^2 \rangle_2 = \frac{1}{3\hbar^2} S_2(S_2+1) g_1^2 g_2^2 \beta^4 \sum_k r_{0k}^{-6} (1 - 3\cos^2\theta_{0k})^2 \qquad (C.4)$$

In other words, in such a system, the total mean square deviation of is given by

$$\langle (\Delta\omega_1)^2 \rangle = \langle (\Delta\omega_1)^2 \rangle_1 + \langle (\Delta\omega_1)^2 \rangle_2$$

The characteristic time constant for the spin-spin interactions is shown by T_2.

iii) Cross-Relaxation

The theory of cross-relaxation was first presented by Bloembergen et al.[64] Since then, it has been applied successfully to interpretation of a number relaxation phenomena which could not be accounted for by considering only T_1 and T_2 time constants. According to this theory, the dipolar interaction between the ions may induce transitions in which the total Zeeman and crystalline field energy is conserved. Consider two different species of ions α and β with corresponding resonance frequencies ω_α and ω_β, and energies E_α

and E_β . Now we ask what is the probability that α "flips up" in spin while β flips down? This probability is proportional to

$$|\langle E_\alpha, E_\beta | \mathcal{H}_{\alpha\beta} | E_\alpha + \hbar\omega_\alpha, E_\beta - \hbar\omega_\beta \rangle|^2$$

where $\mathcal{H}_{\alpha\beta}$ is dipole-dipole interaction Hamiltonian. The characteristic time, which is inversely proportional to the transition probability, is shown by T_{12} due to the fact that its magnitude is commonly between the spin-lattice relaxation time T_1 and the dipolar interaction time T_2. T_{12} increases rapidly as the difference between the resonance frequencies of the two spin systems increases.

2. Saturation Phenomena

If we use only the spin-lattice and spin-spin relaxation times T_1 and T_2 to describe the transient state of the spin system, then the average rate of energy absorption per unit volume of the sample is given by

$$A = \chi_0 \omega_0^2 H_1^2 \frac{T_2}{1 + T_2^2(\omega_0 - \omega)^2 + \gamma^2 H_1^2 T_1 T_2} \qquad \text{(C.5)}$$

which is obtained from the Bloch phenomenological equation.[65] Here

χ_0 = magnetostatic (Curie) susceptibility

H_1 = 1/2 of the amplitude of the microwave field's magnetic component

$\omega = \Delta E_{ij}/\hbar$, where ΔE_{ij} = splitting of energy levels between which transition takes place

ω_0 = fixed frequency of the microwave field

γ = gyromagnetic ratio

Under normal operational condition, the term $\gamma^2 H_1^2 T_1 T_2$, which will be denoted by σ satisfies the condition

$$\sigma \equiv \gamma^2 H_1^2 T_1 T_2 < 1 \tag{C.6}$$

and hence,

$$A_{\sigma<1} \approx \chi_o \omega_o^2 H_1^2 \frac{T_2}{1 + T_2^2(\omega_o - \omega)^2} \tag{C.7}$$

The resonance condition is $\omega = \omega_o$ for which the absorption reaches its peak

$$A_{peak} \approx \chi_o \omega_o^2 H_1^2 T_2$$

We notice that by increasing microwave power, A increases. Figure C.1 shows the shape of absorption line obtained by plotting A vs. $T_2(\omega_o - \omega)$ using Equation (5.7). The width of this curve between the points of half-maximum is

$$\Delta\omega = \frac{2}{T_2} \tag{C.8}$$

The condition (C.6) can be maintained by decreasing the microwave power. However, a limitation is imposed on us by T_1 and T_2. When, for any reason, σ increases so that

$$\gamma^2 H_1^2 T_1 T_2 \gg 1 \tag{C.9}$$

then near resonance, Equation (C.5) takes the following form

$$A_{\sigma \gg 1} \approx \frac{\chi_o \omega^2}{\gamma^2 T_1}$$

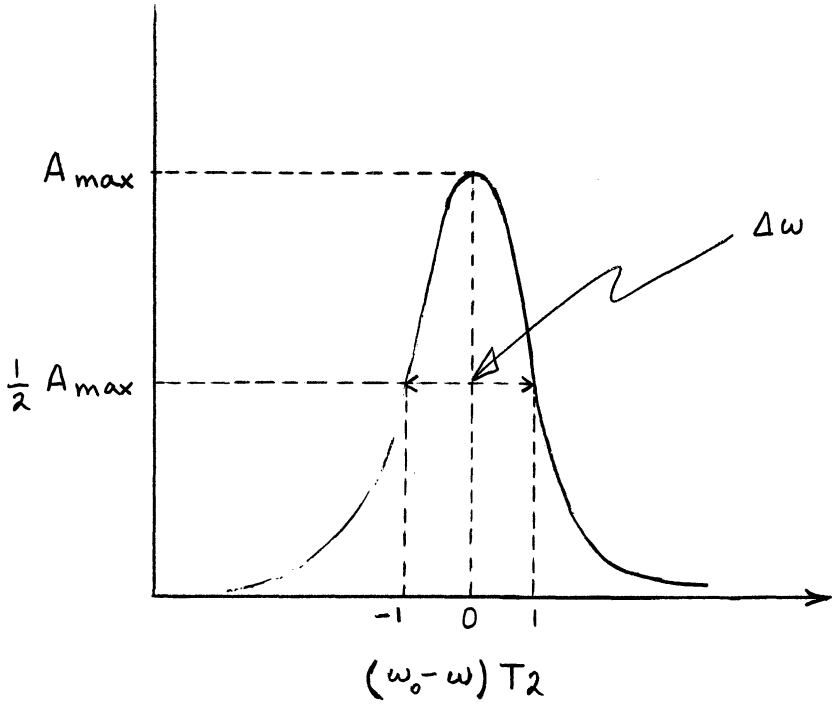

Fig. C4.1. Energy absorption as a function of the microwave frequency.

Under this condition, as we note, the absorption curve levels off and no resonance peak is observed. This situation is called saturation of the ESR signal. It implies that relaxation mechanisms are not powerful enough to carry off the energy put in by the electromagnetic field.

REFERENCES

1. C. F. Hempstead and K. D. Bowers, Paramagnetic Resonance of Impurities in $CaWO_4$. I. Two S-State Ions, Phys. Rev. 118, 131 (1960).

2. P. A. Forrester and C. F. Hempstead, Paramagnetic Resonance of Tb^{3+} Ions in $CaWO_4$ and CaF_2, Phys. Rev. 126, 923 (1962).

3. R. W. Kedzie and M. Kestigian, PMR Determination of Transition Metal Ion Sites and Multiplicity of Rare-Earth Ion Sites in $CaWO_4$, Appl. Phys. Let. 3, 86 (1963).

4. R. W. Kedzie and M. Kestigian, PMR of Nd^{3+} in $CaWO_4$, Appl. Phys. Let. 4, 124 (1964).

5. C. G. B. Garrett and F. R. Merritt, PMR Spectra of Nd^{3+} in Compensated and Uncompensated $CaWO_4$, Appl. Phys. Let. 4, 31 (1964).

6. T. U. Ranon, Electron Spin Resonance of $CaWO_4$:Nd^{3+}, Phys. Let. 8, 154 (Feb. 1964).

7. J. Kirton, PMR of Ho^{3+} Ions in $CaWO_4$, Phys. Rev. 139, A 1930 (1965).

8. I. Z. Potvorova and L. Ya. Shekun, EPR Study of Tetragonal Sm^{3+} Centers in $CaWO_4$, Sov. Phys.-Solid State 7, 2596 (1966).

9. J. Bronstein and V. Voltera, EPR of Eu^{2+} in $CaWO_4$, Phys. Rev. 139, A 1201 (1965).

10. K. Nassau and A. M. Broyer, Calcium Tungstate: Czochrolski Growth, Perfection, and Substitutions, J. Appl. Phys. 33, 3064 (1962).

11. P. Görlich, H. Karras, G. Kotitz and R. Lehmann, Spectroscopic Properties of Activated Laser Crystals I, Physica Status Solidi 5, 437 (1964); II, 6, 277 (1964); III, 8, 385 (1965).

12. L. F. Johnson, "Characteristics of the $CaWO_4$:Nd^{3+} Optical Masers," Quantum Electronics, Paris, Vol. II, 1963, p. 1021.

13. K. Nassau and G. M. Loiacono, Calcium Tungstate-III, Trivalent Rare-Earth Substitution, J. Phys. Chem. Solids 24, 1503 (1963).

14. K. Nassau, Calcium Tungstate-IV, Theory of Coupled Substitution, J. Phys. Chem. Solids 24, 1511 (1963).

15. J. Lambe, R. Ager and C. Kikuchi, ESR of V^{2+} and V^{3+} in Corundum, Bull. Am. Phys. Soc. 4, 261 (1959).

16. J. Lambe and C. Kikuchi, Spin Resonance of V^{2+}, V^{3+}, V^{4+} in α-Al_2O_3, Phys. Rev. 118, 71 (1960).

17. G. H. Azarbayejani and C. Kikuchi, ESR of CaO Doped with Iron-Group Elements, Bull. Am. Phys. Soc. 8, 344 (1963).

18. N. Mahootian and C. Kikuchi, ESR Studies of MgO:V Powder Samples, Bull. Am. Phys. Soc. 9, 245 (1964).

19. R. H. Borcherts and C. Kikuchi, An EPR Investigation of VO^{4+} and X-Ray Produced V^{2+} in Tutton Salt, J. Chem. Phys. 40, 2270 (1964); also R. H. Borcherts, Ph.D. Thesis, Nuc. Engineering Dept., U. Mich. (1963).

20. C. Kikuchi, I. Chen, W. H. From and P. B. Dorain, Spin Resonance of SnO_2:V and the Vanadium 3d Electron Orbital, J. Chem. Phys. 42, 181 (1965).

21. S. Karavelas and C. Kikuchi, Molecular Orbital Theory of Vanadium in the Rutile Structure Crystals SnO_2, TiO_2, Tech. Report 04381-7-T, Univ. Mich. (1964); also S. Karavelas, Ph.D. Thesis, Nuc. Engineering Dept., Univ. Mich. (1964).

22. I. Chen, C. Kikuchi and H. Watanabe, Mechanism of Superhyperfine Structure in SnO_2:V^{4+}, J. Chem. Phys. 42, 186 (1965).

23. I. Chen and C. Kikuchi, On the Theory of Superhyperfine Interaction in Iron Group Ion Complexes, Tech. Report 04381-5-T, Univ. Mich. (1964); also I. Chen, Ph.D. Thesis, Nuc. Engineering Dept., Univ. Mich. (1964).

24. B. Bleaney, D. J. E. Ingram and H. E. D. Scovil, PMR in Vanadous Ammonium Sulphate, Proc. Phys. Soc. A64, 601 (1951).

25. W. Low, PMR of Some Ions of the 3d and 4f Shells in Cubic Crystalline Fields, Phys. Rev. 101, 1827 (1956).

26. See for example J. E. Wertz, P. Auzins, J. H. E. Griffiths and J. W. Orton, Electron Transfer Among Transition Elements in MgO, Disc. Faraday Soc. 26, 66 (1958).

27. J. S. Van Wieringen and J. S. Rensen, Influence of Lattice Imperfection on PMR of V^{2+} and Cr^{3+} in MgO, Proc. 1st Internal. Conf. on PMR in Jerusalem, Edited by W. Low, New York, 1963, Vol. I, p. 105.

28. W. Low and E. L. Offenbacher, ESR of Magnetic Ions in Complex Oxides, Solid State Physics, Edited by F. Seitz et al, Academic Press, New York, 1965, Vol. 17, p. 135.

29. W. Low and R. S. Rubins, PMR of Iron Group and Rare-Earth Impurities in CaO, Proc. 1st Intern. Cof. On PMR in Jerusalem, Edited by W. Low, New York, 1963, Vol. I, p. 79.

30. W. Low and R. S. Rubins, ESR in Cubic Crystalline Field of CaO, Phys. Let. 1, 316 (1962).

31. H. H. Woodbury and G. W. Ludwig, Spin Resonance of Transition Metals in Silicon, Phys. Rev. 117, 102 (1960).

32. T. L. Estle and M. de Wit, ESR of Co^{2+} and V^{2+} in ZnO, Bull. Am. Phys. Soc. 6, 445 (1961).

33. T. P. P. Hall, W. Hayes, R. W. H. Stevens and J. Wilkens, Investigation of Bonding of Iron Group in Fluoride Crystals, J. Chem. Phys. Rev. 38, 1977 (1963).

34. N. Laurance and J. Lambe, Quadrupole Interaction of Vanadium and Manganese in Corundum, Phys. Rev. 132, 1029 (1963).

35. M. D. Sturge, Optical Spectrum of Divalent Vanadium in Octahedral Coordination, Phys. Rev. 130, 639 (1963).

36. G. F. Imbush, W. M. Yen, A. L. Schawlow, D. E. McCumber and M. D. Sturge, Temperature Dependence of the Width and Position of the $^2E \rightarrow {}^4A_2$ Fluorescent Lines of Cr^{3+} and V^{2+} in MgO, Phys. Rev. 133, A 1029 (1964).

37. G. M. Zverev and A. M. Prokhorov, EPR of the V^{3+} Ion in Sapphire, Sov. Phys. JETP 7, 707 (1958).

38. M. H. L. Pryce and W. A. Runciman, The Absorption Spectrum of Vanadium Corundum, Disc. Faraday Soc. 26, 34 (1958).

39. H. H. Woodbury and G. W. Ludwig, Impurity Studies in Compound Semiconductors by Electron Spin Resonance, Bull. Am. Phys. Soc. 6, 118 (1961).

40. W. C. Holton, J. Schneider, and T. L. Estle, Electron Paramagnetic Resonance of Photosensitive Iron Transition Group Impurities in ZnS and ZnO, Phys. Rev. 133, A 1938 (1964).

41. H. J. Gerritsen and H. R. Lewis, PMR of V^{4+} in TiO_2, Phys. Rev. 119, 1010 (1960).

42. G. M. Zverev and A. M. Prokhorov, EPR of Vanadium in Rutile, Sov. Phys. JETP 12, 160 (1961).

43. J. A. Marley and T. C. McAvoy, Air Force Cambridge Research Laboratories AFCRL-62-771, 186 (1962).

44. I. Siegel, PMR of Vanadium in Amorphous and Polycrystalline GeO_2, Phys. Rev. 134, A 193 (1964).

45. C. A. Hutchinson Jr. and L. S. Singer, PMR Absorption in Salts of V and Mn, Phys. Rev. 89, 256 (1953).

46. B. M. Kozyrev, PMR in Solutions of Electrolytes, Disc. Faraday Soc. 19, 135 (1955).

47. G. E. Pake and R. H. Sands, Hyperfine Structure in PMR of Vanadium Ions in Solutions, Phys. Rev. 98, 266A (1955).

48. R. H. Sands, PMR Absorption in Glass, Phys. Rev. 99, 1222 (1955).

49. D. E. O'Reilly, PMR of Vanadyl Etiporphyrin I, J. Chem. Phys. 29, 1188 (1958).

50. R. J. Faber and M. T. Rogers, PMR Spectra of Absorbed Mn (II), Cu (II), and Oxovanadium (IV), J. Am. Chem. Soc. 81, 1849 (1959).

51. R. N. Rogers and G. E. Pake, Paramagnetic Relaxation in Solution of Vo^{2+}, J. Chem. Phys. 33, 1107 (1960).

52. E. M. Roberts, W. S. Koski and W. S. Coughey, ESR of Some Vanadyl Porphyrins, J. Chem. Phys. 34, 591 (1961).

53. R. W. G. Wyckoff, Crystal Structures. Interscience Publishers, Inc., New York (1951), Vol. II, Ch. VIII; Also, International Tables for X-Ray Crystallography, Vol. I, The Kynoch Press, Birmingham, England (1952).

54. M. I. Kay, B. C. Grazer and I. Almodovar, Neutron Diffraction Refinement of $CaWO_4$, J. Chem. Phys. 40, 504 (1964).

55. A. Zalkin and D. H. Templeton, X-Ray Diffraction Refinement of the $CaWO_4$ Structure, J. Chem. Phys. 40, 501 (1964).

56. S. Karavelas and C. Kikuchi, Molecular Orbital Calculation of Vanadium in $CaWO_4$, Bull. Am. Phys. Soc. 10, 614 (1965); Also Univ. Mich. Tech. Report 06029-30-T, Sept. 1965.

57. L. Pauling, The Nature of the Chemical Bond, 3rd Edition, Cornell Univ. Press, Ithica, New York (1960).

58. S. A. Al'tshuler and B. M. Kozyrev, Electron Paramagnetic Resonance, Academic Press, Inc., New York (1964).

59. H. B. G. Casimir and F. K. du Pre, Note on Thermodynamic on Paramagnetic Relaxation Phenomena, Physica 5, 507 (1938).

60. J. H. Van Vleck, The Puzzle of Spin-Lattice Relaxation at Low Temperatures, Quantum Electronics, A symposium Edited by C. H. Townes, Columbia Univ. Press, 1960, p. 392.

61. C. Gorter, L. C. Van Der Marel and B. Bolger, PMR Relaxation in the Temperature Region of Liquid Helium, Physica 21, 103 (1955).

62. J. H. Van Vleck, The Dipolar Broadening of Magnetic Resonance Lines in Crystals, Phys. Rev. 74, 1168 (1948).

63. W. J. C. Grant and M. W. P. Strandberg, Statistical Theory of Spin-Spin Interactions in Solids, Phys. Rev. 135, A 715 (1964).

64. N. Blombergen, S. Shapiro, P. S. Pershan and J. O. Artman, Cross Relaxation in Spin Systems, Phys. Rev. 114, 445 (1959).

65. George E. Pake, Paramagnetic Resonance, W. A. Benjamin, Inc., New York, 1962.

66. R. V. Pound and E. M. Purcell, A Nuclear Spin System at Negative Temperature, Phys. Rev. 81, 279 (1951).

67. J. A. Giordmaine, L. E. Alsop, F. R. Nash and C. H. Townes, PMR Relaxation at Very Low Temperature, Phys. Rev. 109, 302 (1958).

68. R. Pappalardo and D. L. Wood, Crystal Field Calculation for the Ca Site of the Scheelite Structure, J. Mol. Spect. 10, 81 (1963).

69. J. W. Mellor, A Comprehensive Treatise on Inorganic and Theoretical Chemistry, Vol. IX, Longmans, Green, and Company (1949).

70. G. D. Watkins and J. W. Corbett, Defects in Irradiated Silicon: EPR and ENDOR of the Si-E Center, Phys. Rev. 134, A 1359 (1964).

71. H. S. Gutowsky and A. Saika, Dissociation, Chemical Exchange and the Proton Magnetic Resonance in Some Aqueous Electrolytes, J. Chem. Phys. 21, 1688 (1953).

72. Charles P. Slichter, Principles of Magnetic Resonance, Harper and Row, New York, 1963.

73. G. D. Watkins, Motion of Mn^{++}-Cation Vacancy Pairs in NaCl: Study by ESR and Dielectric Loss, Phys. Rev. 113, 91 (1959).